AD-A031 794 EDO CORP COLLEGE POINT N Y F/G 17/1
ACOUSTIC TRANSIENT SIGNAL STUDY.(U)
JUN 66 A A WINDER, A N COHEN NONR-3346(00)
UNCLASSIFIED EDO-7087 NL

1 OF 2
AD A031794

Acoustic Transient Signal Study

INTERIM YEARLY
ENGINEERING REPORT
1 SEPT 1964 - 1 SEPT 1965

[illegible]
[illegible]

MOST Project 1

Report 7087
Edo SC-119

1622-01

ACOUSTIC TRANSIENT SIGNAL STUDY

INTERIM YEARLY ENGINEERING REPORT

PERIOD: 1 SEPT. 1964 - 1 SEPT. 1965

CONTRACT NO. NOnr 4678(00)

Authors:
Research Project Engineer:
A. A. Winder

Research Senior Engineer:
A. N. Cohen

Approval:
Chief Engineer Advanced Programs:
J. Bernstein

Distribution of this document is unlimited

Edo Corporation
COLLEGE POINT 56, N.Y.C., N.Y.

TABLE OF CONTENTS

LIST OF ILLUSTRATIONS

LIST OF ILLUSTRATIONS (cont)

LIST OF ILLUSTRATIONS (cont)

LIST OF ILLUSTRATIONS (cont)

LIST OF ILLUSTRATIONS (cont)

ABSTRACT

The objective of Edo's efforts in the field of acoustic transients is to establish the operational feasibility for employing these signals in applications such as detection, classification, communication, and bottom contour mapping. In the process of carrying out this objective, an experimental-study program was conducted to characterize the waveshape, reproducibility, energy spectra, and directivity of a mechanical impact generator, the IMP MOD X-1. The influence of the propagating medium upon the acoustic properties of the generated shock-wave was also investigated. The results of the program and a recommended future program of work are given in this report.

ACKNOWLEDGEMENT

The work reported here is part of the Acoustic Transient Signal Study supported by the Office of Naval Research under Contract Nonr-4678(00). The program was under the technical guidance of Dr. Philip L. Stocklin and the administrative coordination of Dr. Aubrey W. Pryce, Director, Acoustics Programs. We extend our deepest appreciation to ONR for encouraging Edo's contact with other leading activities in the area of acoustic transients through various symposia and informal meetings. The resulting stimulating discussions matured our thinking and made our work more meaningful.

We are indebted to the personnel of the Johns Hopkins University (Electrical Engineering Department) for their contribution in analyzing the data, in particular to Dr. William Huggins, Dr. Stephen S. Wolff, Dr. John R. Sopko, and Mr. J. Yang. Their work substantially enhanced the results of the program.

We would also like to take this opportunity to express our appreciation to the Underwater Sound Reference Laboratory (Orlando, Florida) for the calibration of the receiving probes, to the Naval Underwater Ordnance Station (Newport, Rhode Island) for their cooperation and advice concerning the tests conducted there from May through July 1965, and to the computer group at the Edo Corporation, specifically Mr. Frank F. Taranto, for programming our data analyses.

SECTION 1

INTRODUCTION

This report describes the Edo investigation of the effects of the acoustic medium on the spatial and temporal properties of transient signals.

Data was recorded at the Edo Corporation and the NUOS Torpedo Range, and analyzed by various signal representations programmed on a digital computer. The results given are an extension of those presented in an earlier report entitled "A Survey of Acoustic Transient Processes and Experimental Evaluation of IMP MOD X-1," Edo Report 6299 January, 1964 (reference 1).

The wideband characteristic of an acoustic transient make it very receptive to the nonlinear and dispersive properties of the transmission medium. When a complex signal is transmitted, the received waveform will have the same amplitude-phase structure as the original signal only if all of its Fourier components are attenuated equally and if they all propagate at the same phase velocity. Therefore, distortionless transmission requires that the attenuation coefficient be independent of frequency and that the phase coefficient be linearly proportional to frequency. However, these conditions are generally not satisfied. An interesting propagation effect is the anomaly produced by a sound wave traveling with a finite amplitude (reference 2). This is characterized by a steepening of the wavefront which enhances the high frequency content with respect to the low frequencies and is opposed by the broadening due to high frequency absorption. Finite amplitude therefore represents a departure from the linear acoustic wave equation. Distortion or fluctuations in a signal's parameters (amplitude, phase, frequency and pulsewidth) may also be attributed to multipaths, and the space and time variability of the geophysical properties of the ocean.

The high peak pressure and short time duration which distinguish a transient signal often impose limitations upon the test instrumentation. Examples of such constraints are the requirements for high dynamic range and short time of analysis. Also, signal processing techniques should accommodate the changes in frequency and pulsewidth due to propagation to detect and classify targets effectively.

It is desirable that the transient signal have certain properties, such as:

- ★ Reproducibility with respect to waveshape
- ★ High directionality
- ★ An energy distribution that will propagate
- ★ A bandwidth-time product sufficient for processing.

An additional requirement for employing acoustic transients is that there be knowledge of the time dependence of the directivity pattern. This refers not only to the propagation of such patterns but also to their temporal growth and decay at a given range.

An experimental-study program was designed to determine the properties of an acoustic transient, as discussed above. The tests at Edo were at ranges of 1 foot to 4 yards and those at NUOS at ranges up to 750 yards. The transient generator used was the IMP MOD X-1, (references 3 and 4), the mechanical impact source designed and developed by the late Harold Sawyer of the Woods Hole Oceanographic Institution. The IMP MOD X-1 was selected because its waveshape is highly predictable and reproducible. Mechanical impact design theory (reference 5) permits the peak pressure, pulsewidth, rise time, and rate of decay to be independently and accurately controlled. This makes the IMP MOD X-1 an excellent tool for carrying out the aims of the program. The purpose of the tests at short ranges was to determine the operation and characteristics of the IMP MOD X-1 so that the effects of the medium on the transient signal at the longer ranges could be properly analyzed.

The tests consisted of recording the waveform to determine its structural characteristics as a function of bearing and range, and superimposing many waveforms to establish the degree of reproducibility. Peak and iso-time patterns* were calculated, including the effective C-W pressure patterns** having the amplitude-phase spectra of the transients generated on-axis. Spectral analyses** and signal decompositions** were performed in cooperation with the Johns Hopkins University.

In section 2, the results of the program are summarized and compared with those of previous programs wherever possible. In section 3, the test instrumentation and facilities are described in detail to facilitate an understanding of the results. In section 4, the results of the measurements and analyses are extensively discussed. In section 5, the future acoustic transient program is outlined.

*Defined on page 4D-1.
**Defined in Part 4A

SECTION 2

SUMMARY OF RESULTS

The IMP MOD X-1 acoustic transient program had two principal goals, namely:

a. To characterize the operation of the mechanical impact generator

b. To record and analyze the propagation of a shock wave in the near and far field.

This section contains a summary of the results of the experimental-study program for the following areas:

- ★ Waveform
- ★ Energy spectra
- ★ Directivity
- ★ Orthogonal exponential decomposition

The experimental data, and the methods and techniques used in the analyses are discussed in section 4.

WAVEFORM

The pressure waveform was found to be highly reproducible with respect to peak pressure, pulsewidth, rise time and decay. This was determined by superimposing five pulses over the average time intervals of 15 and 50 seconds. The peak pressure measured was 141 db re 1 microbar at 1 yard from the acoustic window, on-axis, with a pulsewidth* of 33 microseconds. The rise time, 4 microseconds, is the integration of the wideband probe. The value of peak pressure recorded at 1 yard shows excellent correlation with those measured in other programs. The results of these previous programs are listed below.

	NUOS (1965)	WHOI (1964)	EDO[1] (1963)	WHOI[4] (1959)
Peak Pressure at 1 yard (db re 1 μbar)	141	143.7	140	144

(Superscripts refer to references)

* The "pulsewidth" is defined as the first positive portion of the pressure waveform.

At the ranges of 1 foot to 5 yards, the peak pressures followed a spreading loss dictated by a 0.75 power of the range. This indicates a transition region or intermediate zone between spherical and cylindrical spreading. For the other ranges from 30 to 750 yards, the spreading loss appeared to be spherical.

At a range of 5 yards, the pulsewidth decreased to approximately 26 microseconds and remained at this value for all other test ranges. The rise time was constant at 4 microseconds to approximately 250 yards. Above 250 yards, the rise time appeared to increase slowly. This may be attributed to either one or both of the following factors:

a. The high frequency attenuation due to absorption becoming more pronounced.

b. The increasing inaccuracy of the data due to surface and bottom reflections at ranges greater than 250 yards.

The tests at Edo were conducted at a depth of 10 feet and those at NUOS at a depth of 25 feet. Although the cavitation limit for C-W intensity was greatly exceeded during these tests, there was no evidence of cavitation. Also, there were no bubble pulses generated after radiation of the shock-wave. This facilitates pulsing repetitively and will result in greater control and reproducibility in shaping the energy spectrum. The variation in the firing time delay of the impulse generator was about ±10 milliseconds.

ENERGY SPECTRA

The energy spectrum was determined by initially computing the correlation function of the transient signal and then taking its Fourier transform. The slope of the energy spectra on-and-off-axis, with the average values of the signals removed, was + 6 db per octave at the low frequency end. The high frequency fall-off rate was more difficult to determine due to the effects of truncation, aliasing and manual sampling, but appeared to be about -12 db per octave. The positions of the maximum energy densities were generally between 4 to 6 kc.

The cumulative energy spectra of the waveforms on-axis in general showed that 50% of the energy was below 14 kc and 85% was below 35 kc (approximately the reciprocal of the pulsewidth). Thus, the low frequencies are major contributors to the energy. An interesting occurence was that for similar ranges at Edo (3 and 4 yards) and NUOS (5 yards), there

was a shift of energy to the higher frequencies. At greater ranges, the energy maxima returned to their previous positions.

Off-axis, the total energy decreased with increased bearing deviation. This was characterized primarily by a reduction in the high frequency energy. Generally, the spatial selectivity increases with increasing frequency for a fixed-size projector. Therefore, the high frequencies will contribute small amounts of energy at large deviations from the acoustic axis.

A measure of the amount of information contained in a signal and the complexity of the instrumentation necessary for processing it is the rms bandwidth-time product. The average rms time and frequency durations computed, and their products, were:

	EDO	NUOS
RMS Time Duration (μsecs)	25.7	40.8
RMS Frequency Duration (kc)	33.3	35.3
RMS Bandwidth-time Product	0.85	1.43

A bandwidth-time product of about unity implies that there are two samples available for coherent processing for every signal pulse received.

DIRECTIVITY

The transient signal generated was highly directional. Its directive properties were characterized by peak and iso-time patterns. The iso-time pattern was computed at the time that the pressure waveform reached its maximum value on-axis. Both patterns were rather symmetrical at all ranges. At the time of the peak maxima on-axis, the pressures at other bearings had not reached their peak values due to the increase in rise time which resulted in the iso-time pattern being steeper than the peak pattern. The increase in rise time was caused by the high frequency content off-axis being significantly reduced as compared to the on-axis spectra.

The beamwidths at the-3 db levels for both patterns were practically identical for all ranges greater than 1 yard. At 1 yard, the beamwidth measured approximately 30° at Edo and 26° at NUOS. For ranges greater than 3 yards, the patterns were narrower and the beamwidth varied from 14° to 20° (17°± 3°). In a previous program (reference 4), the peak

directivity patterns taken at 23, 75, and 105 feet indicated a -3 db beamwidth of 30°.

The effective C-W pressure patterns having the amplitude-phase spectra of the transient signals generated on-axis were computed by utilizing the law of linear superposition. These patterns were generally much broader and more consistent with range than the peak or iso-time patterns and had a -3 db beamwidth of 22°. These pattern differences may have been caused by selecting an incorrect "single frequency" directivity pattern for spectral weighting (the IMP MOD X-1 was considered a rigid circular piston) or by the presence of anomalies in propagating through the medium.

The temporal growth and decay of the directivity pattern was determined for ranges of 1 yard and 67 yards. The temporal decay resembled the transition of a "sum-type pattern" (at the time of peak response on-axis) to a "difference-type pattern" (at a time approaching the pulsewidth on-axis) due to natural suppression of the high frequency content off-axis.

ORTHOGONAL EXPONENTIAL DECOMPOSITION

Waveforms at ranges of 1, 2, 3, 4, and 12 feet were sampled and analyzed using orthogonal exponential techniques. Accuracy (in the mean-squared sense) of 2.66% or better was obtained using five complex conjugate pairs of decaying exponentials to represent each signal. Characteristic of the mean-squared error criterion, the fidelity of waveform reproduction was best when the signals were large, but deteriorated in the low-amplitude signal tails. Energy spectra of the representations were computed analytically and were found to agree closely with spectra estimated from the data.

SECTION 3

TEST INSTRUMENTATION AND FACILITIES

This section describes the test instrumentation and facilities used to obtain the data for the acoustic transient program. The areas discussed are:

- ★ IMP MOD X-1

  The generation and control of the transient signal

- ★ Wideband Receiving Probes

  The fidelity of reproduction of the received transient

- ★ Control Cabinet

  The monitoring of the operation of the IMP and the recording of data

- ★ Receiving Platforms

  The supporting structure for the receiving instrumentation

- ★ Test Facilities

  The bounds imposed by the testing environment, such as surface and bottom reflections

- ★ Data Analysis

  The various analyses performed on the data

MECHANICAL IMPULSE GENERATOR, IMP MOD X-1

The generator, as shown in figure 3-1, is 3 feet long and has an outer radiating diameter of 1 foot. A cutaway drawing depicting its internal structure is shown in figure 3-2. The acoustic energy is generated by the impact of two masses under accurately controlled conditions. One of the masses is a stationary radiating piston. The other mass or impacting slug (driver) moves at a very high velocity at the time of contact with the piston. The slug obtains its motion through the release of several hydraulically loaded compressed helical springs. Therefore, the transient process is one in which the primary energy is the potential energy stored in helical springs

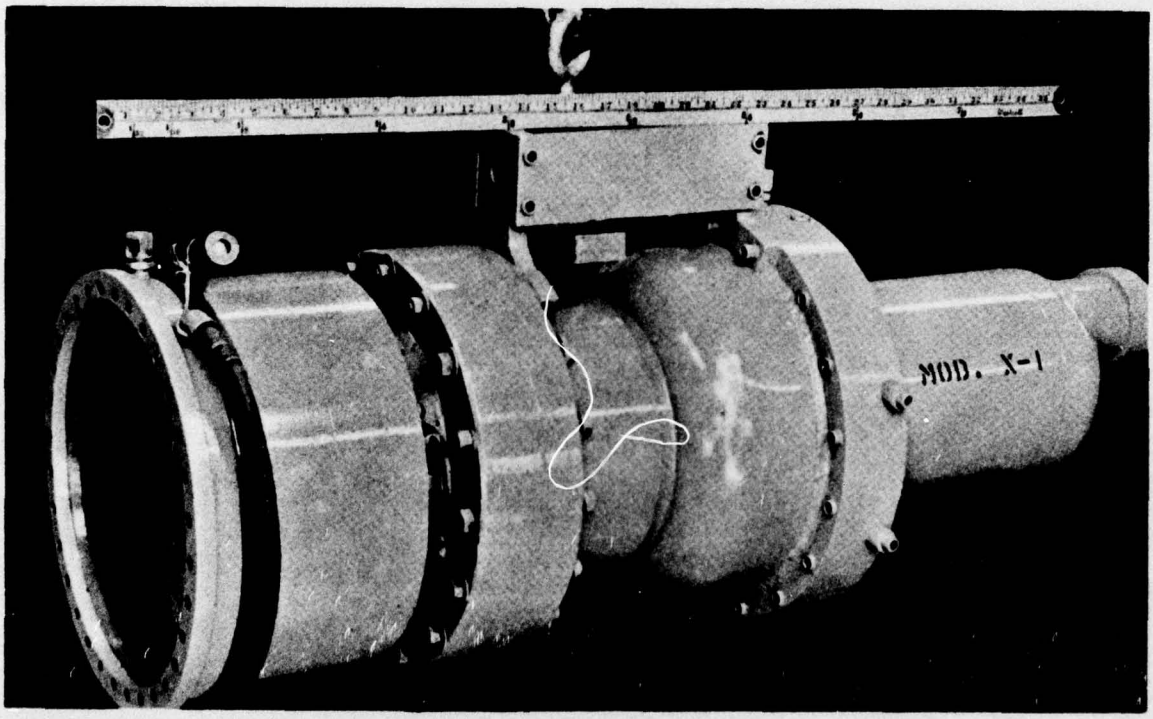

(Figure 1 of "Acoustic Transients and Impact-Energized Sound Source Research: "Final Report" by A. E. Sharp, WHOI, ref. no. 64-23, June 1964.)

Figure 3-1. IMP

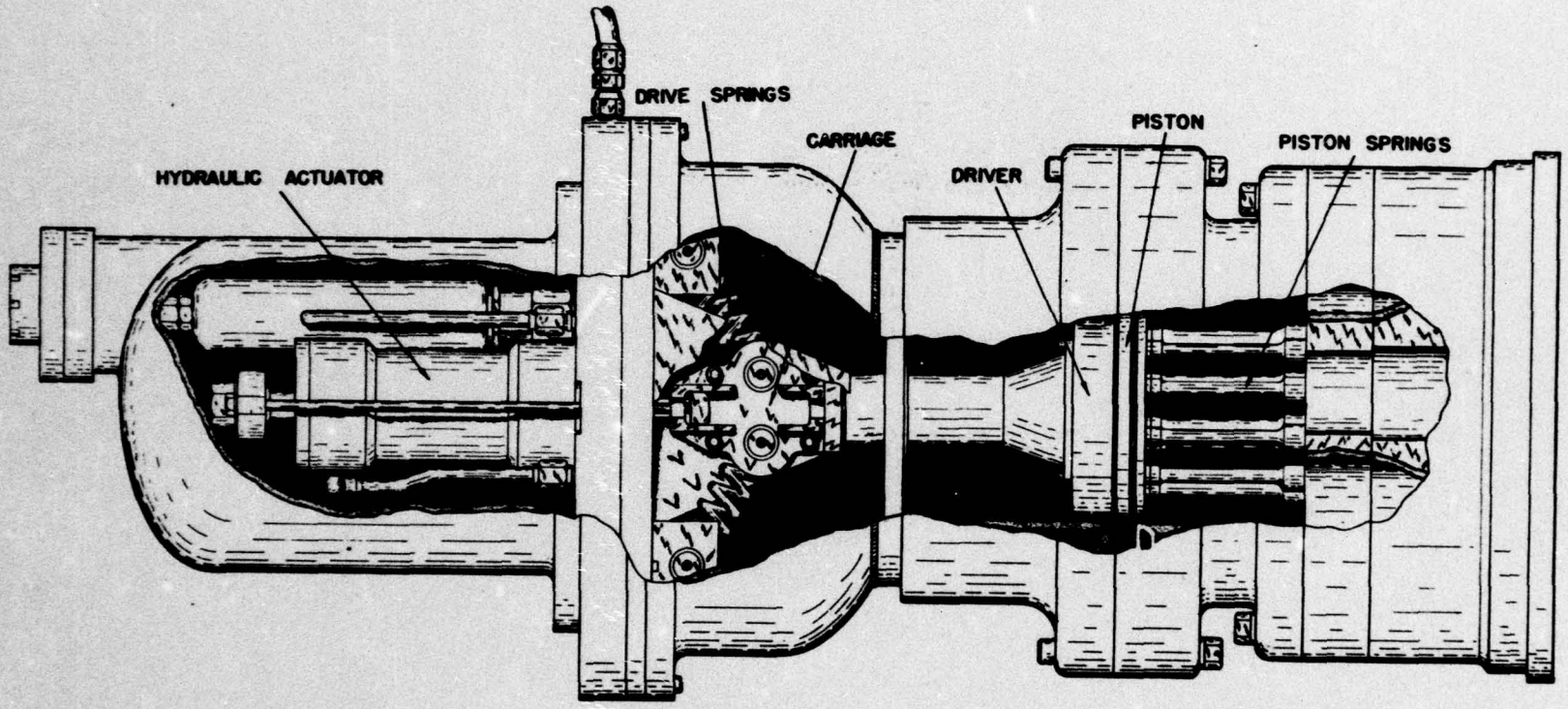

(Figure 2 of "Acoustic Transients and Impact-Energized Sound Source Research: Final Report" by A. E. Sharp, WHOI, ref. no. 64-23, June 1964.)

Figure 3-2. Cutaway Drawing of IMP

and converted into acoustic energy by the impact of a rapidly moving slug with the stationary, radiating piston. Upon impact, an extremely high pressure shock-wave is radiated into the water with no subsequent bubble pulsations.

The rear chamber of the IMP contains the slug, helical springs, and the hydraulic cylinder and accumulator which, together with a remote power and control unit, are required to draw back ("load") the springs and to release ("fire") them. The power and control unit (or hydraulic generator) is shown in figure 3-3 and consists of a motor-driven pump, a control valve, and a hydraulic fluid reservoir. One end of the cylinder is connected to a hose leading to the control valve and the other end is connected through another hose to the accumulator, which is filled with compressed air.

To load the helical springs, the control valve is set so that oil may be pumped through the hose to the cylinder at a pressure of 1200 psi, drawing the springs back until they pass a neutral position. When "loaded", the springs are in a locked position in much the same manner as a toggle latch. To "fire", the springs must be pushed past the neutral position. The second oil hose is used to transmit pressure from the accumulator to the rear of the piston-rod in the cylinder. This forces the slug past the neutral position since the piston-rod is connected to the slug through suitable linkage. The linkage is arranged so that the helical springs, piston-rod, etc., are disengaged from the slug just prior to impact. Thus, the pressure impulse is due only to the momentum of the slug. The area between the helical springs and the impact side of the piston is evacuated to a pressure of a 100 microns or less to prevent air from cushioning the impact. An air cushion between the slug and piston causes the impact to be applied more slowly, which results in a reduced peak pressure and the elimination of high-frequency components.

The slug and piston are circular steel plates with a diameter of 5.5 inches, and a thickness of approximately 1.5 and 1.35 inches, respectively. The velocity of the slug is approximately 22 feet per second. The piston is supported in its position by a spring system consisting of 15 hollow tension-compression springs. The springs prevent bending or vibration

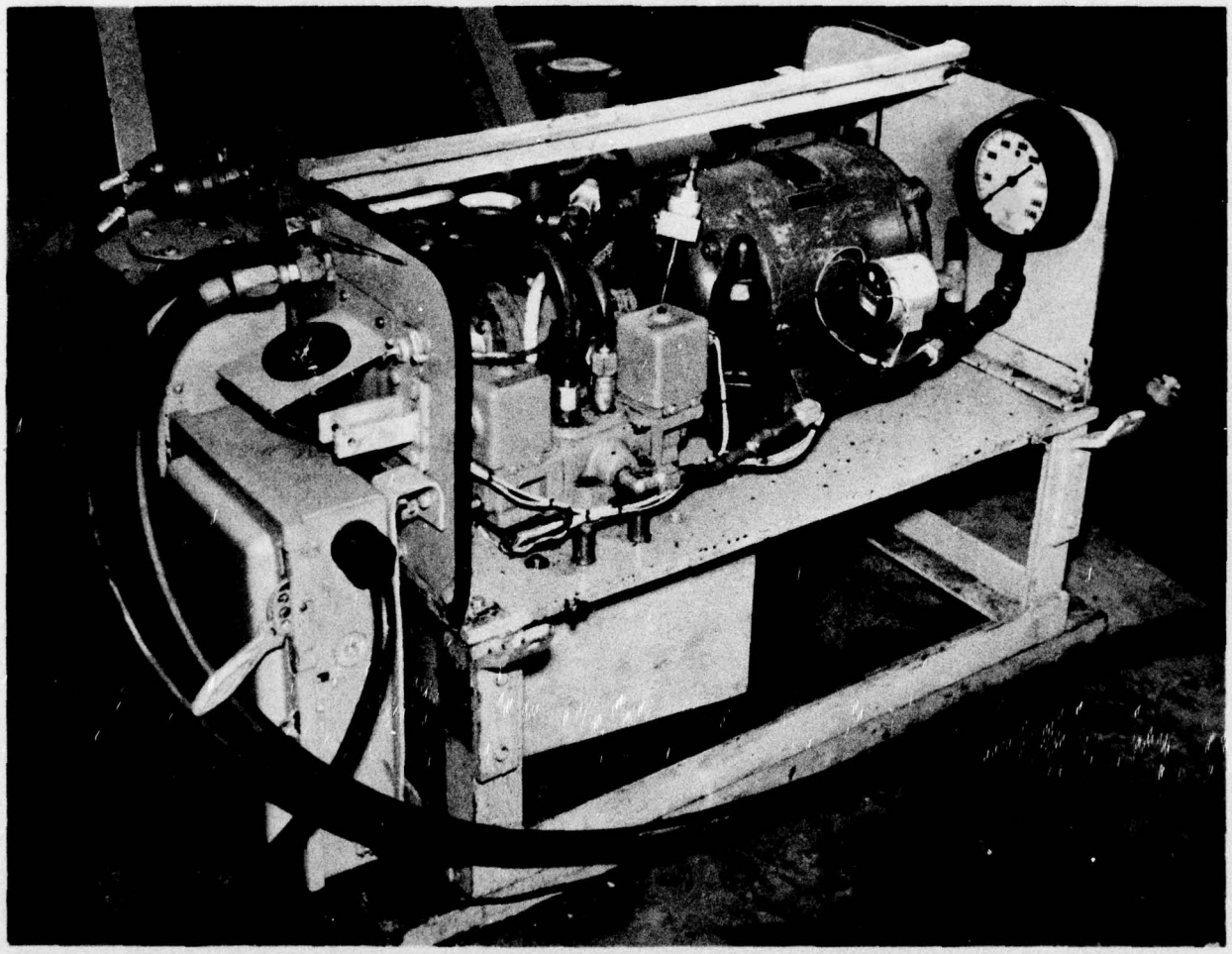

Figure 3-3. Power and Control Unit (Hydraulic Generator)

of the piston and are necessary for producing a plane shock-fronted pulse. The outer end of the sound source is a stainless steel cover plate or "acoustic window" which is 10 inches away and parallel to the radiating piston. The space between the window and the piston is filled with castor oil, which acts to couple the acoustic pulse to the medium.

The pressure at the piston-fluid interface will depend upon the acoustic impedance of the piston, spring system, and fluid. In the IMP, the resultant system was designed as a rapidly damped oscillator with a natural frequency of 3 kc.

Since the velocity of sound in steel is much faster than that in castor oil, a result of the 10-inch separation between the radiating piston and acoustic window is that the acoustic energy traveling through the springs and connecting steel paths reaches the acoustic window about 100-120 microseconds before the main shock wave traveling through the castor oil. This is designated a "precursor," and has been confirmed experimentally.

WIDEBAND RECEIVING PROBES

The relative position of the IMP and the receiving probe are shown in figure 3-4. The sensor is made of lead zirconate titanate and is one of two types - either an LC-10 wideband probe or a modified LC-10 (designated LC-10M-1), obtained from the Atlantic Research Corporation. The sensing elements for both probe models are approximately 1/4-inch in diameter, which gives a transit or integration time of about 4 microseconds. This is the time interval required for the probe to reach full value.

The specific probes used were the:

- ★ LC-10M-1 with a 50-foot cable
- ★ LC-10 with a 52-foot cable (LC-10A)
- ★ LC-10 with a 175-foot cable (LC-10B)

A comparative measure of their fidelity in reproducing a wideband signal was obtained by examining their responses to the IMP pressure waveform at a range of 1 foot on-axis, shown in figure 3-5. The characteristics of these waveforms are listed below.

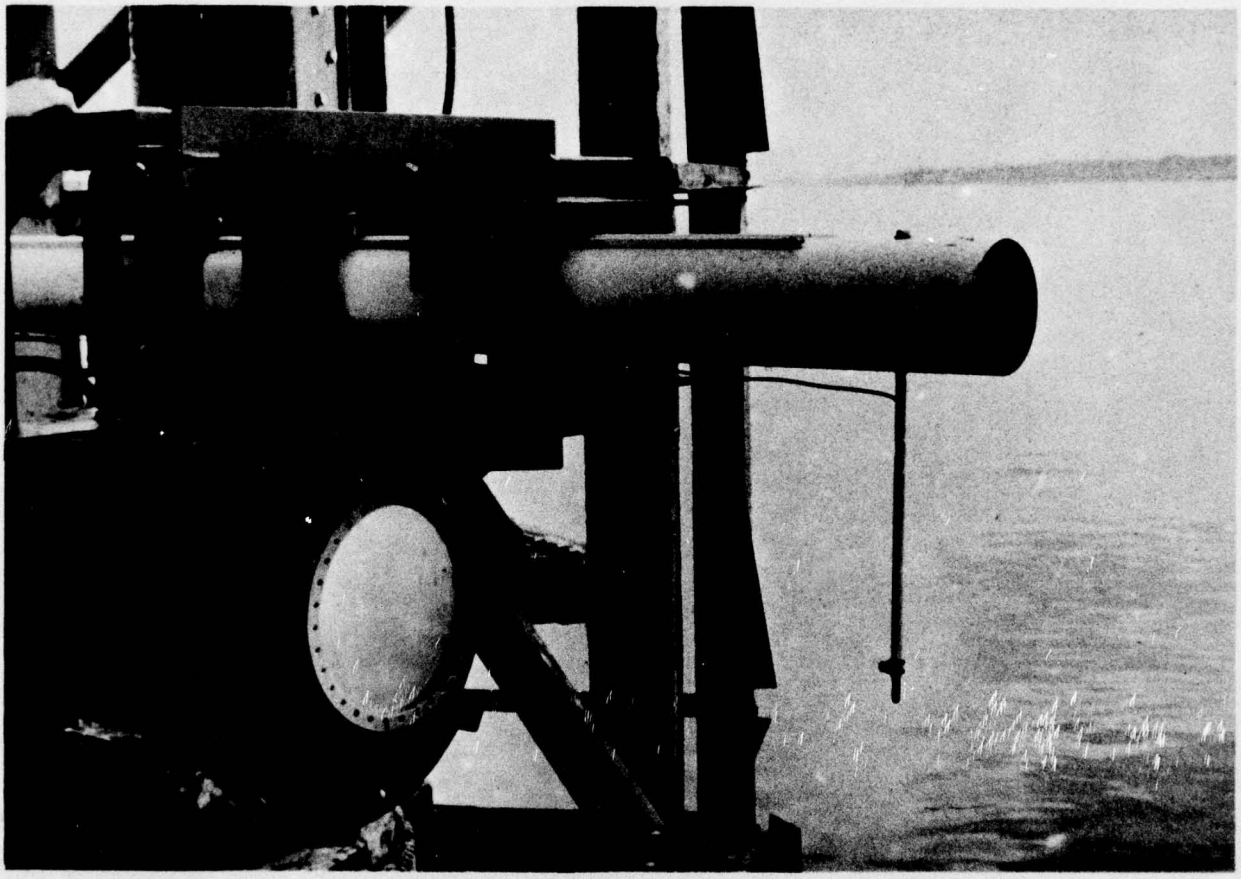

Figure 3-4. Relative Position of IMP MOD X-1 and Receiving Probe.

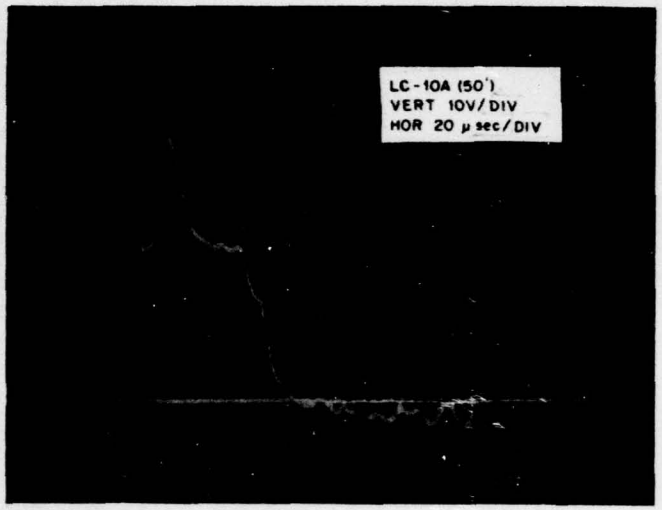

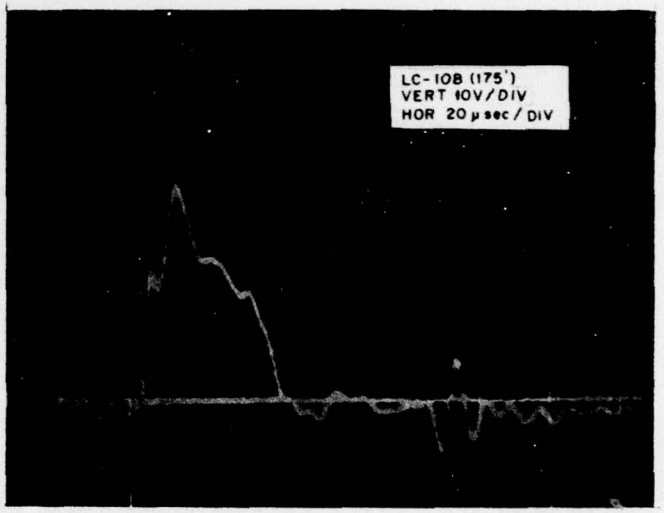

Figure 3-5. Pressure Waveform at a Range of One (1) Foot, On-Axis, with Various Wide-band Probes.

PROBE	PEAK LEVEL (db)	PULSEWIDTH (microseconds)	RISE TIME (microseconds)
LC-10M-1	25.7	40	10
LC-10A	31.4	44	10
LC-10B	29.8	40	10

The waveforms were recorded at Edo at a depth of 10 feet.

The LC-10M-1 and LC-10A were calibrated at the Underwater Sound Reference Laboratory in Orlando, Florida. The receiving response (open-circuit voltage) of the LC-10A is shown in figure 3-6. The response is rather flat at -110 db re 1 microbar from 100 cps to 5 kc, slowly decreases to -112 db re 1 microbar at 7 kc and remains at this level, ± 2 db, to 150 kc. The LC-10M-1 does not have the usual mounting sleeve and is slightly smaller, more omnidirectional, and has less sensitivity than the LC-10A. Its response, shown in figure 3-7, is relatively flat at -114 db re 1 microbar from 100 cps to 20 kc, slowly decreases to -118 db re 1 microbar at 55 kc, and increases to -115 db re 1 microbar at 110 kc.

Spectral analysis of the IMP pressure waveforms on-axis indicated that 85 percent of the energy was concentrated below 35 kc. Therefore, the receiving response for determining the absolute peak pressure level incident on the probe was taken as -112 db re 1 microbar for the LC-10A and -114 db re 1 microbar for the LC-10M-1. The increased shunt capacitance of the 175-foot cable, compared with that of the 52-foot cable, was computed to result in a voltage reduction of 3 db. The receiving response of the LC-10B was then taken as -115 db re 1 microbar.

CONTROL CABINET

Figure 3-8 shows the Control Cabinet used for remote electrical operation, hydraulic pressure monitoring and recording data. Remote electrical operation was accomplished by replacing the manually operated control valve with a solenoid-activated valve. The hydraulic pressure was monitored by the insertion of an electrial transducer in the oil line with a meter read-out on the Control Cabinet panel. The repetition rate with the present instru-

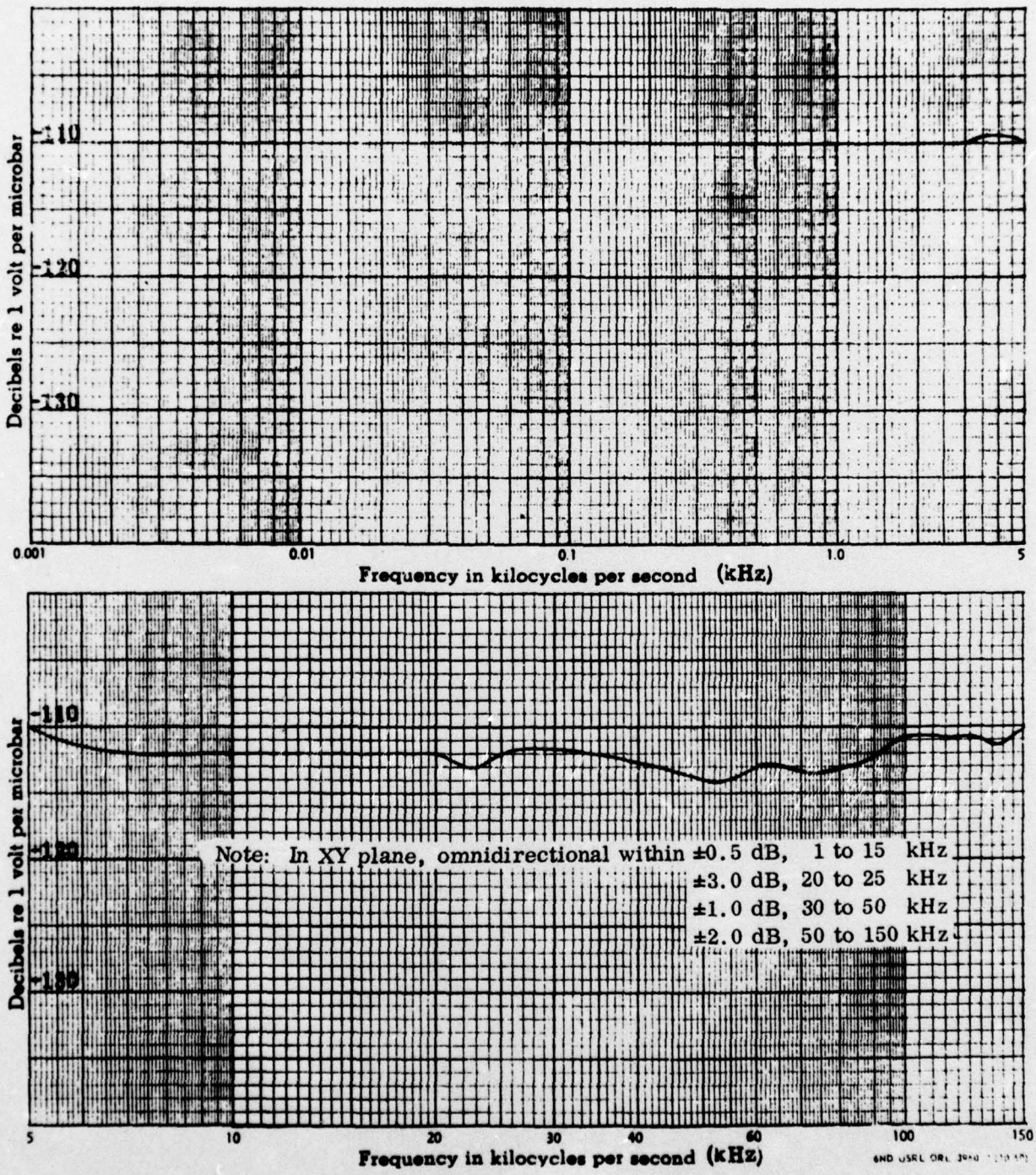

Figure 3-6. Calibration of LC-10A (52-ft cable)

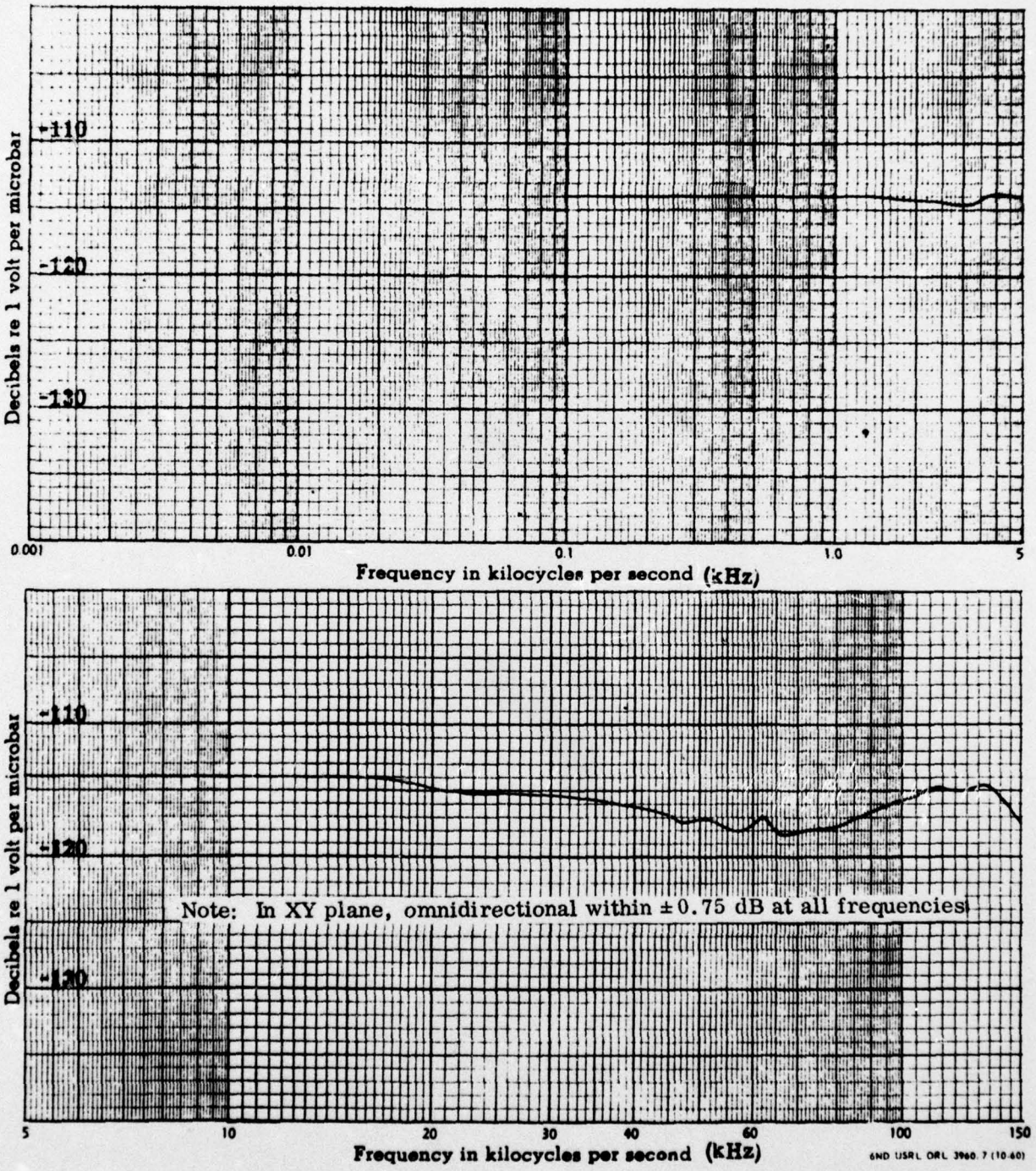

Figure 3-7. Calibration of LC-10 M-1 (50-ft cable)

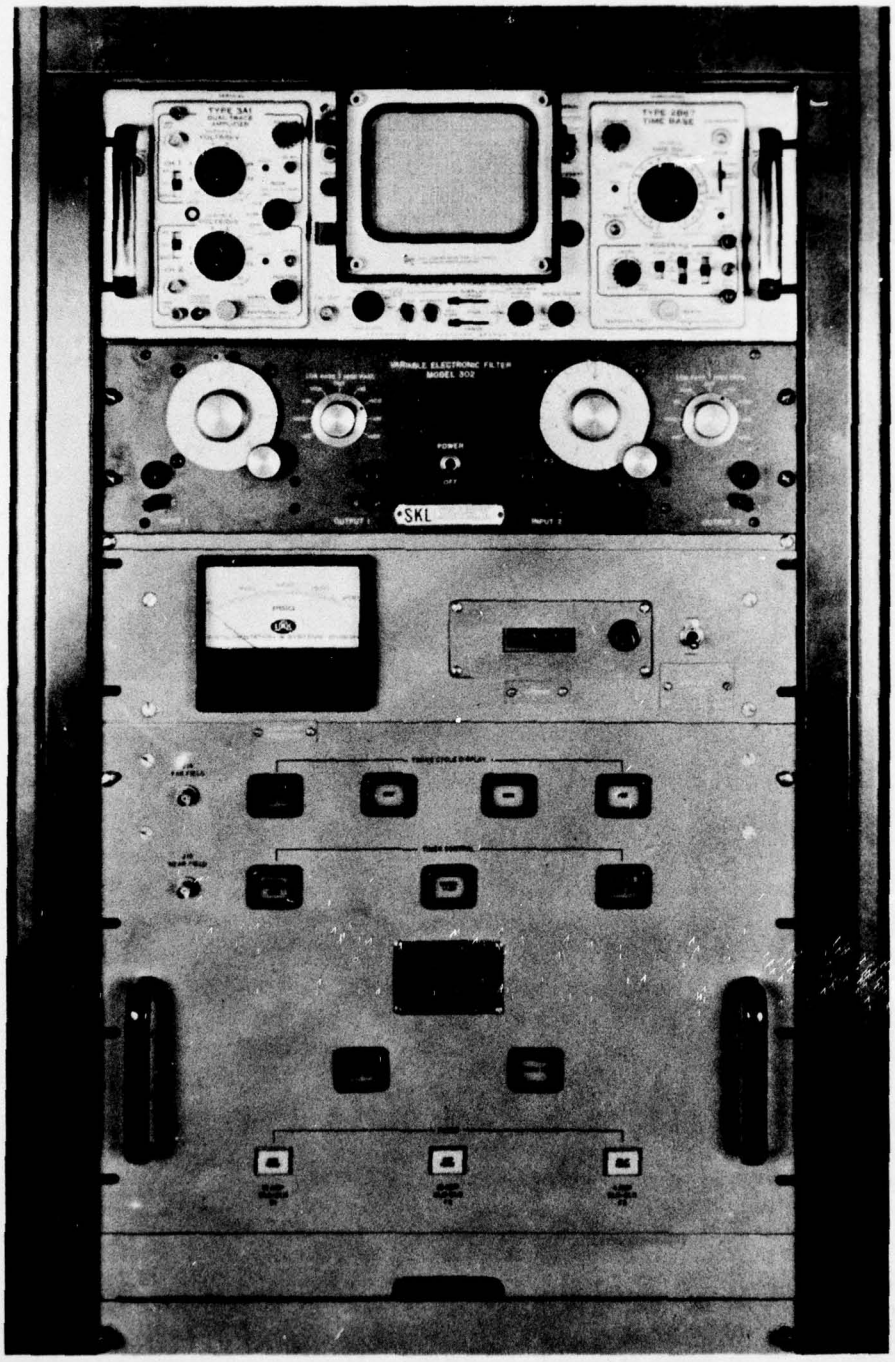

Figure 3-8. Control Cabinet

mentation was 1 cycle every 10 seconds, using hose lengths of 100 feet. However, with shorter hose lengths, the repetition rate could be reduced to 1 cycle every 3 seconds. Variations of these repetition rates were within ± 10 milliseconds.

All data taken was in the form of oscillographs obtained with a 564 Tektronix dual trace storage oscilloscope having a DC to 10 MC passband, and a Tektronix C-27 trace-recording camera with a f/1.4, 1:1 lens which preserved the resolution of the scope on film. A counter was used for recording the number of firings as a measure of the generator's mechanical reproducibility. Although more than 6000 firings had been made, there were no significant changes in the waveshape, peak pressure, or pulsewidth due to mechanical wear. (An SKL active filter, which can produce an arbitrary bandpass within the total frequency range of 20 cps to 200 kc, is indicated in figure 3-8. However, it was not employed in tests described in this report.)

RECEIVING PLATFORMS

In tests at Edo and NUOS, a boom, shown in figure 3-4, was used to locate the receiving probe accurately and to fix it at distances of 1 foot to 5 yards on-axis from the acoustic window of the IMP. The boom, having an outer diameter of 6 inches, was a free flooding cylindrical shell made of 1/8-inch thick aluminum. To permit the investigation of the directive properties of the transient, the boom could be rotated about an axis lying in the plane of the acoustic window. The cross-section was designed to be equal to or less than 1/15 of a wavelength of the significant frequencies contained in the transient signal. Acoustic theory and tests of sonar dome structures show that measurements will be unaffected by the supporting structure. The longitudinal axis of the boom is parallel to and 18 inches from the acoustic axis of the IMP. In addition to considering reflections, the boom was designed for azimuthal and vertical deflections of 1/2-inch at the cantilever end. This assumed a current of 1.5 knots and a 1/2-pound load, representing the weight of the probe. However, the current strengths observed during tests were less than 1 knot and the probe weighed only three ounces, so that the actual deflections were appreciably less than that designed for.

A pictorial diagram of the test setup at NUOS for ranges greater than 5 yards is illustrated in figure 3-9.

The properties of the generated transient were determined at a given range by placing the tower-tripod, shown in figure 3-10, at the desired location. The platform supported the receiving instrumentation and consisted of a telescoped pair of 20-foot aluminum tubes which permitted the vertical height to be adjusted from 20 to 40 feet so that the probe mounted at the top of the tower could be aligned with the acoustic axis of the IMP. The tower-tripod was designed to deflect a maximum of 3.5 inches when fully extended with a current of 1.5 knots. The deflection was smaller, since the current did not exceed 1 knot. Thus, the errors introduced in the measurements by standing waves due to reflections, and by non-alignment due to deflections of the receiving platforms (boom and tower-tripod) were quite negligible.

At ranges of 30 yards and greater, amplification of the electrical pressure waveform was required to balance the loss due to spreading in transmission in order to have sufficient voltage to drive the cable and oscilloscope. The output of the receiving probe was sent to a transistorized amplifier which was direct-coupled to a 3000-foot RG-58 A/U coaxial cable connected to the control cabinet on shore. The amplifier was obtained from Ithaco, Inc. and had an adjustable gain from 10 db to 80 db in 1.0-db steps. Its amplitude-frequency response is shown in figure 3-11 and although the bandwidth was rated from 0.5 cps to 100 kc, its upper 3-db frequency was measured to be approximately 200 kc. What is also desirable is its gradual fall-off response up to about 500 kc. In general, the shape of the fall-off characteristic is of greater importance in the faithful reproduction of transients than that of the portion during which the amplitude remains flat. The power for the amplifier was supplied by a Burgess sealed nickel cadmium battery with a 24 v, 4.0 amp-hr. capacity. The amplifier and battery were packaged in a watertight cannister and fastened to a leg of the tripod.

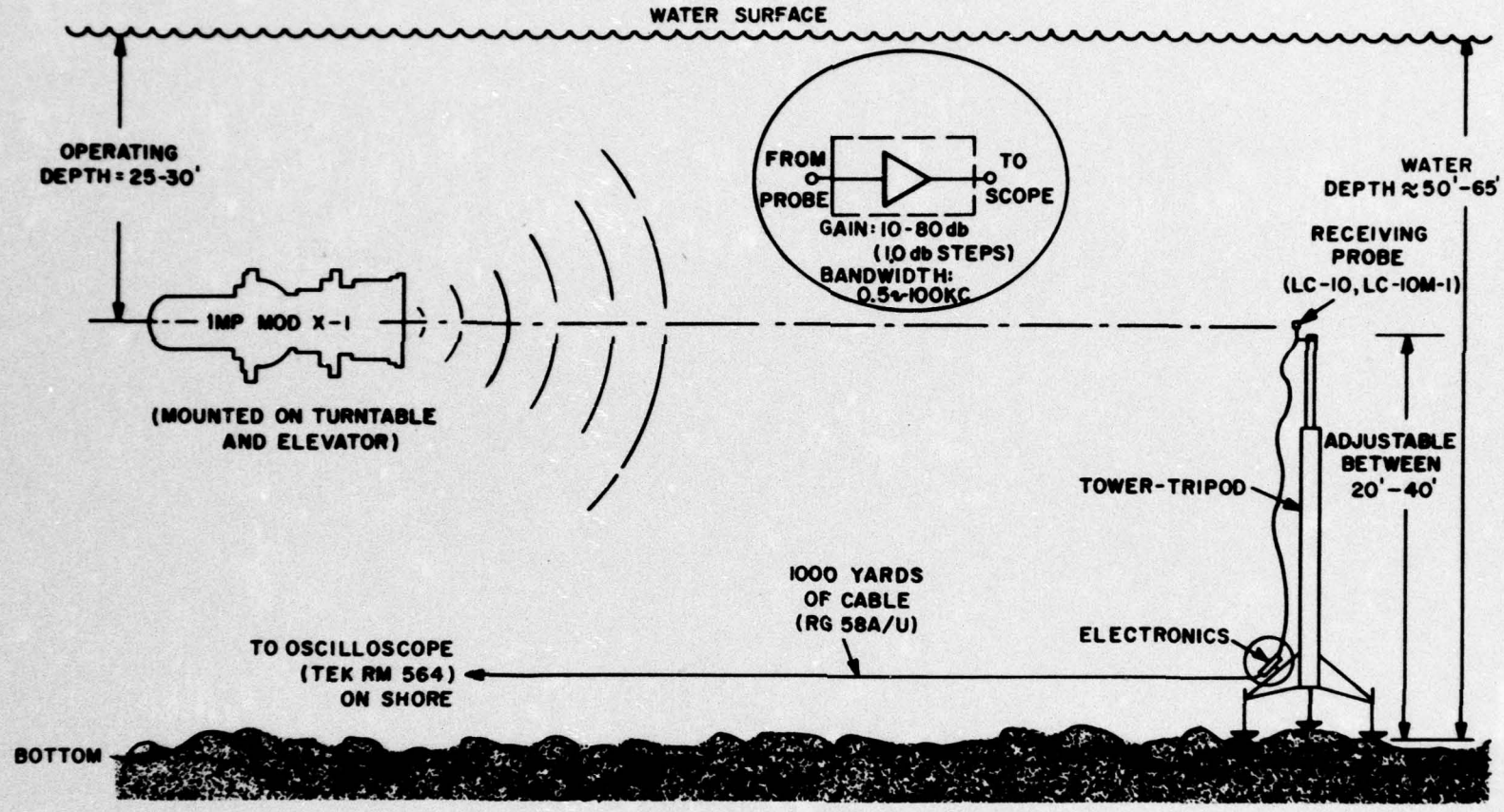

Figure 3-9. Pictorial Diagram of Test Set-up at NUOS

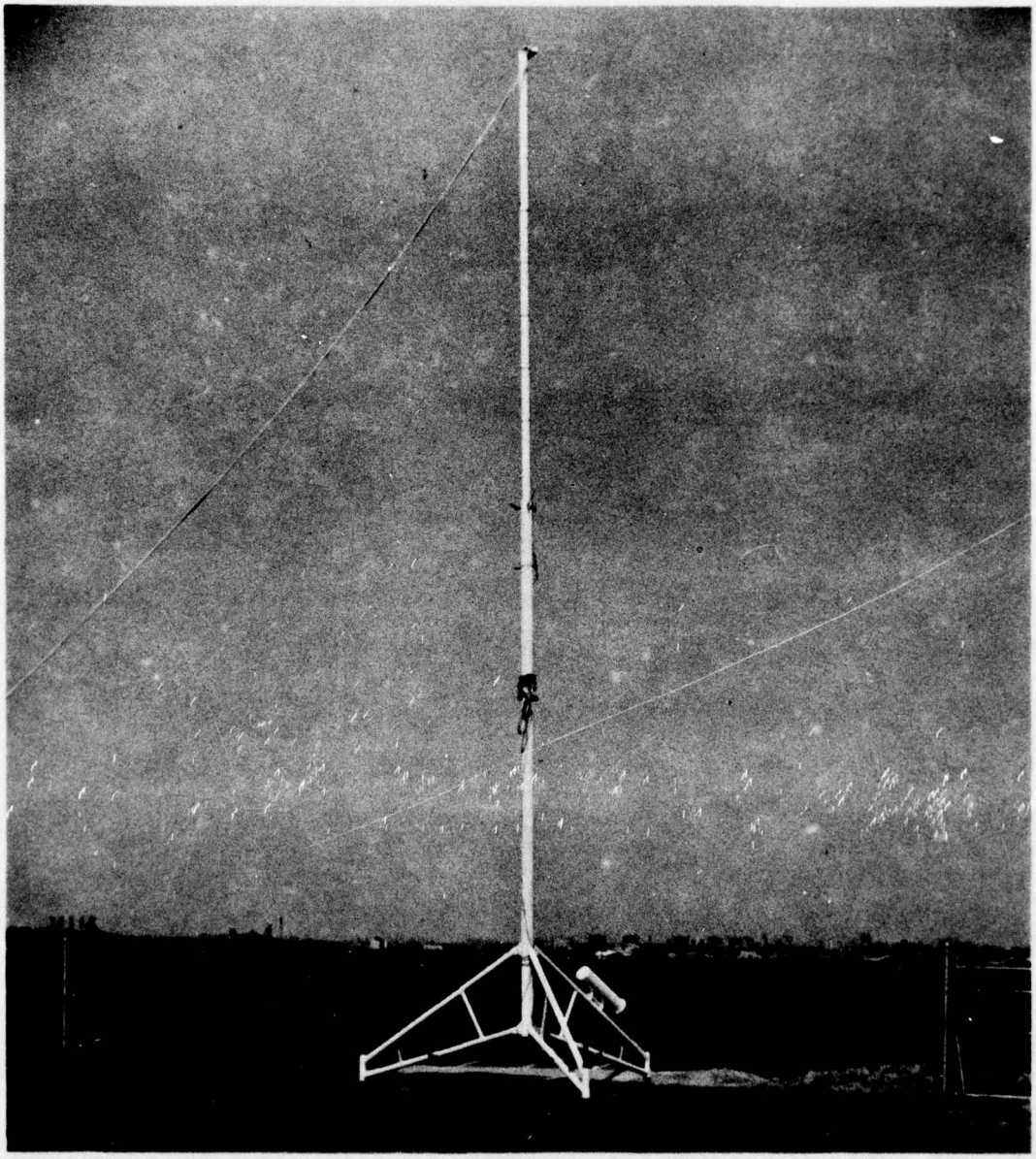

Figure 3-10. Tower-Tripod

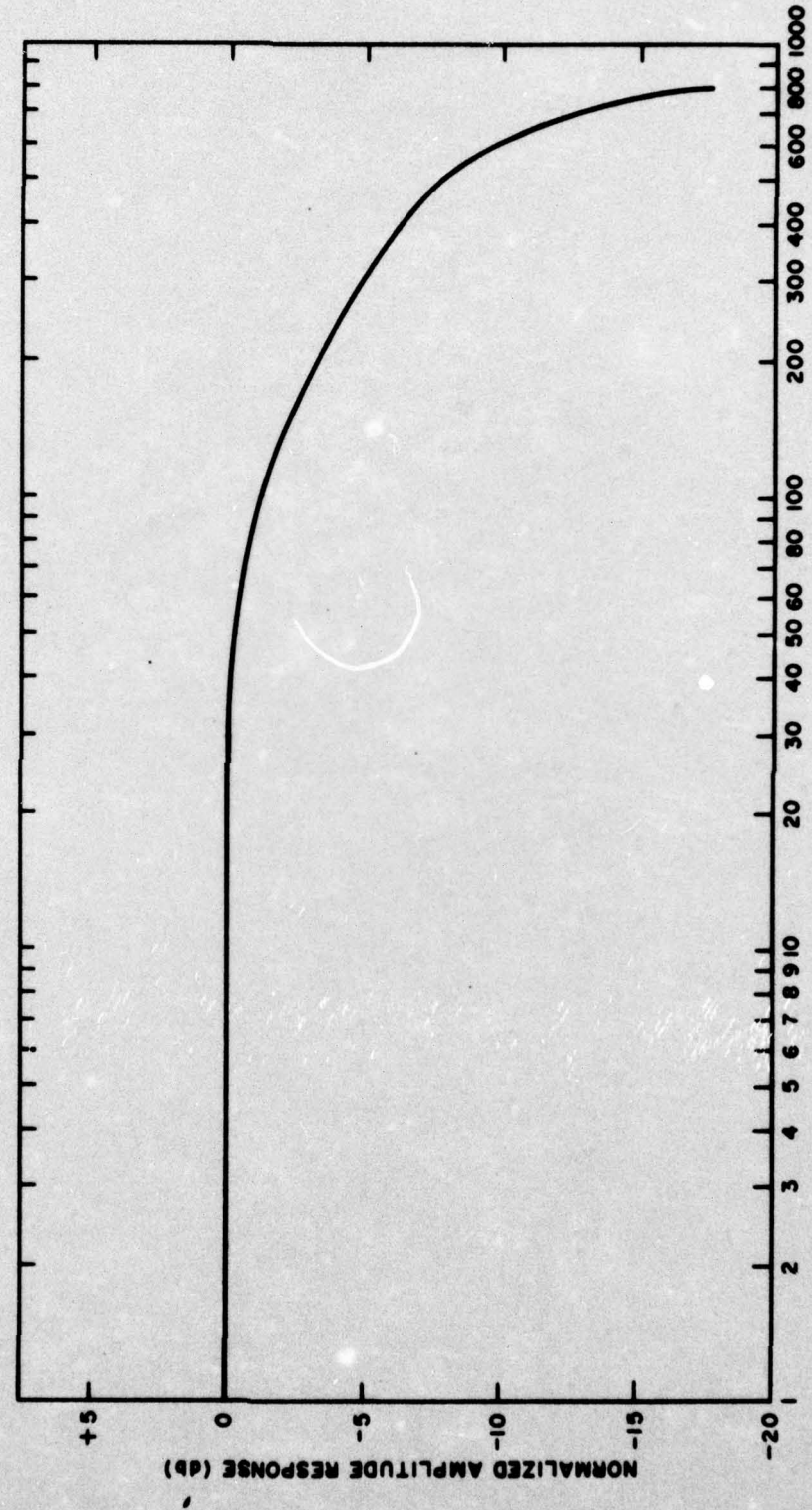

Figure 3-11. Amplitude-frequency Response of Driver Amplifier

The coaxial cable had a characteristic impedance of 50 ohms and was matched at both ends to eliminate electrical reflections; the D-C-coupled output resistance of the amplifier was 50 ohms and a 47-ohm resistive load was placed across the input terminals of the oscilloscope. There was the usual 6.0-db loss at the input to the cable due to impedance matching. For a rapidly changing signal, the time required for the signal to travel the length of the cable cannot be assumed negligible. For a total distributed capacitance C (in microfarads) and a characteristic impedance R_o (in ohms), the transit time (in microseconds) = $R_o C$. Therefore, for a 3,000 foot RG-58 A/U cable with a capacitance of 30 $\mu\mu$f per foot and a 50-ohm characteristic impedance, the transit time of the cable was 4.5 microseconds. The cable can be considered as a simple lumped circuit for signals which change insignificantly over such time intervals, i.e., for signal frequencies much less than 222 kc. This is quite sufficient for receiving the pressure waveforms of the IMP.

TEST FACILITIES

The test facility employed at Edo is indicated by an arrow in figure 3-12. Tests were conducted during the months of February and March 1965, in water approximately 21 feet deep (high tide). Directivity measurements were performed at ranges of 1 foot to 4 yards with the IMP at a depth of 10 feet and the receiving probe (LC-10M-1) mounted in the boom and connected directly to the control cabinet.

The test facility at NUOS comprised Gould Island and the associated torpedo range, as shown (arrow) in figure 3-13. The tests extended from May through July 1965, and included ranges from 1 foot to 750 yards. The IMP and boom were mounted on the integrated turntable-elevator assembly shown in figure 3-14. The turntable and elevator were normally employed in the launching of torpedoes and could be lowered to a maximum depth of 30 feet and rotated through a 90-degree sector. The depth of water was from 50 to 65 feet (water depths are indicated on the map in figure 3-13). As a result of these depths, surface and bottom reflections made the data unobtainable at ranges greater than 750 yards on-axis and at ranges greater than 250 yards off-axis.

Figure 3-12. Location of Edo Test Facility

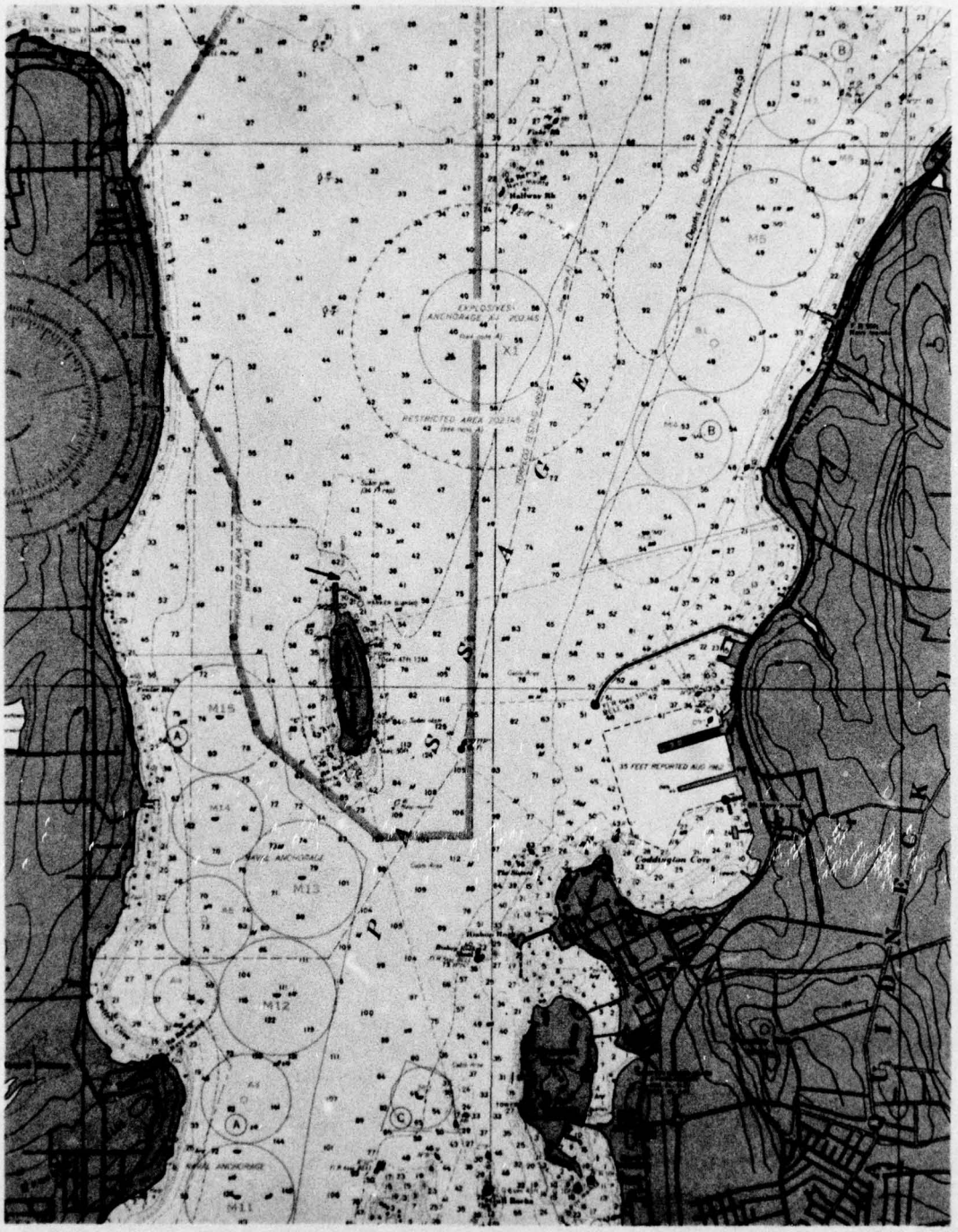

Figure 3-13. Location of NUOS Test Facility

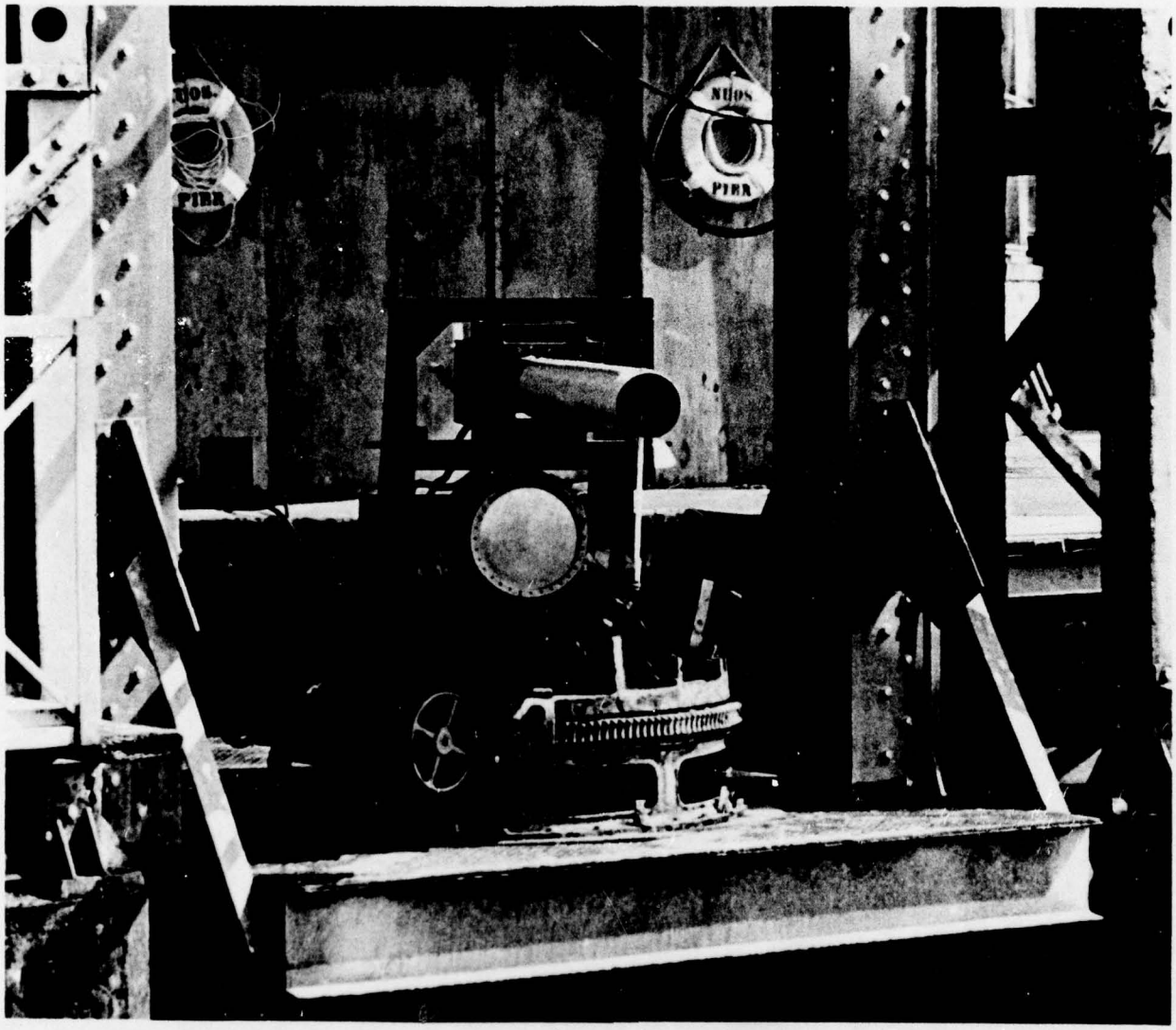

Figure 3-14. IMP MOD X-1 and Boom Mounted on Turntable - Elevator Assembly at NUOS

DATA ANALYSIS

An IBM 1620 computer was employed in the analysis of the data. Various signal representations were programmed such as:

- ★ Autocorrelation Function
- ★ Crosscorrelation Function
- ★ Smoothed and Unsmoothed Power Spectra
- ★ Fourier Amplitude - Phase Spectra
- ★ RMS Frequency Duration
- ★ RMS Time Duration
- ★ Effective C-W Pressure Pattern
- ★ Effective C-W Power Pattern

The data was sampled by hand, which generally introduces high frequencies into the analysis. This and the errors due to truncation and aliasing are extensively discussed in the following section.

SECTION 4

DATA ANALYSIS AND TEST RESULTS

This section discusses in detail the analytical and empirical basis for the results of the transient program summarized in section 2. The acoustic data recorded and analyzed will be presented according to the following areas:

- ★ Part 4-A: Data Analysis Program
- ★ Part 4-B: Waveform
- ★ Part 4-C: Energy Spectra
- ★ Part 4-D: Directivity
- ★ Part 4-E: Orthogonal Exponential Decomposition

Part 4-A

Data Analysis Program

To perform the data analysis, oscillographs of the IMP waveforms having a time scale of 20 microseconds per centimeter were sampled and digitized manually at 4 microsecond intervals. The set of discrete data, a minimum of 30 samples, was then processed digitally to obtain the desired representations. These consisted of autocorrelations, amplitude-phase and energy spectra, rms time and frequency durations, effective C-W pressure patterns, peak and iso-time patterns, and orthogonal exponential decompositions. The formulation employed for the analysis techniques will be reviewed.

CORRELATION ANALYSIS

The autocorrelations of the IMP signals were obtained by computing the mean-lagged products.

$$R_{xx}(j) = \Delta t \sum_{i=j}^{N} x_i \, x_{i-j} \quad \text{for } j \geq 0 \tag{4A-1}$$

where x_i = Sampled value of signal x (t) within the interval

$$o \leq t_i = i \Delta t \leq N \Delta t$$

$N + 1$ = Number of data points

Δt = Time interval between data points

$|j|$ = Delay increment = 0, 1, 2, ... $M \leq N$

i = Sample instant = 0, 1, 2, ... N

M = Maximum correlation lag

This equation is valid only for signals having finite energy such as transients. The value of the autocorrelation function for $j = o$, $R_{xx}(o)$, is the total signal energy. The autocorrelation function also has the properties of $|R_{xx}(j)| \leq R_{xx}(o)$ and $R_{xx}(j) = R_{xx}(-j)$.

ENERGY SPECTRUM

The estimates of the energy spectrums (reference 6) were computed by performing a discrete finite Fourier transformation on the empirical correlation functions given in equation 4A-1. The one-sided spectral estimate $P_{xx}(\omega)$ was expressed as

$$P_{xx}(m\,\Delta f) = 2\,\Delta t\ \left[R_{xx}(o) + 2\sum_{j=1}^{M} R_{xx}(j)\cos(2\pi\, m\,\Delta f\, j\,\Delta t)\right] \qquad (4A\text{-}2)$$

where Δf = Resolution of spectral estimate = $1/2\,M\,\Delta t$ (cps)

m = Frequency index

To improve the spectral estimate, the index (m) was given non-integral values. The value of the spectrum at each frequency (f) is a weighted average of the spectrum in the band $f \pm 1/2M\,\Delta t$.

CUMULATIVE ENERGY SPECTRA

The cumulative energy spectra C(f) represents the amount of signal energy present below the specified frequency (f). The normalized spectra in percent is

$$C(m\Delta f) = \frac{\Delta f \sum_{m=o}^{M} P_{xx}(m\,\Delta f)}{R_{xx}(o)} \times 100\% \qquad (4A\text{-}3)$$

The frequency summation was determined by employing the trapezoidal rule for integration.

RMS TIME AND FREQUENCY DURATIONS

The rms time duration (D_t) of the signal x (t) was calculated as the second moment of $\left|x(t)\right|^2$ with respect to the origin. This is defined as (reference 7),

$$D_t^2 = \frac{(\Delta t)\sum_{i=o}^{N} (i\,\Delta t)^2 \left|x\ (i\,\Delta t)\right|^2}{R_{xx}(o)} \qquad (4A\text{-}4)$$

If $X(\omega) = A(\omega)e^{j\phi(\omega)}$ is the Fourier transform of x(t), then the rms frequency duration (D_ω) of $X(\omega)$ is given by

$$D_\omega^2 = \frac{(2\pi\Delta f)\sum_{m=0}^{M}(2\pi m\Delta f)^2 A^2 (2\pi m\Delta f)}{R_{xx}(o)} \qquad (4A-5)$$

where $$X(2\pi m\Delta f) = \Delta t \sum x(i\Delta t)\, e^{-j2\pi m\Delta f i\Delta t} \qquad (4A-6)$$

If x(t) decreases at infinity faster than $1/\sqrt{t}$, then the uncertainty principle states that the rms bandwidth-time product must satisfy the inequality

$$D_\omega D_t \geq \sqrt{\frac{\pi}{2}} \qquad (4A-7)$$

The equality is obtained when the signals are of Gaussian form. The time duration D_t may also be expressed as

$$D_t^2 = \frac{1}{2\pi}\int_{-\infty}^{\infty}\left[\left(\frac{dA}{d\omega}\right)^2 + A^2\left(\frac{d\phi}{d\omega}\right)^2\right]d\omega \qquad (4A-8)$$

Equation 4A-8 indicates that a high ripple in the amplitude or phase spectrum of $X(\omega)$ results in signals of long duration.

EFFECTIVE C-W PRESSURE PATTERN

The radiation pattern produced by a signal characterized by a finite spectral width is generally broader and has a higher sidelobe radiation (with a smoothing of the lobe structure) than the single-frequency pattern (reference 8). If

$X(\omega) \equiv A(\omega)e^{j\phi(\omega)}$ = The Fourier transform of the signal x(t)

and

$g(\theta, \omega) \equiv$ The radiation pattern for a C-W sine wave of frequency (ω)

then the effective C-W pressure pattern (normalized) for the signal x(t) is defined as

$$\left|G(\theta_i)\right| = \left| \frac{\sum_q g(\theta_i, \omega q)\, A(\omega q)\, e^{j\phi(\omega q)}}{\sum_q A(\omega q)\, e^{j\phi(\omega q)}} \right| \qquad (4A\text{-}9)$$

where $\omega q = 2\pi q \Delta f = \frac{\pi q}{M \Delta t}$ (radians/second)

θ_i = The angle between the normal to the plane of the transducer and the bearing of the direction vector $\vec{i}$. A broadband pattern is most sensitive to the signal phase characteristic $\phi(\omega)$.

In computing the effective C-W pressure pattern, the IMP Mod X-1 was considered a rigid circular piston whose steady-state pattern $g(\theta, \omega)$ is given by (reference 9),

$$g(\theta_i, \omega_q) = \frac{2 J_1(\psi_{iq})}{\psi_{iq}} \qquad (4A\text{-}10)$$

where $J_1(\psi_{iq})$ = Bessel function of the first order and first kind

$\psi_{iq} = \frac{\pi q \Delta f D}{v} \sin\theta_i$

D = Diameter of piston (feet)

v = Velocity of sound (feet/sec)

This pattern has a first minor lobe whose maximum value is 0.132 (-17.8 db) of the major lobe level. In the calculations, the diameter was taken to be 1 foot.

ORTHOGONAL EXPONENTIAL DECOMPOSITION

The class of one sided decaying exponentials

$$\phi_i(t) = \begin{cases} 0 & t < t_o \\ \varepsilon^{s_i (t - t_o)} & t \geq t_o \quad \mathrm{Re}(s_i) < 0 \end{cases} \qquad (4A\text{-}11)$$

has been shown to be an appropriate basis for the approximate representation of a wide variety of pulse-like signals (reference 10). In terms of the ϕ_i, an observed signal f is represented by an approximating signal f_a in the form of

$$f \approx f_a = \sum_1^N A_i \phi_i \qquad (4A\text{-}12)$$

In practice an exact representation ($f = f_a$) is never sought. Theoretically it is possible since there are infinitely many sequences of functions in equation 4A-11, which are complete in $L_2(t_o, \infty)$. Instead, a number N is chosen and the set of numbers $\left\{A_i\right\}_1^N$ and $\left\{s_i\right\}_1^N$ determined so that the error signal $e = (f - f_a)$ is, in some sense, acceptably small. The signal f may be considered approximately as the output of an impulsively excited linear, time-invariant, lumped parameter system, and since the signals ϕ_i are the eigen-signals of such systems, a representation in the form of equation 4A-12 should be possible with relatively small N, provided the exponents $\left\{s_i\right\}_1^N$ are chosen appropriately.

In representing the IMP signals, the mean-squared-error criterion was used for mathematical tractability and its intuitive content. For fixed N it was attempted to find the $\left\{A_i\right\}_1^N$ and $\left\{s_i\right\}_1^N$ to minimize the expression

$$\left\langle e^2 \right\rangle = \int [f(t) - f_a(t)]^2 \, dt \qquad (4A\text{-}13)$$

where the integral extends over the duration of the data. Formulating this least-squares problem in the Laplace transform domain leads to the equations of Aigrain and Williams (reference 11), which have the following geometrical interpretations. Let Φ be the signal space spanned by $\left\{\phi_i\right\}_1^N$ and Φ' the signal space orthogonal to Φ spanned by the derivatives of $\left\{\phi_i\right\}_1^N$ with respect to the $\left\{s_i\right\}_1^N$. Then the $\left\{s_i\right\}_1^N$ should be chosen so that the projection of f on Φ' is zero, while the $\left\{A_i\right\}_1^N$ are simultaneously chosen so that f_a, the projection of f on Φ, has maximum length. These relationships are shown in figure 4A-1. Since the Aigrain-Williams equations are simultaneous transcendental equations in 2N unknowns, no general solution exists. However, for fixed $\left\{s_i\right\}_1^N$, the coefficients $\left\{A_i\right\}_1^N$ are soluble in closed-form.

CLASS OF ONE-SIDED DECAYING EXPONENTIALS: $\phi_i(t) = \begin{cases} 0 & t < t_o \\ e^{s_i(t-t_o)} & t \geq t_o \quad R_e(s_i) > 0 \end{cases}$

Φ = SIGNAL SPACE SPANNED BY $\left\{\phi_i\right\}_1^N$

Φ' = SIGNAL SPACE ORTHOGONAL TO Φ SPANNED BY THE DERIVATIVES OF THE $\left\{\phi_i\right\}_1^N$ WITH RESPECT TO THE $\left\{s_i\right\}_1^N$

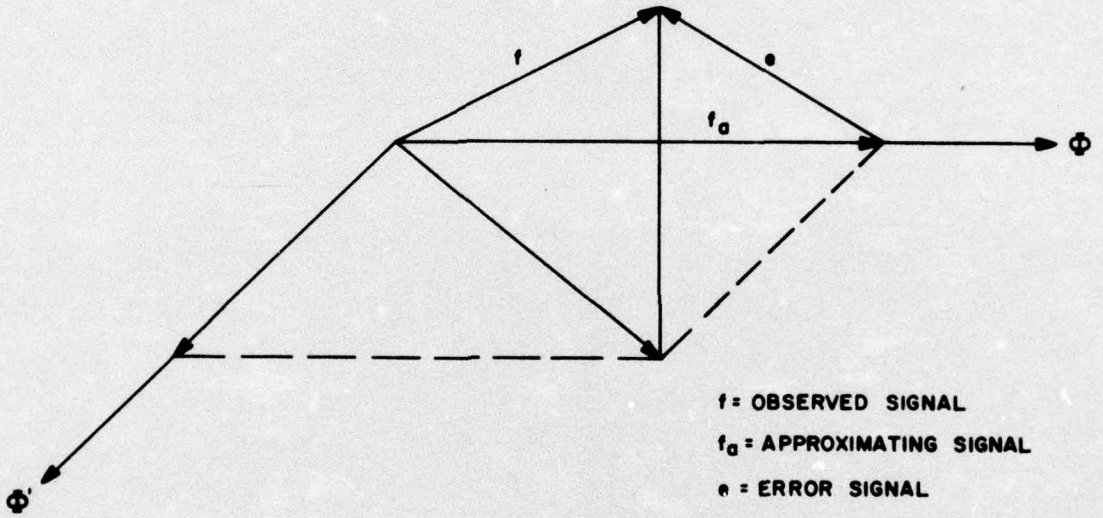

f = OBSERVED SIGNAL

f_a = APPROXIMATING SIGNAL

e = ERROR SIGNAL

Figure 4A-1. Geometrical Interpretation of Least-squares Problem in Signal Representation

The digital computer program used to analyze the IMP signals* was an iterative one. Given an intial guess for $\left\{s_i\right\}_1^N$ it computed the optimum $\left\{A_i\right\}_1^N$ and the projection of f on Φ'. It then adjusted the $\left\{s_i\right\}_1^N$ (thus rotating both Φ and Φ' with respect to f) so as to reduce the projection on Φ'.

ERRORS IN THE SPECTRAL ESTIMATE

The major sources of error in estimating the energy spectra of the IMP signals were those due to truncation, aliasing, manual digitization and high-frequency ripple in the probe response.

Consider an experimental record of finite length (T) which is less than the signal duration. This implies that the signal under analysis, $x_T(t)$, may be considered to be the product of the actual signal, x(t), and a "window" or rectangular pulse, $p_T(t)$,

$$x_T(t) = x(t)\ P_T(t) \qquad (4A\text{-}14)$$

where $P_T(t) = 1 \qquad 0 \leq t \leq T$

$= 0 \qquad$ elsewhere

Equation (4A-14) expresses the temporal truncation of a signal. The effect of this truncation may be readily seen from the frequency convolution theorem in Fourier analysis which states that the Fourier transform $X_T(\omega)$ of the product $x(t)\ p_T(t)$ of two functions equals the convolution $X(\omega) * P_T(\omega)$ of their respective transforms $X(\omega)$ and $P_T(\omega)$ divided by 2π

$$X_T(\omega) = \mathcal{F}\left\{x_T(t)\right\} = \frac{1}{2\pi}\int_{-\infty}^{\infty} X(\beta)\,P_T(\omega-\beta)\,d\beta \qquad (4A\text{-}15)$$

where

$$P_T(\omega) = \mathcal{F}\left\{p_T(t)\right\} = \frac{2\sin\ \omega\ T/2}{\omega}\ e^{-j\omega T/2} \quad . \qquad (4A\text{-}16)$$

*Routine developed by Lt. J. R. Sopko, a graduate student in the Electrical Engineering Department, The Johns Hopkins University.

Therefore, the amplitude-phase spectrum of $x_T(t)$ is expressed as

$$X_T(\omega) = \frac{e^{-j\,\omega\,T/2}}{\pi} \int_{-\infty}^{\infty} X(\beta)\, \frac{\sin\,(\omega - \beta)\,T/2}{\omega - \beta}\, e^{j\,\beta\,T/2}\, d\beta \qquad (4A\text{-}17)$$

Equation (4A-17) suggests that the maxima and minima of sin x/x may generate a similar but suppressed fluctuation in the spectrum $X_T(\omega)$. This effect would also be observed in the energy spectrum $P_T(\omega)$ of $x_T(t)$ since

$$P_T(\omega) = X_T(\omega)\; X_T^*(\omega) \qquad (4A\text{-}18)$$

The energy spectrum $P_{xx}(m\,\Delta\,f)$ defined by equation (4A-2) is actually the discrete estimate of $P_T(2\,\pi\,f)$. In the spectra of the IMP signals shown in figures 4C-1 through 4C-13, the fluctuations below 15 kc may be attributed primarily to truncation.

Digital computation involves performing many different kinds of operations on numbers. Data "numbers" are generally obtained by sampling the continuous time record at equally spaced values of time. If the sampling interval is Δt such that,

$$t = 0,\ \Delta t,\ 2\,\Delta t,\ \ldots,\ N\,\Delta t$$

then the highest frequency f_N considered in the spectral estimate is $f_N = \frac{1}{(2\,\Delta\,t)}$. The spectral estimate will then vanish for $f > f_N$, although the true spectrum may not, which is generally the case. Frequencies above f_N will contribute some energy to the band from 0 to f_N. In addition, each of these frequencies ($f > f_N$) will be indistinguishable from one in the band. This is called <u>aliasing</u> or <u>spectrum folding</u> and is a consequence of data taken or read at equal intervals. A sampling interval of 4 microseconds was used to analyze the data which gave a maximum spectrum frequency of 125 kc. The rapid fluctuations in the IMP spectra above 35 kc are believed to be due primarily to aliasing.

The rapid spectrum fluctuations above 35 kc may also have been enhanced by digitizing the data manually. A comparison of the log energy spectra of two earthquake records digitized electronically (CHP 13, CHP 14) and manually (CHP 13H, CHP 14H) are shown in

figure 4A-2 (reference 12). It appears that manual digitization tends to introduce high frequencies in the spectral analysis. In addition, as the high-frequency energy in a waveform increases, it becomes more difficult to digitize manually resulting in greater deviations in the spectral estimates.

The calibration curves of the LC-10A and LC-10M-1 test probes, shown in figures 3-6 and 3-7, indicate that the LC-10A has a higher amplitude-frequency ripple above 20 kc that the LC-10M-1. From the expression for the rms time duration D_t given by equation 4A-8, it is anticipated that D_t will be longer using the LC-10A (NUOS tests) than the LC-10M-1 (Edo tests). This was verified in the program where the average rms time duration was computed to be 40.8 microseconds at NUOS and 25.7 microseconds at Edo (see page 4C-19). The average rms frequency durations at both test sites were almost equal. Thus, the rate-of-change of the amplitude-frequency response of the probe will strongly influence the signal duration and the degree of fluctuations in the estimated spectra.

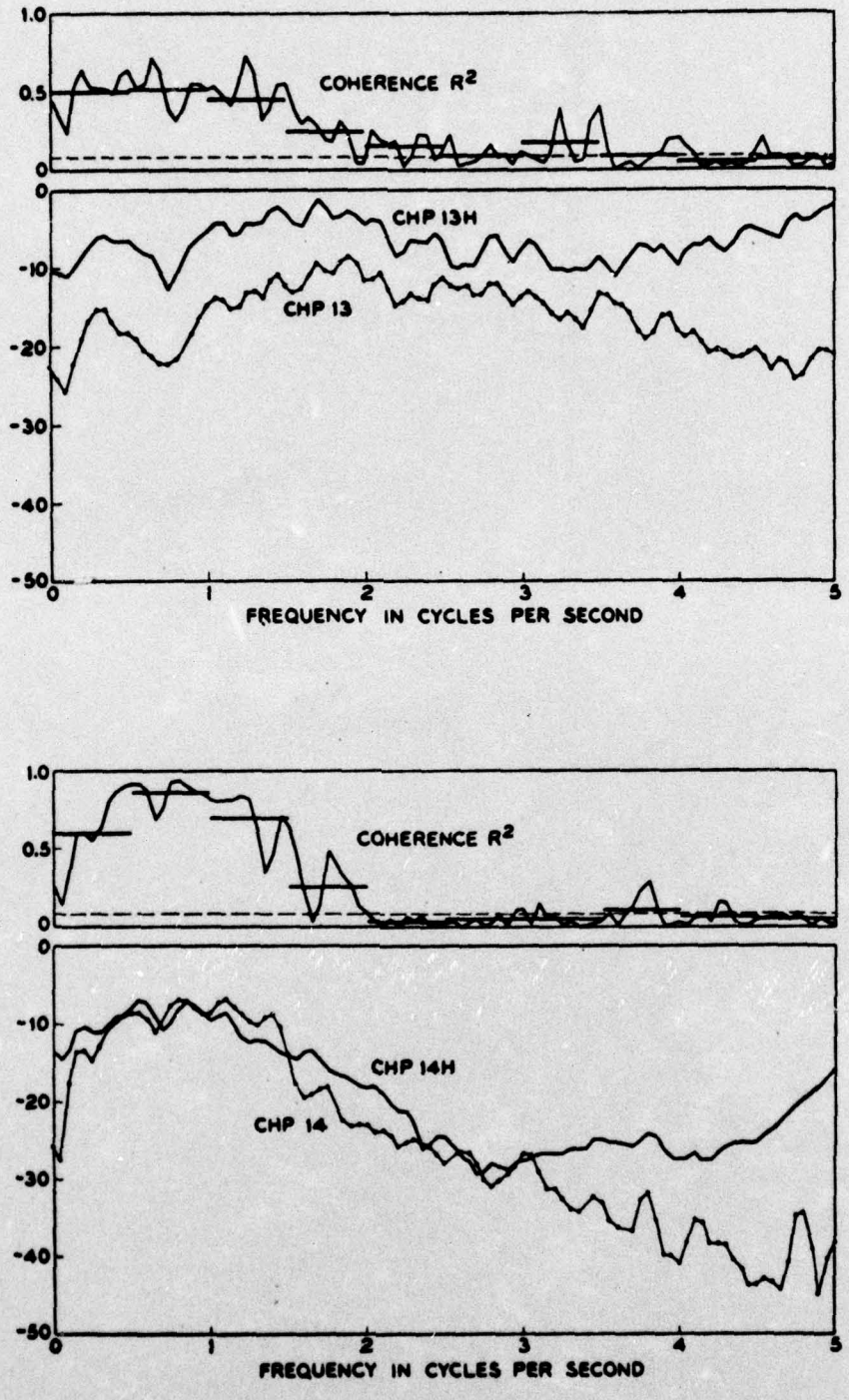

Figure 4A-2. Comparison of Manual and Electronic Digitization on Log Energy Spectra and Coherence R^2

Part 4B
Waveform

The pressure waveform of the IMP is highly predictable and reproducible. Mechanical impact design theory predicts a pulse having an instantaneous rise to peak pressure and a decay in the form of discrete steps where the length of each is equal to twice the acoustic travel time through the piston. The peak pressure is determined by the velocity of impact and the elastic properties of the piston and fluid. The IMP was designed to provide a peak pressure of 160 db re 1 microbar at the piston-fluid interface with a total peak power of 1 megawatt for 10 microseconds.

Figures 4B-1 through 4B-12 show the pressure waveform on-axis, at ranges of 1 foot to 107 yards from the acoustic window. With the exception of figure 4B-10, all of the waveforms have five pulses superimposed. This clearly depicts the excellent reproducibility of this type of transient generation in peak pressure, pulsewidth, rise time, and decay. The average time interval for superimposing a set of five pulses was 15 seconds at Edo and 50 seconds at NUOS (caused by the use of longer hose lengths). The increased time interval at NUOS may account for the greater lack of coherence in the "tails" of the NUOS waveforms as compared to those recorded at Edo. The coherence was also influenced by near-field effects. Examination of the NUOS data showed the overall reproducibility increased as the transient signal propagated from 1 foot to 107 yards.

All waveforms exhibited a "precursor" which is a threshold-type response prior to the epoch of the shock-wave (refer to page 3-6 of this report). The recorded maximum duration of the "precursor" was 96 microseconds as shown in figure 4B-8 which agrees well with the predicted duration of 100 to 120 microseconds. The "precursor" was highly reproducible and present for the total duration of the signal. The data indicates that it was probably the primary component 80 to 100 microseconds after the epoch (for the ranges shown).

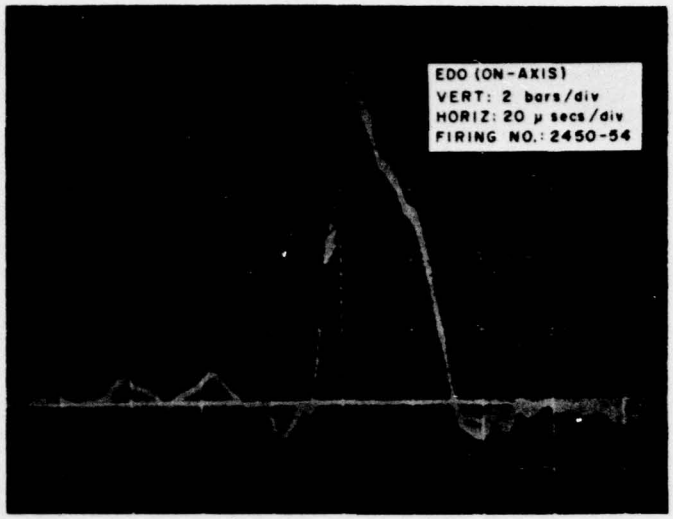

Figure 4B-1. Pressure Waveform (1 Foot)

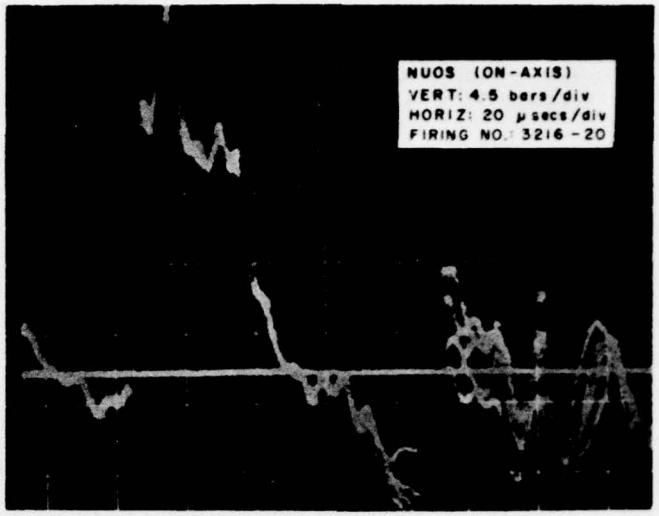

Figure 4B-2. Pressure Waveform (1 Foot)

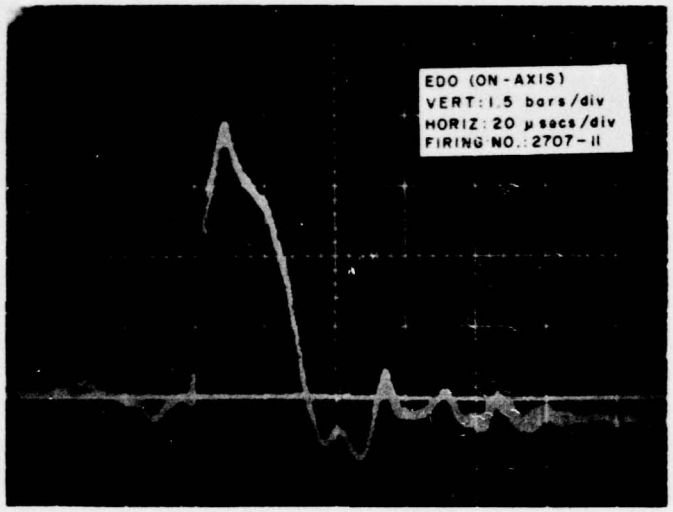

Figure 4B-3. Pressure Waveform (2 Feet)

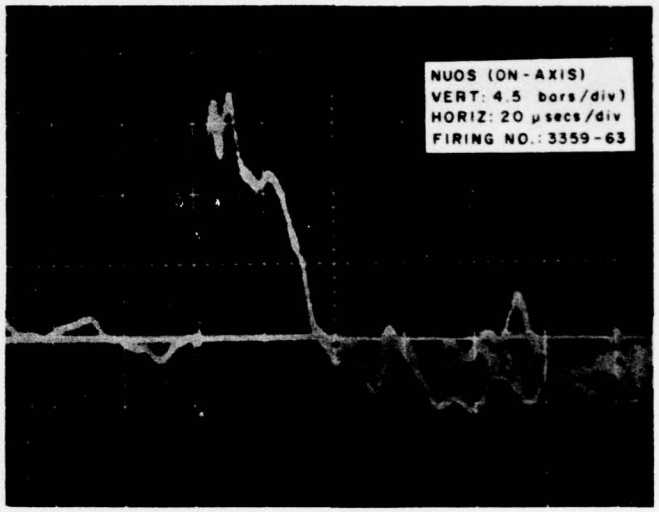

Figure 4B-4. Pressure Waveform (2 Feet)

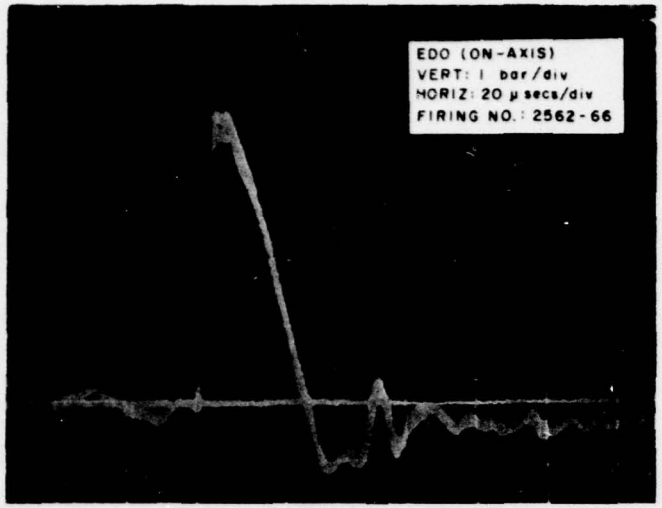

Figure 4B-5. Pressure Waveform (1 Yard)

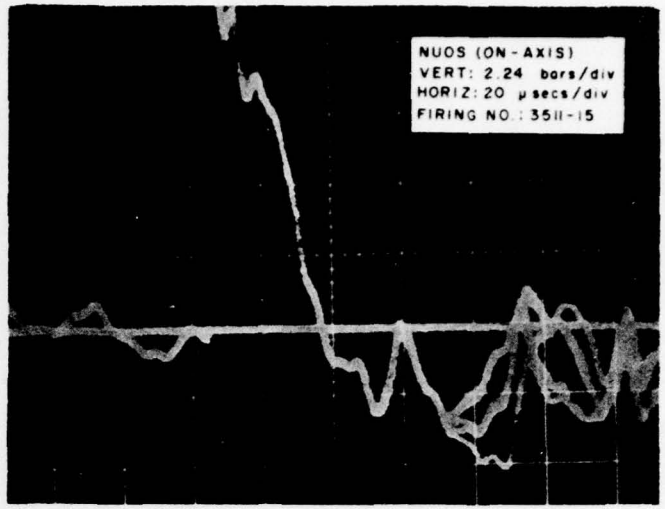

Figure 4B-6. Pressure Waveform (1 Yard)

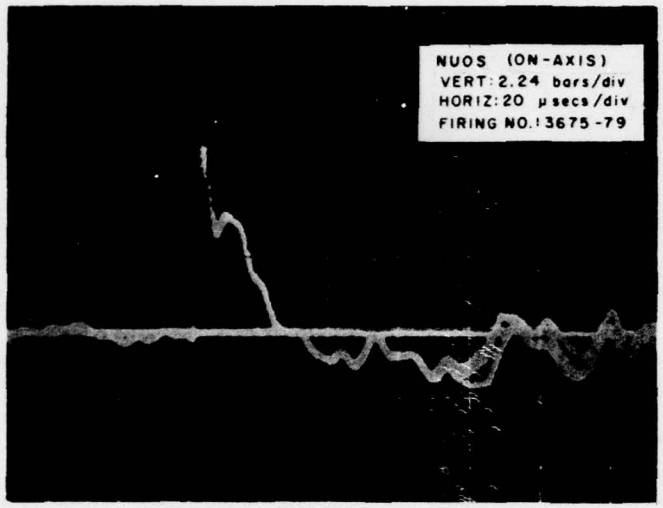

Figure 4B-7. Pressure Waveform (3 Yards)

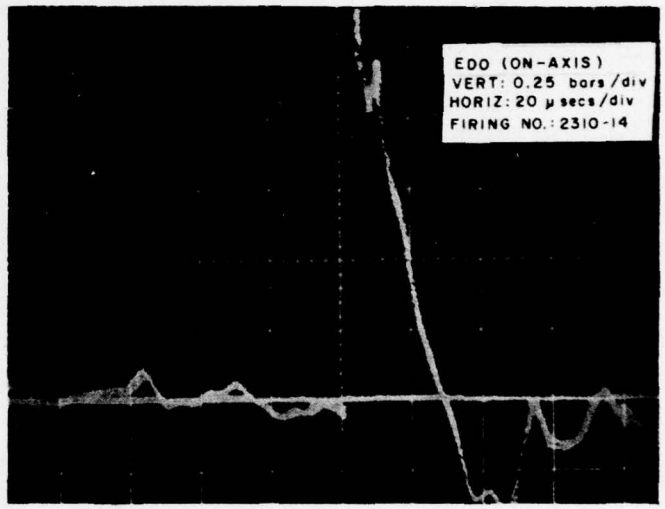

Figure 4B-8. Pressure Waveform (4 Yards)

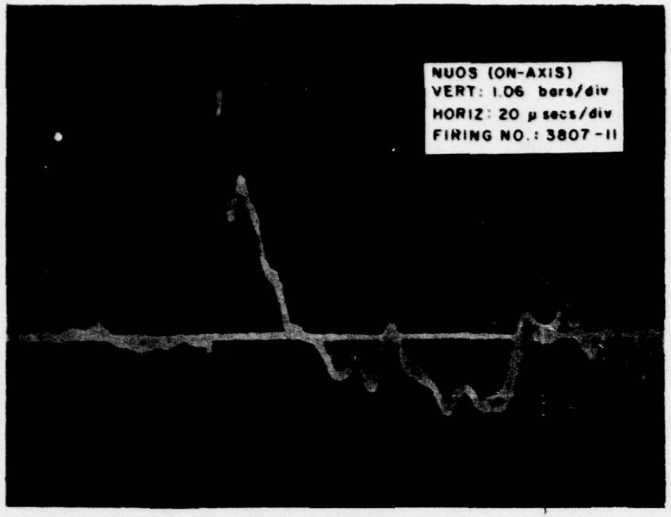

Figure 4B-9. Pressure Waveform (5 Yards)

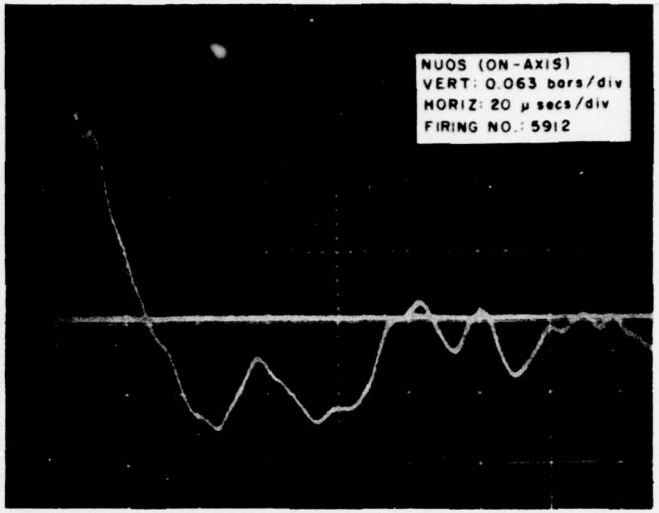

Figure 4B-10. Pressure Waveform (30 Yards)

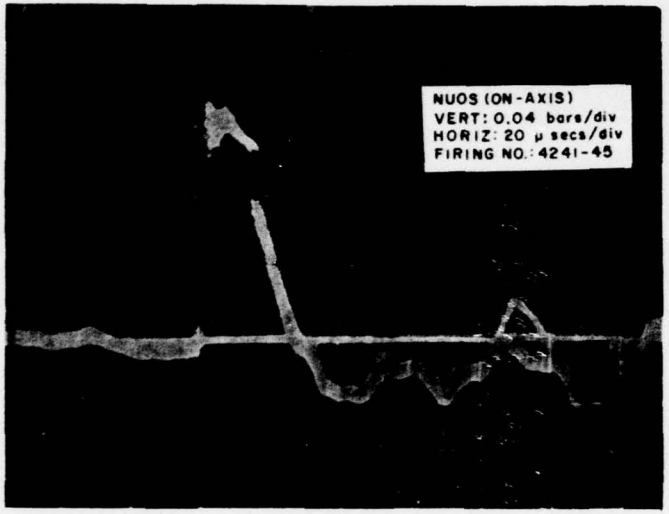

Figure 4B-11. Pressure Waveform (67 Yards)

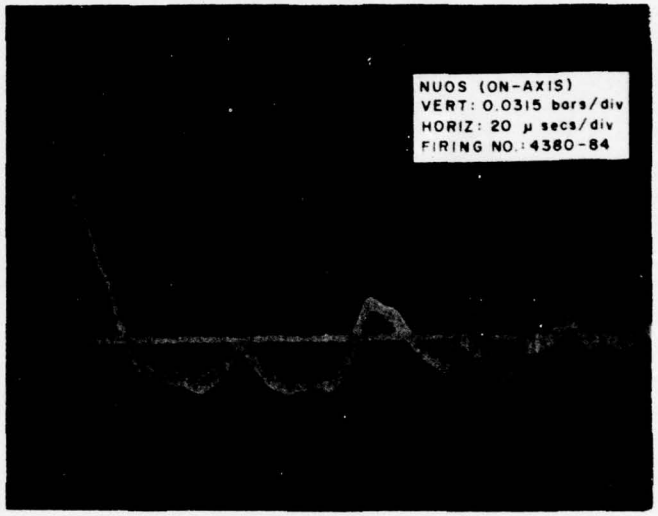

Figure 4B-12. Pressure Waveform (107 Yards)

A secondary peak is indicated in figure 4B-8 which was taken at Edo at a range of 4 yards. This characteristic was not present in some of the other waveforms recorded at Edo such as those shown in figures 4B-1, 4B-3 and 4B-5. However, the secondary peak appeared in all NUOS tests and approached the main peak at ranges greater than 5 yards. This behavior may be related to the propagation of the coherent structure of the shock-wave.

The output of the receiving probe was coupled directly to the oscilloscope. A measure of the ambient noise background was obtained by triggering the time-base sweep and examining the trace. The IMP was then fired and the received waveform superimposed on the trace. All tests were carried out under conditions of very high signal-to-noise ratio.

Although the cavitation limit for CW intensity was greatly exceeded during the tests, there was no evidence of cavitation. This is due to the stress-time relationship which permits materials to be stressed for a short duration far in excess of that allowable under static conditions. Also, there were no bubble pulses generated after radiation of the shock-wave which is a consequence of this particular type of transient generation. This facilitates pulsing repetitively and results in greater reproducibility.

The peak pressure at 1 yard from the acoustic window, on-axis, was measured at 141 db re 1 microbar and showed excellent agreement with measurements in previous programs (references 1 and 4).

The peak pressure* on-axis as a function of range is shown in figure 4B-13. The

---

*The maximum value of the pressure (P_{max}) incident on the receiving probe at a given range was computed as:

$$P_{max} = V_{meas} - RR \left[- A + 6\right] \quad \text{(db re 1 microbar)}$$

where:

V_{meas}	=	measured voltage	(db re 1 volt)
RR	=	receiving response	(db re volt/microbar)
A	=	amplifier gain	(db re 1 volt)
6	=	loss due to impedance matching	(db re 1 volt)

The dotted portion was required for computing P_{max} at ranges $\geq$ 30 yards (details given on pages 3-14 and 3-18).

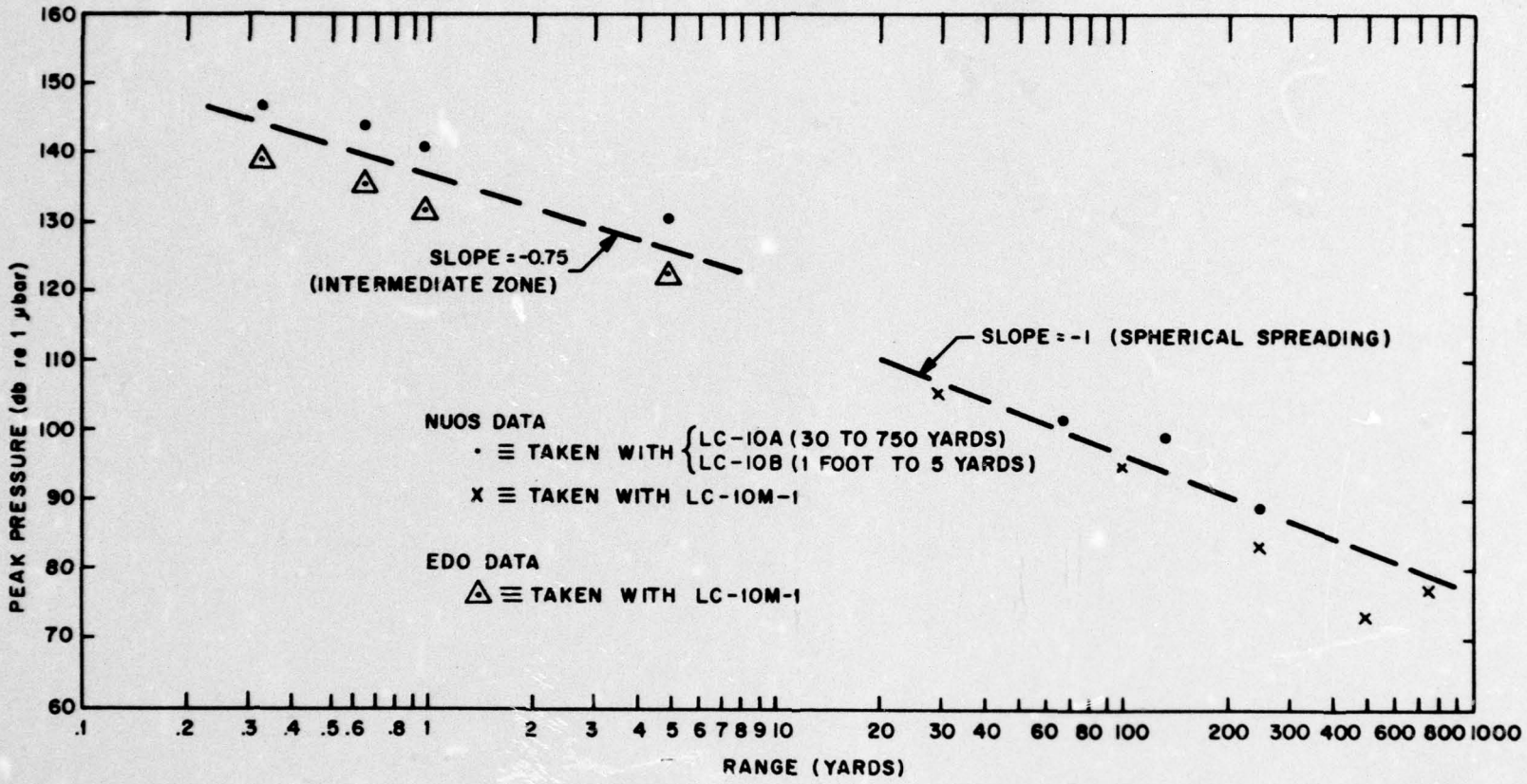

Figure 4B-13. Peak Pressure vs Range (On-Axis)

broken lines refer only to slope dependence and do not imply any empirical curve-fitting. At ranges of 1 foot to 5 yards, the peak pressure followed a spreading loss dictated by a 0.75 power of the range which indicates an intermediate zone between spherical (R^{-1}) and cylindrical ($R^{-0.5}$) spreading. For the other ranges from 30 to 750 yards, the spreading loss appeared to be spherical.

The pulsewidth* and rise time on-axis as a function of range is shown in figure 4B-14. At a range of 1 yard, the pulsewidth was 31 to 33 microseconds. It decreased to approximately 26 microseconds at 5 yards and remained at this value for all other test ranges. The rise time was constant at 4 microseconds from 1 yard to approximately 250 yards. This 4 microsecond build-up time was the integration time of the wideband probes. Above 250 yards, the rise time appeared to increase slowly which may be attributed to the high frequency attenuation due to absorption becoming more pronounced and/or the increasing data inaccuracy caused by reflections. An example of such reflections is the direct wave and surface reflection at 107 yards, as shown in figure 4B-15. The average coherence between the direct and surface arrivals, although not computed, appeared to be high. The surface arrival was accompanied by the usual phase inversion and a loss of 6db in peak amplitude.

*The pulsewidth is defined as the first positive portion of the pressure waveform.

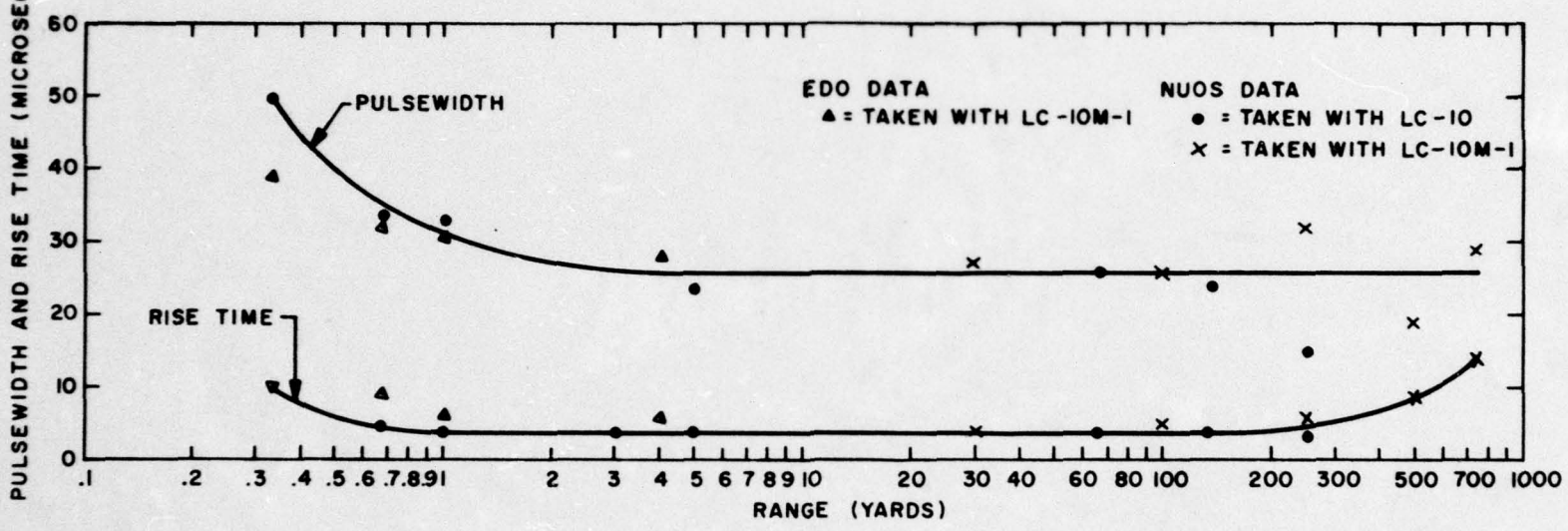

Figure 4B-14. Pulsewidth and Rise Time vs Range (On-Axis)

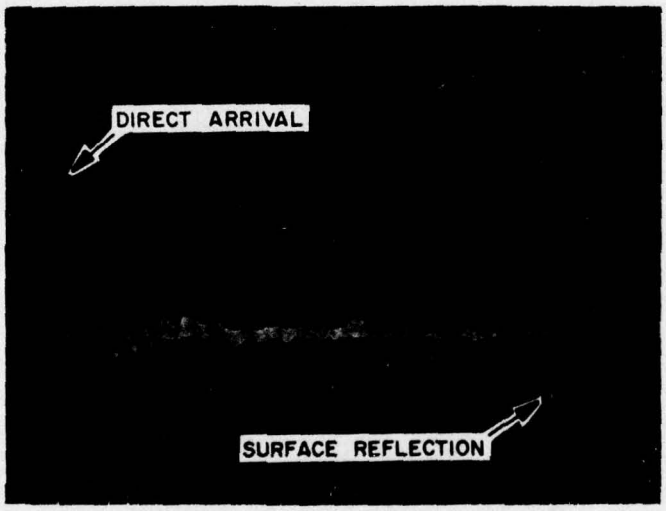

Figure 4B-15. Direct Wave and Surface Reflection at 107 Yards (On-Axis)

Vert. Scale: 0.0315 bars/div
Horiz. Scale: 100 usecs/div

Part 4C

Energy Spectra

The energy spectrum and the cumulative energy spectra for the waveforms shown in part 4B are plotted in figures 4C-1 through 4C-13. In general, the spectra computed from the Edo and NUOS data showed very good agreement in structure and degree of energy concentration. The rapid fluctuations of the energy spectrum for both sets of data were the effects of truncation, aliasing and sampling. However, the energy spectrum levels at Edo were about 7 to 10 db lower than those at NUOS. Also, the Edo spectra decreased somewhat more smoothly above 20 kc. These differences were primarily due to the different frequency responses of the LC-10 and LC-10M-1 probes.

The slope of the energy spectra on- and off-axis, with the average values of the signals removed, was +6 db per octave at the low frequency end. The high frequency fall-off rate was more difficult to determine due to the effects given above, but appeared to be about -12 db per octave. The positions of the maximum energy densities were generally between 4 to 6 kc. An interesting occurrence was that for similar ranges at Edo (3 and 4 yards) and NUOS (5 yards), there was a shift of energy to the higher frequencies. At greater ranges, the energy was redistributed to the lower frequencies.

The cumulative energy spectra of the waveforms on-axis in general showed that 50% of the energy was below 14 kc and 85% was below 35 kc (approximately the reciprocal of the pulsewidth). Thus, the low frequencies were major contributors to the total energy content and implies that the IMP waveform will propagate over long distances.

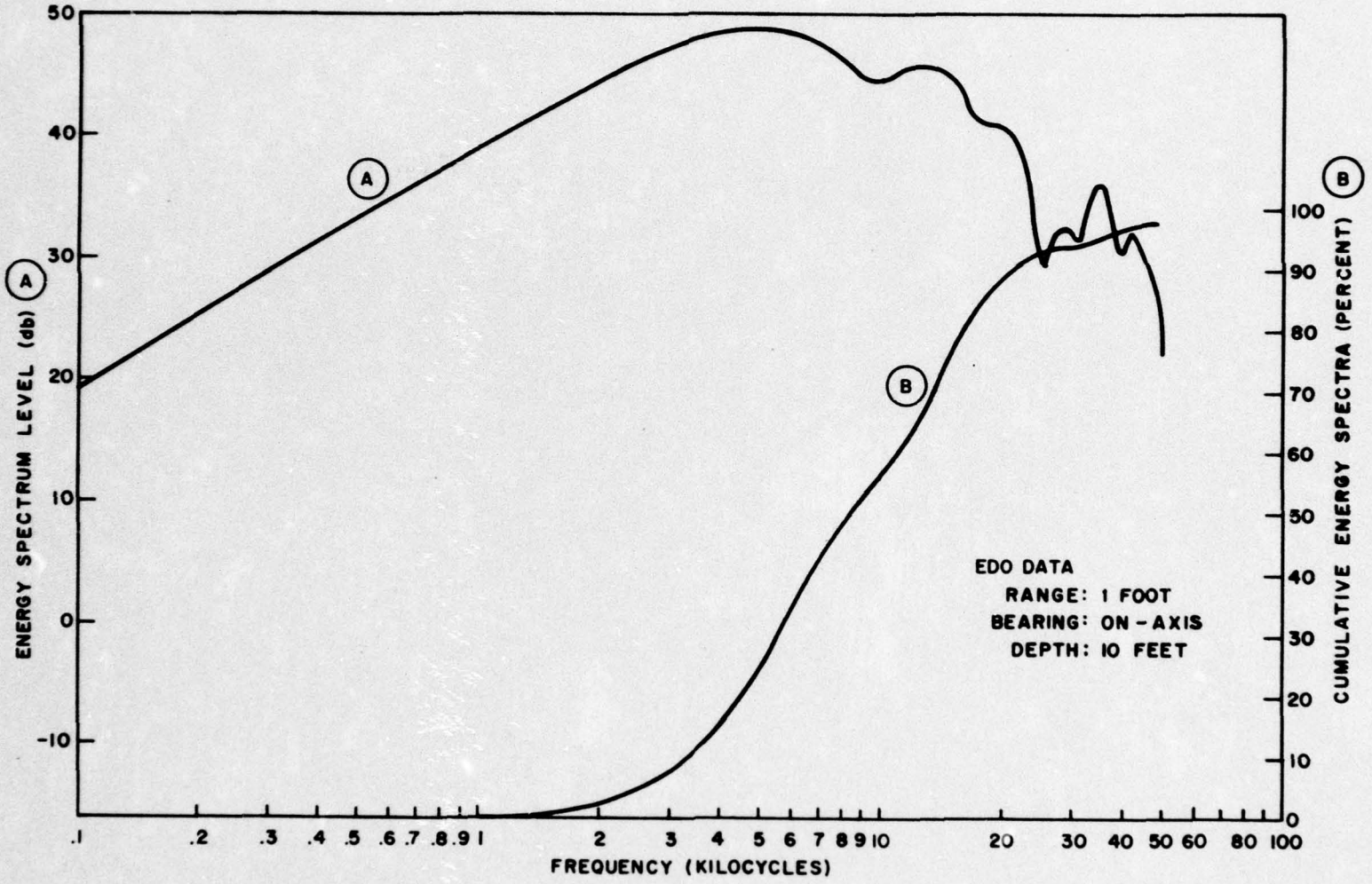

Figure 4C-1. Energy Spectrum and Cumulative Energy Spectra

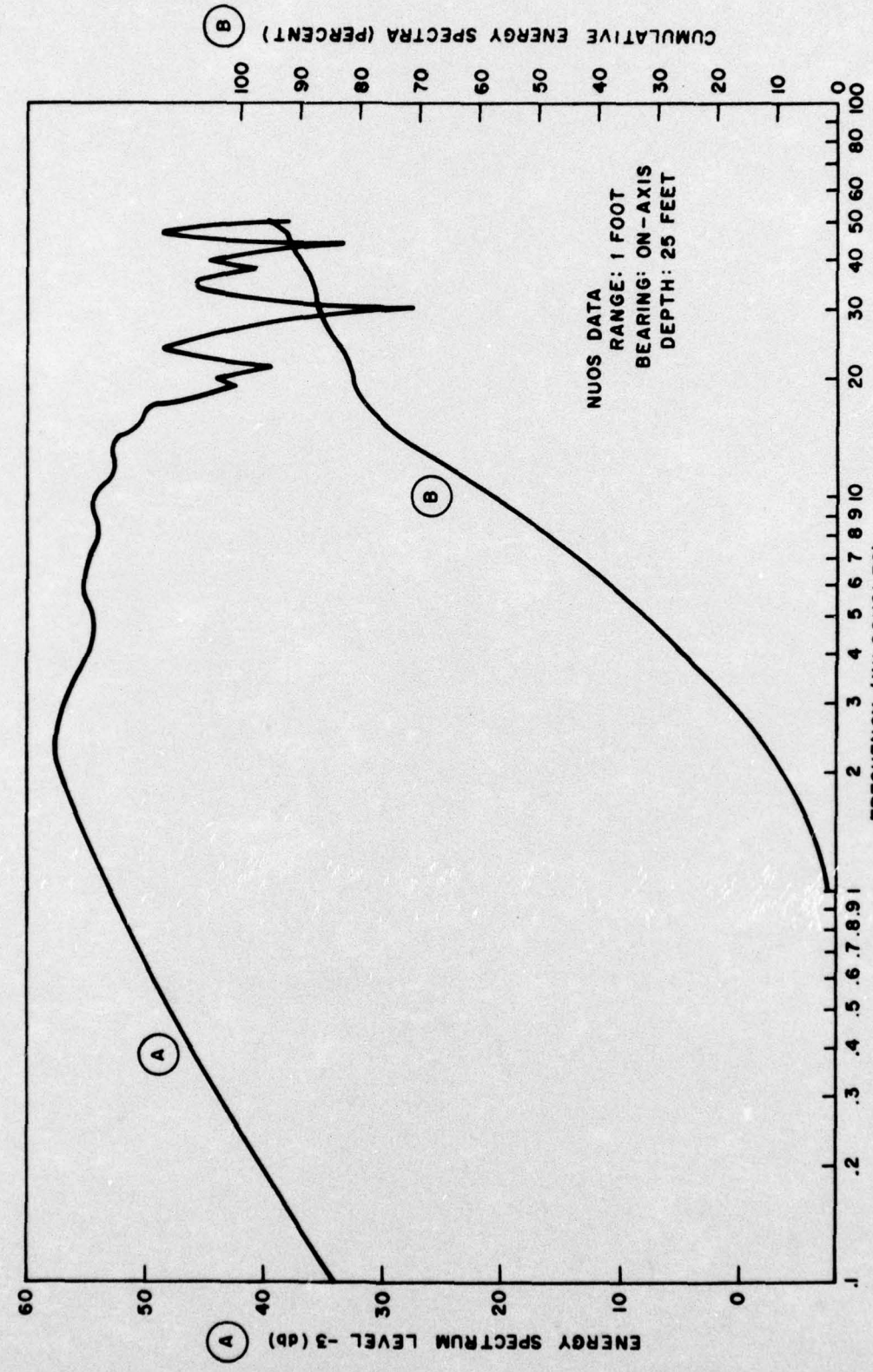

Figure 4C-2. Energy Spectrum and Cumulative Energy Spectra

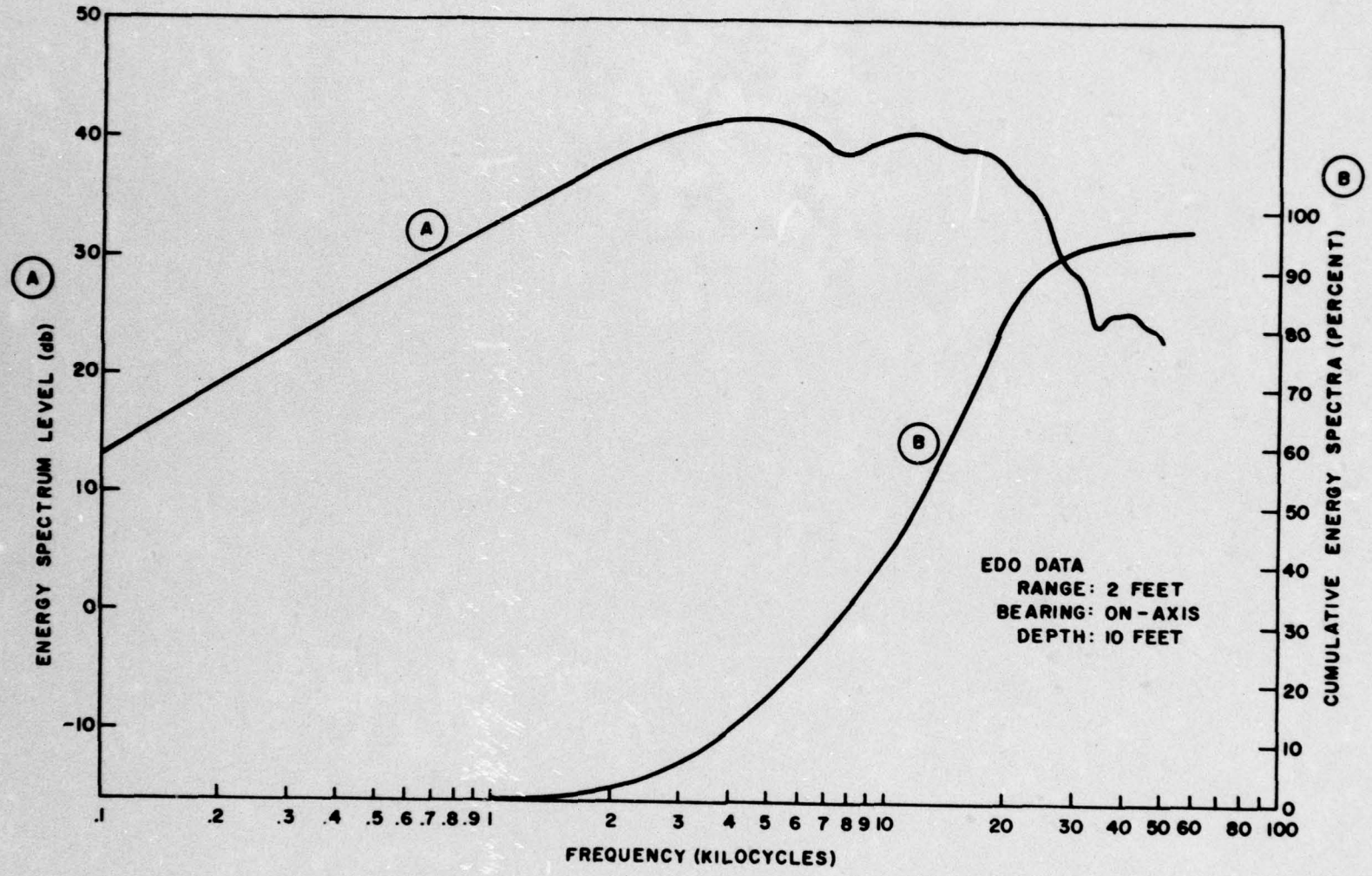

Figure 4C-3. Energy Spectrum and Cumulative Energy Spectra

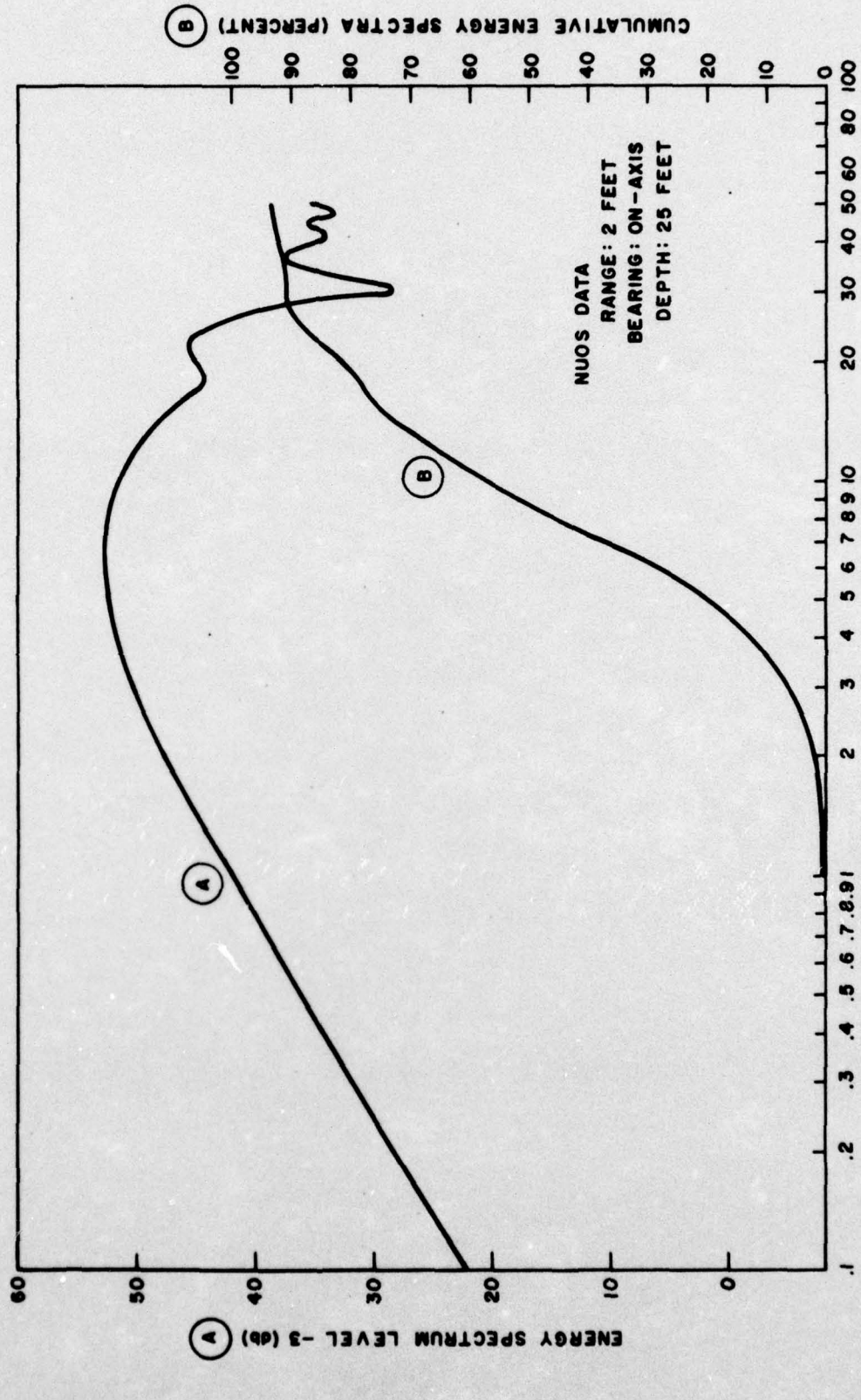

Figure 4C-4. Energy Spectrum and Cumulative Energy Spectra

Figure 4C-6. Energy Spectrum and Cumulative Energy Spectra

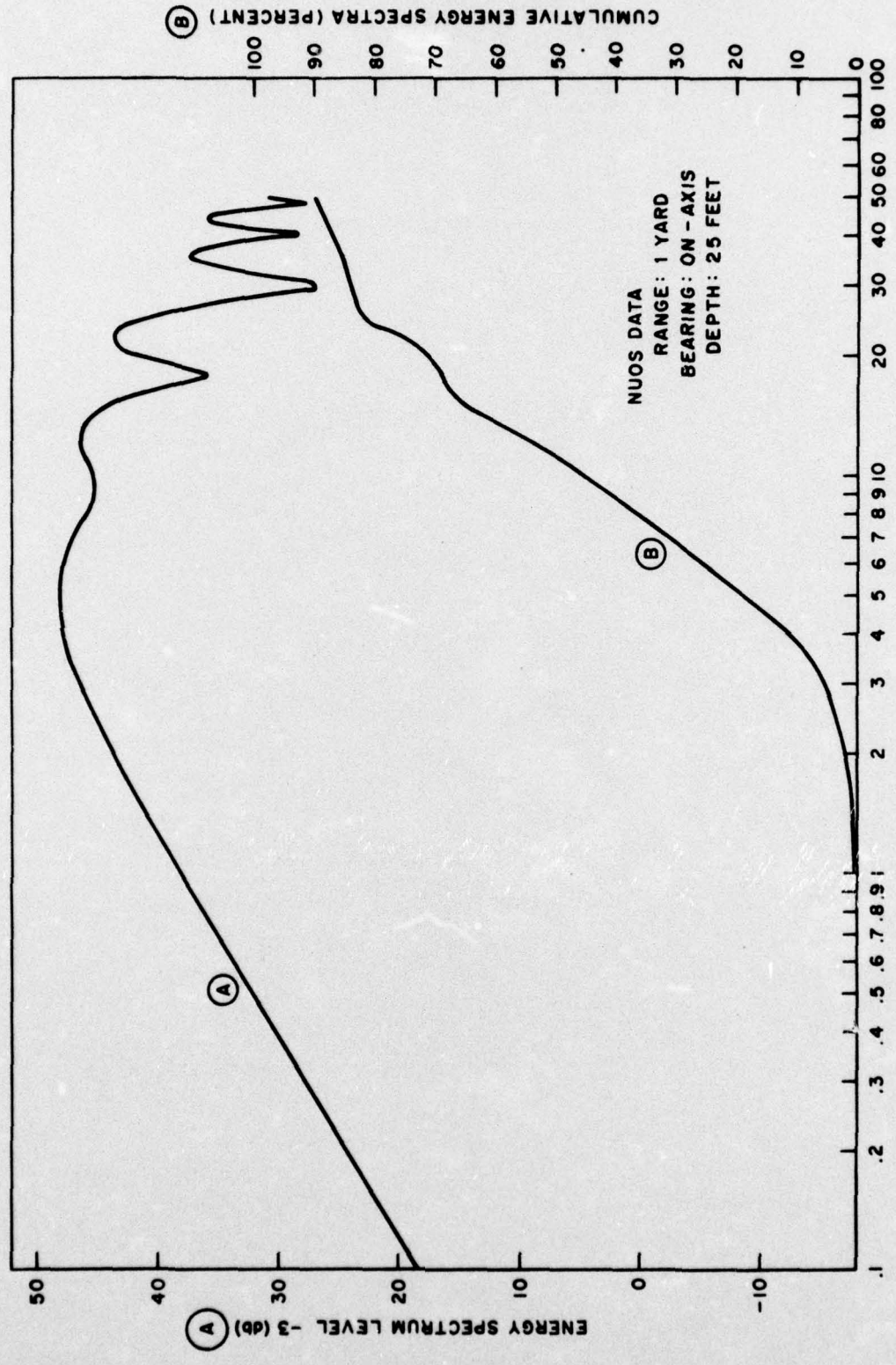

Figure 4C-6. Energy Spectrum and Cumulative Energy Spectra

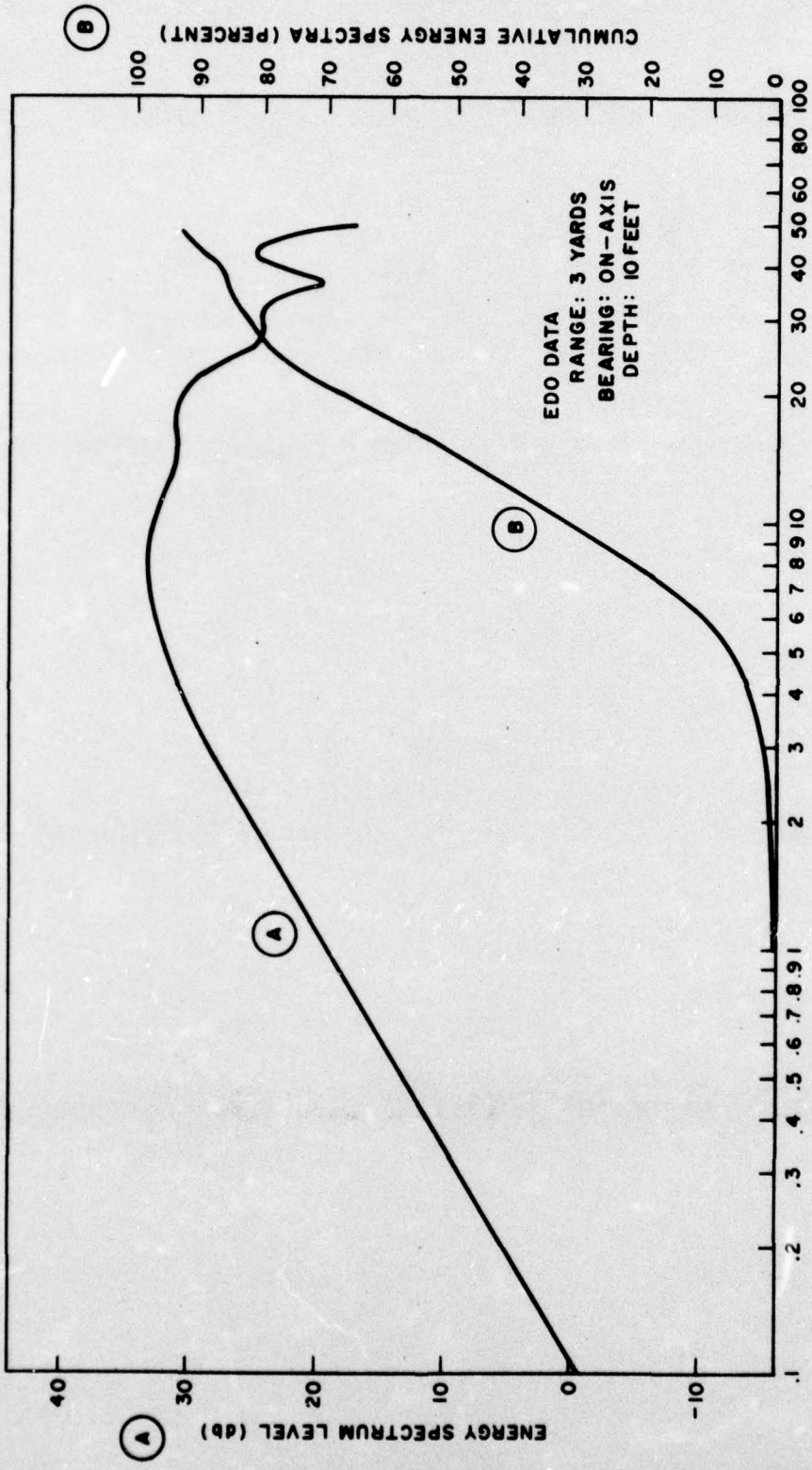

Figure 4C-7. Energy Spectrum and Cumulative Energy Spectra

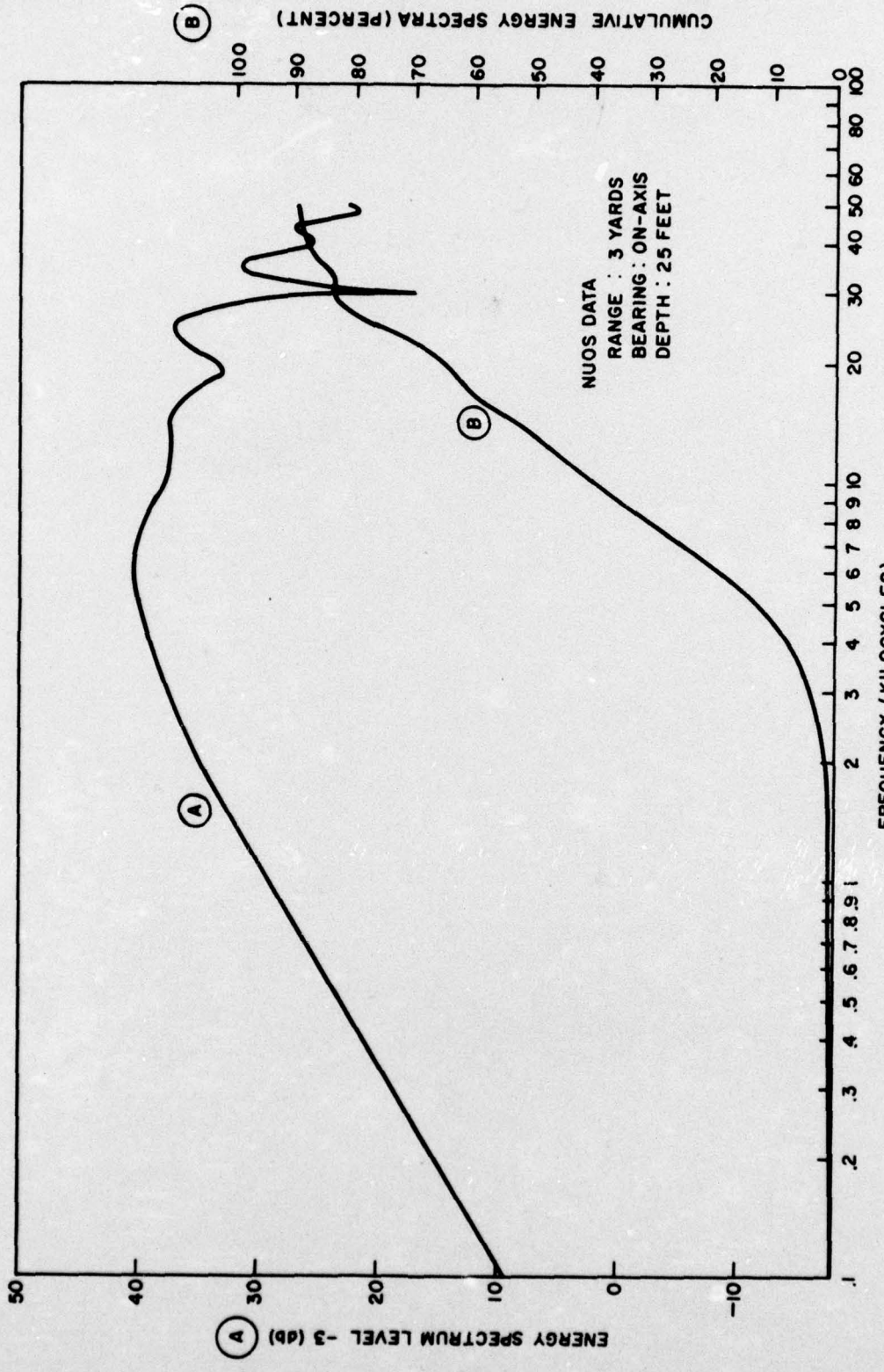

Figure 4C-8. Energy Spectrum and Cumulative Energy Spectra

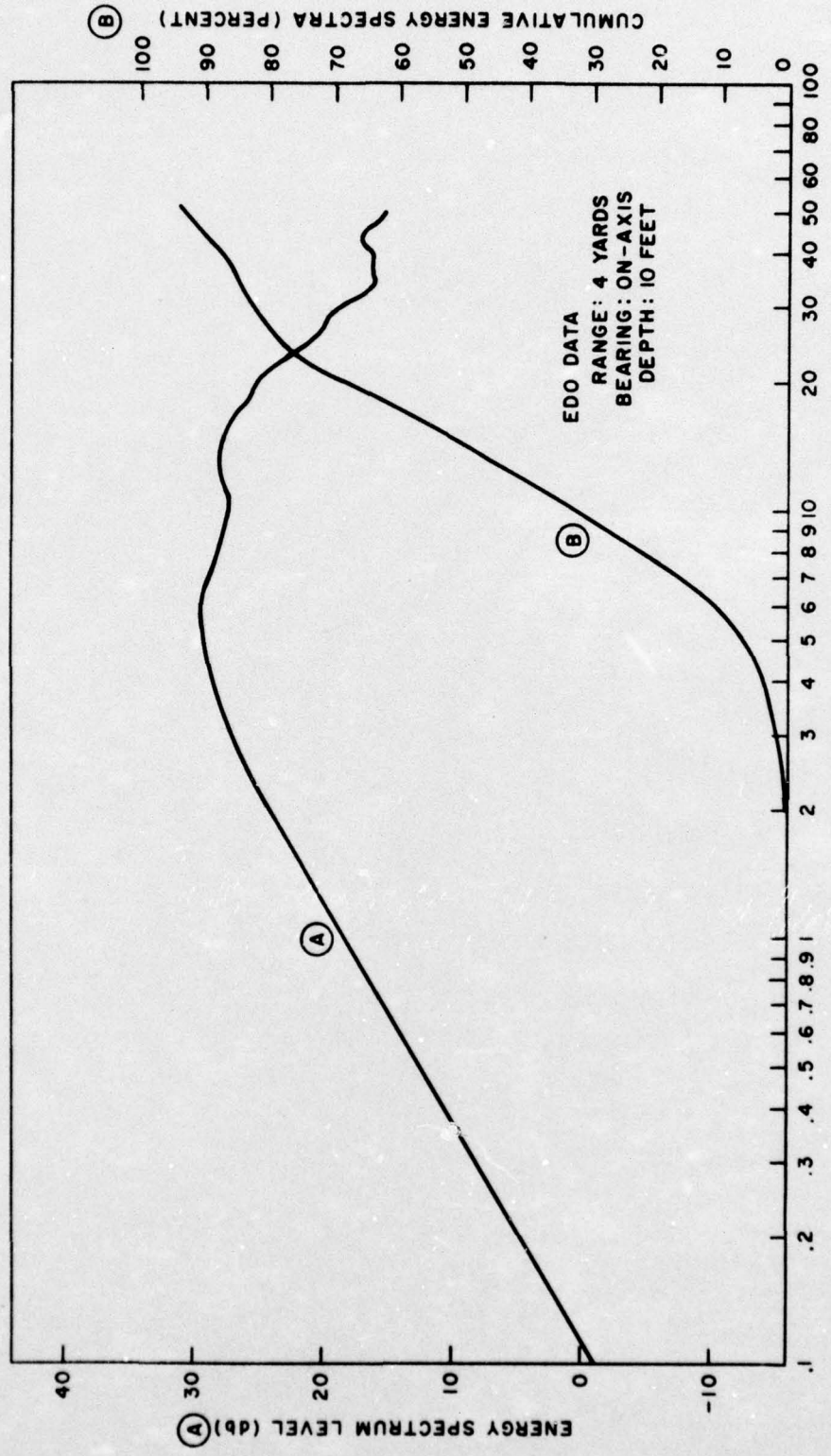

Figure 4C-9. Energy Spectrum and Cumulative Energy Spectra

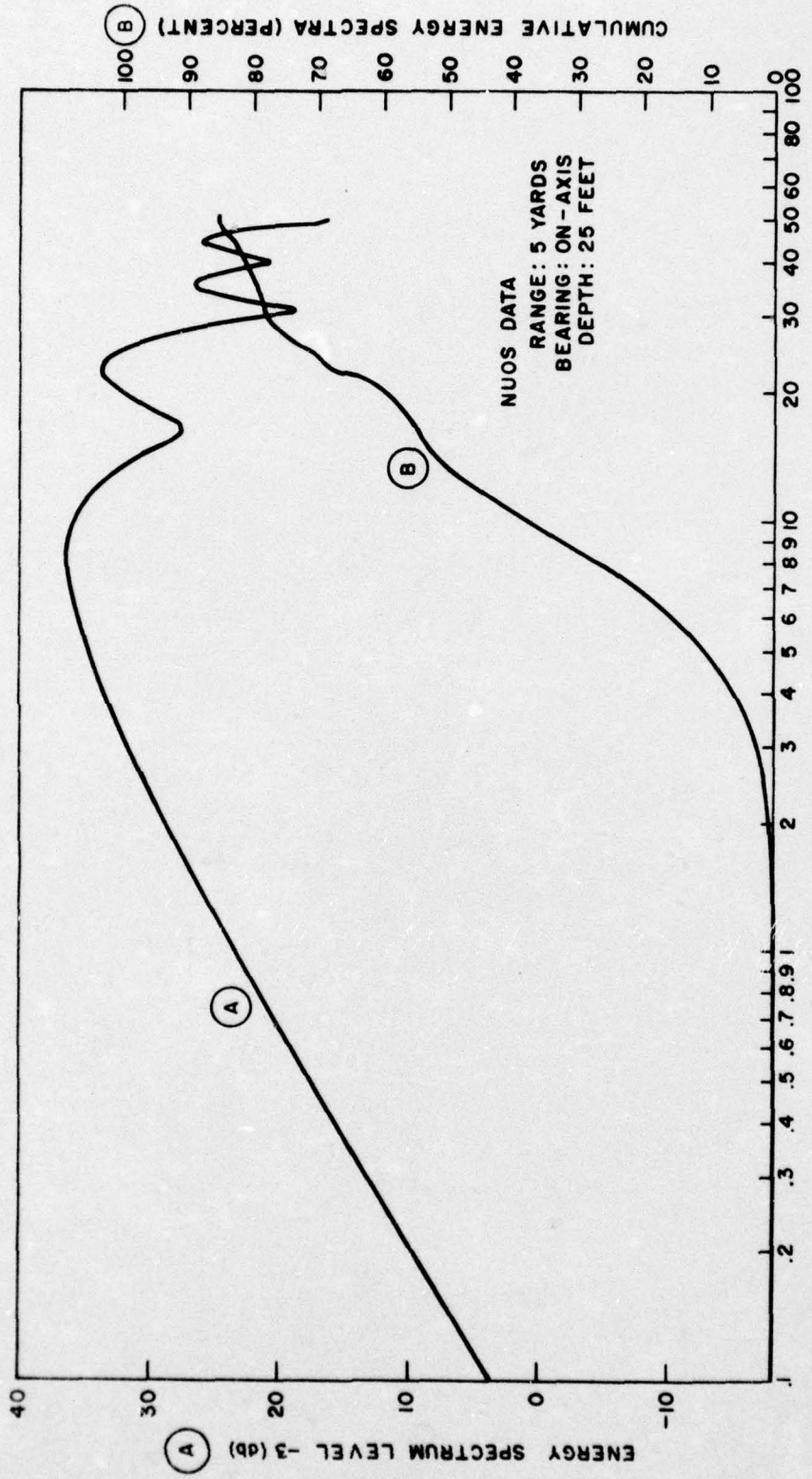

Figure 4C-10. Energy Spectrum and Cumulative Energy Spectra

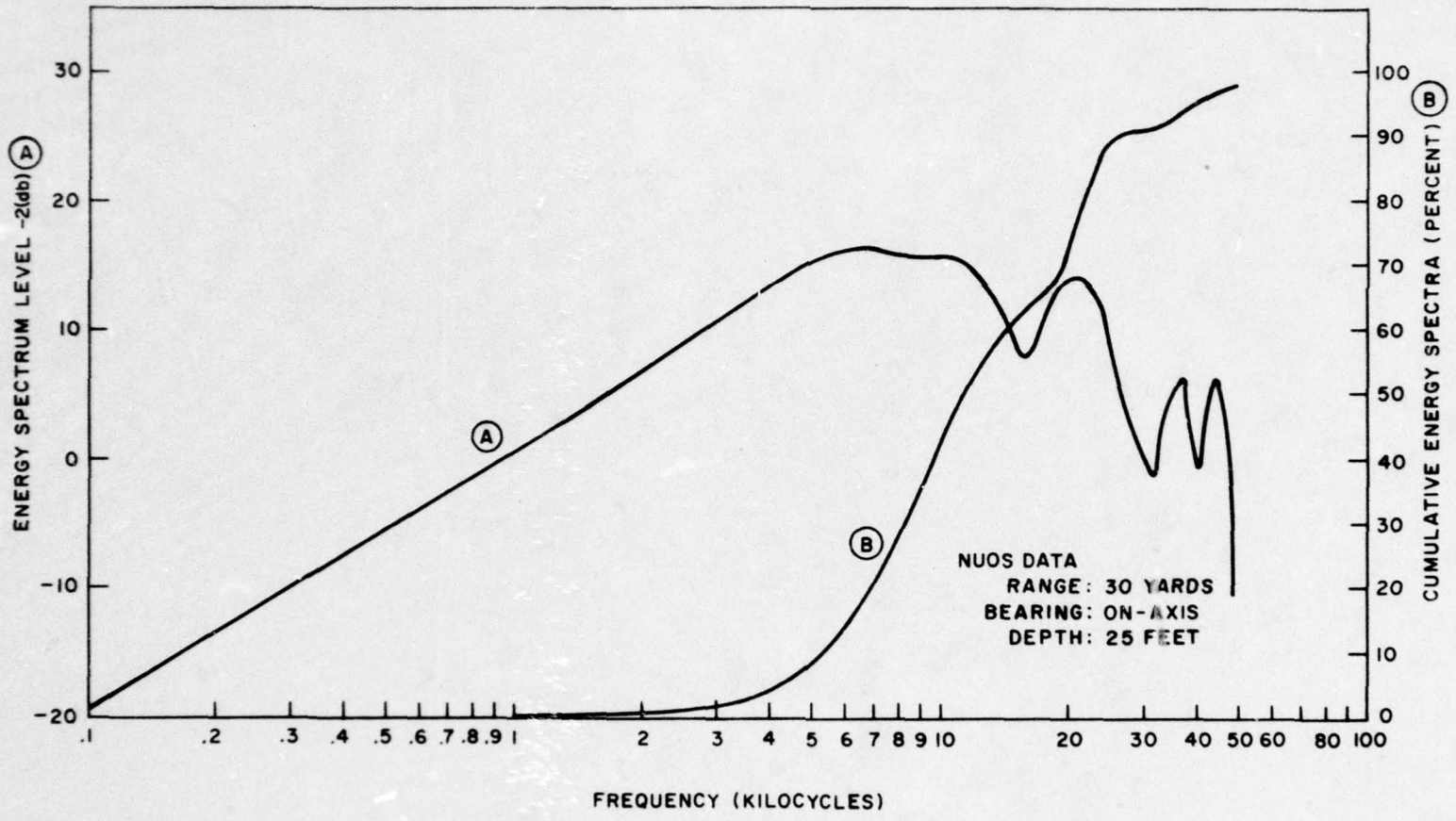

Figure 4C-11. Energy Spectrum and Cumulative Energy Spectra

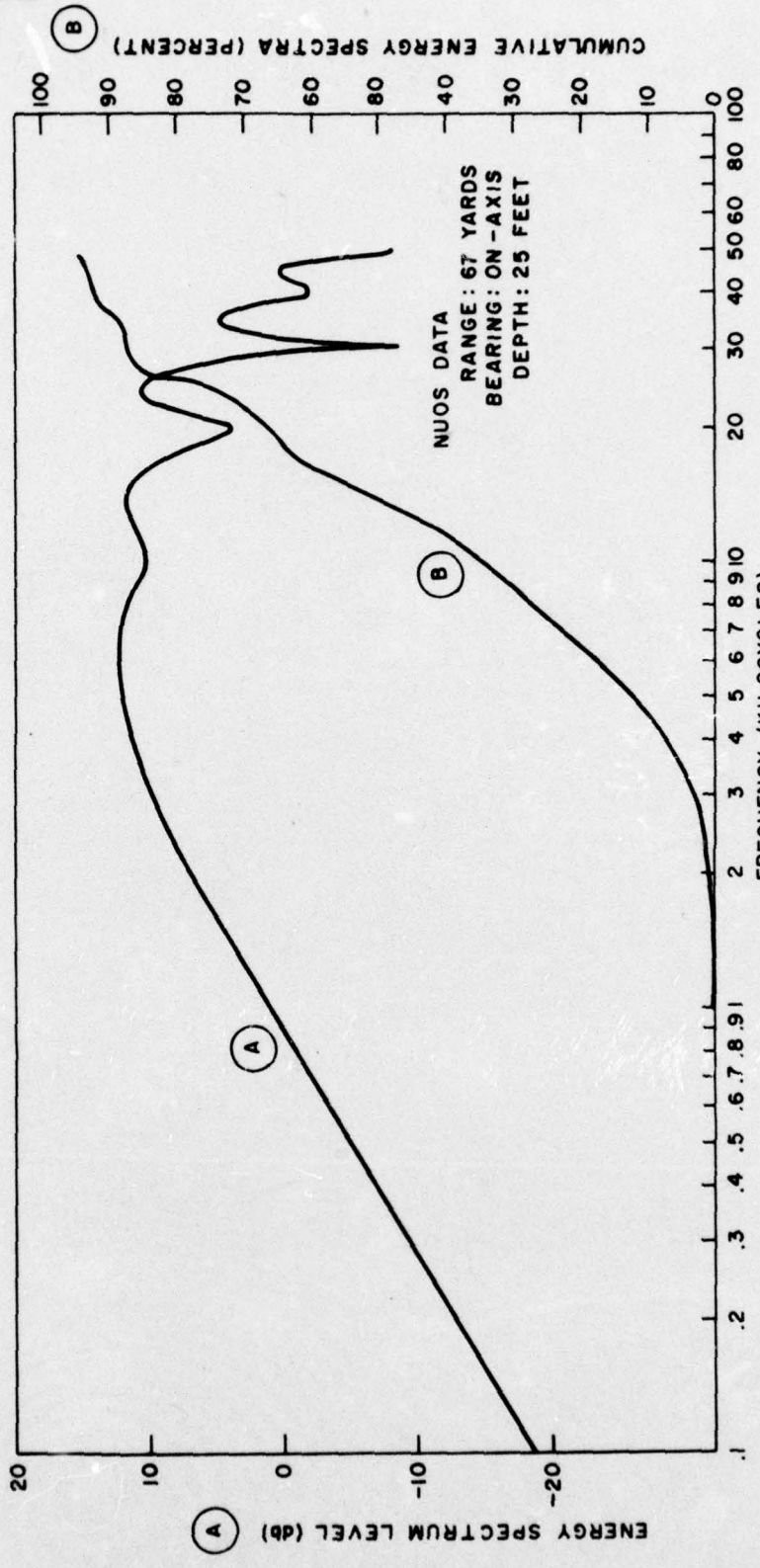

Figure 4C-12. Energy Spectrum and Cumulative Energy Spectra

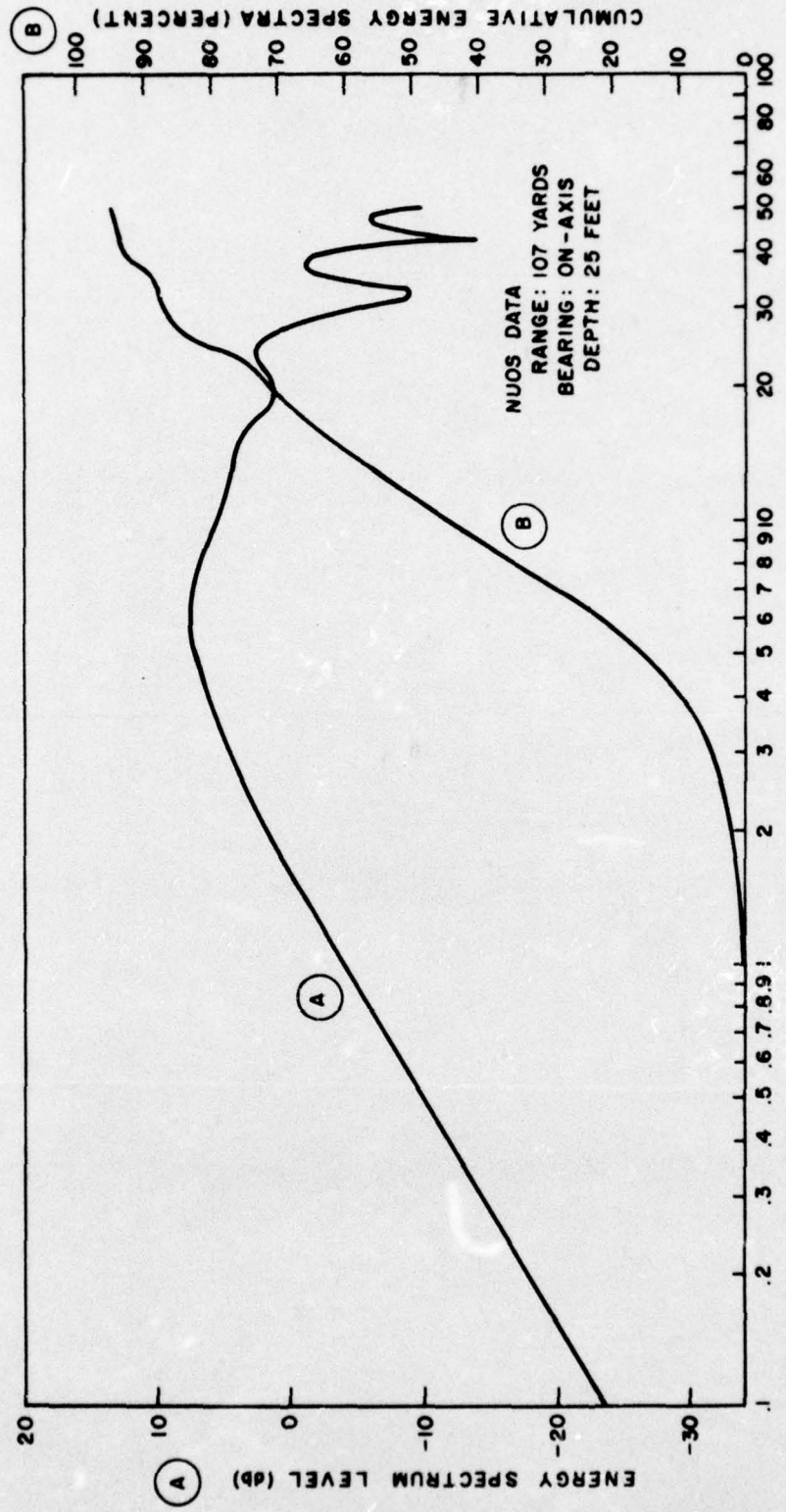

Figure 4C-13. Energy Spectrum and Cumulative Energy Spectra

The beamwidth for a fixed-size projector increases with increasing frequency. Therefore, the high frequencies have narrow spatial selectivity and contribute small amounts of energy at large deviations from the acoustic axis. This reduction in the high frequency energy was characterized by the energy spectra 25° off-axis at 1 yard in figure 4C-14 and 15° off-axis at 67 yards in figure 4C-15. The corresponding waveforms at these ranges are shown in figures 4C-16 and 4C-17. A comparative measure of the significant acoustic parameters depicted in figures 4C-14 through 4C-17 is summarized below.

PARAMETER	1 YARD		67 YARDS	
	ON-AXIS	25° OFF-AXIS	ON-AXIS	15° OFF-AXIS
Peak Pressure (db re 1 ubar)	141	134.5	102	94.3
Pulsewidth (microseconds)	33	50	26	60
Risetime (microseconds)	4	6	4	14
50% of Energy	$\leq$ 11 kc	$\leq$ 7 kc	$\leq$ 14 kc	$\leq$ 6.3 kc
85% of Energy	$\leq$ 35 kc	$\leq$ 19 kc	$\leq$ 27 kc	$\leq$ 12 kc
Spectrum Maxima (db)	51	48	12.5	11.5
Frequency of Spectrum Maxima (kc)	5.0	2.5	6.0	5.5

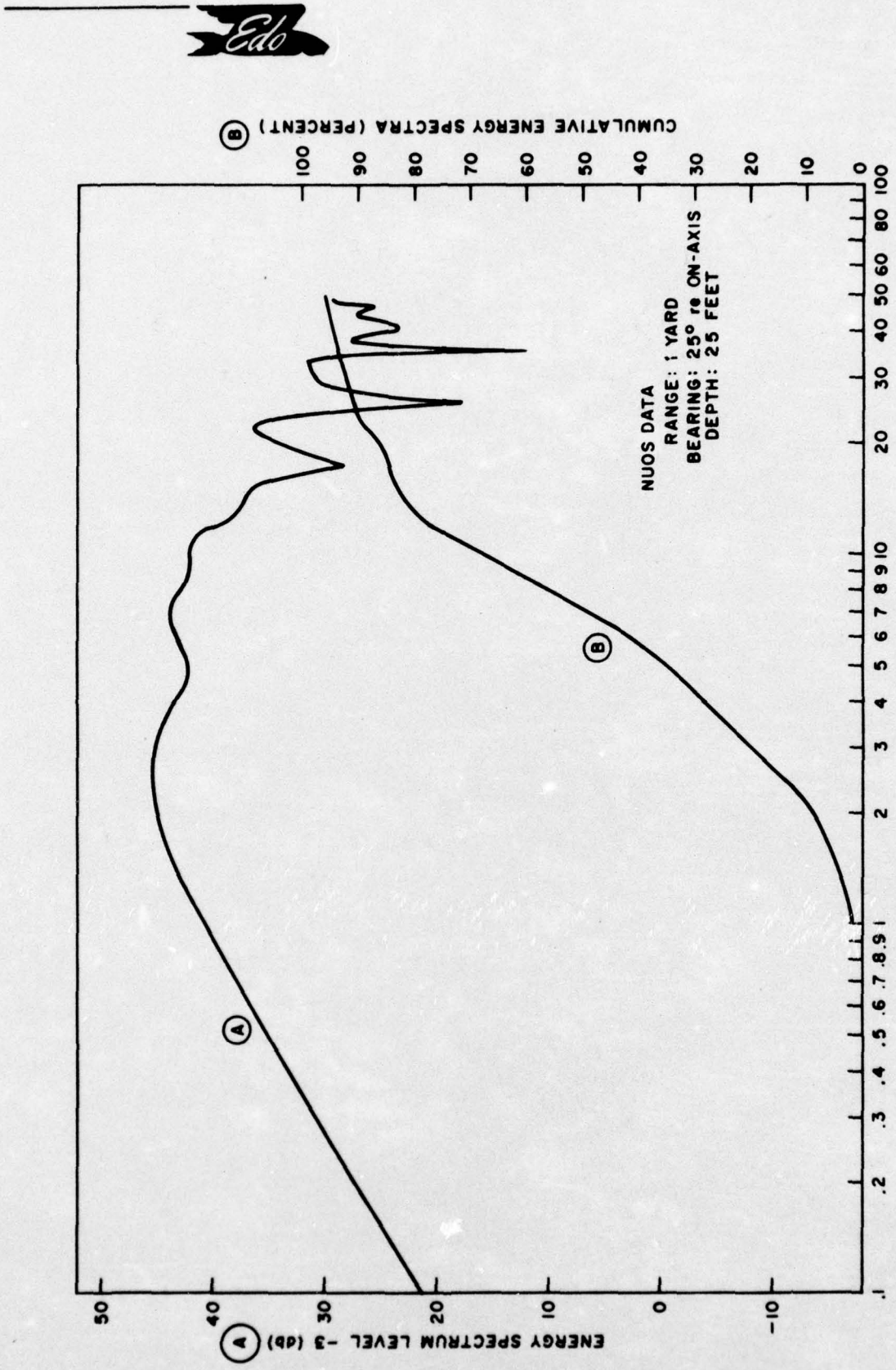

Figure 4C-14. Energy Spectrum and Cumulative Energy Spectra

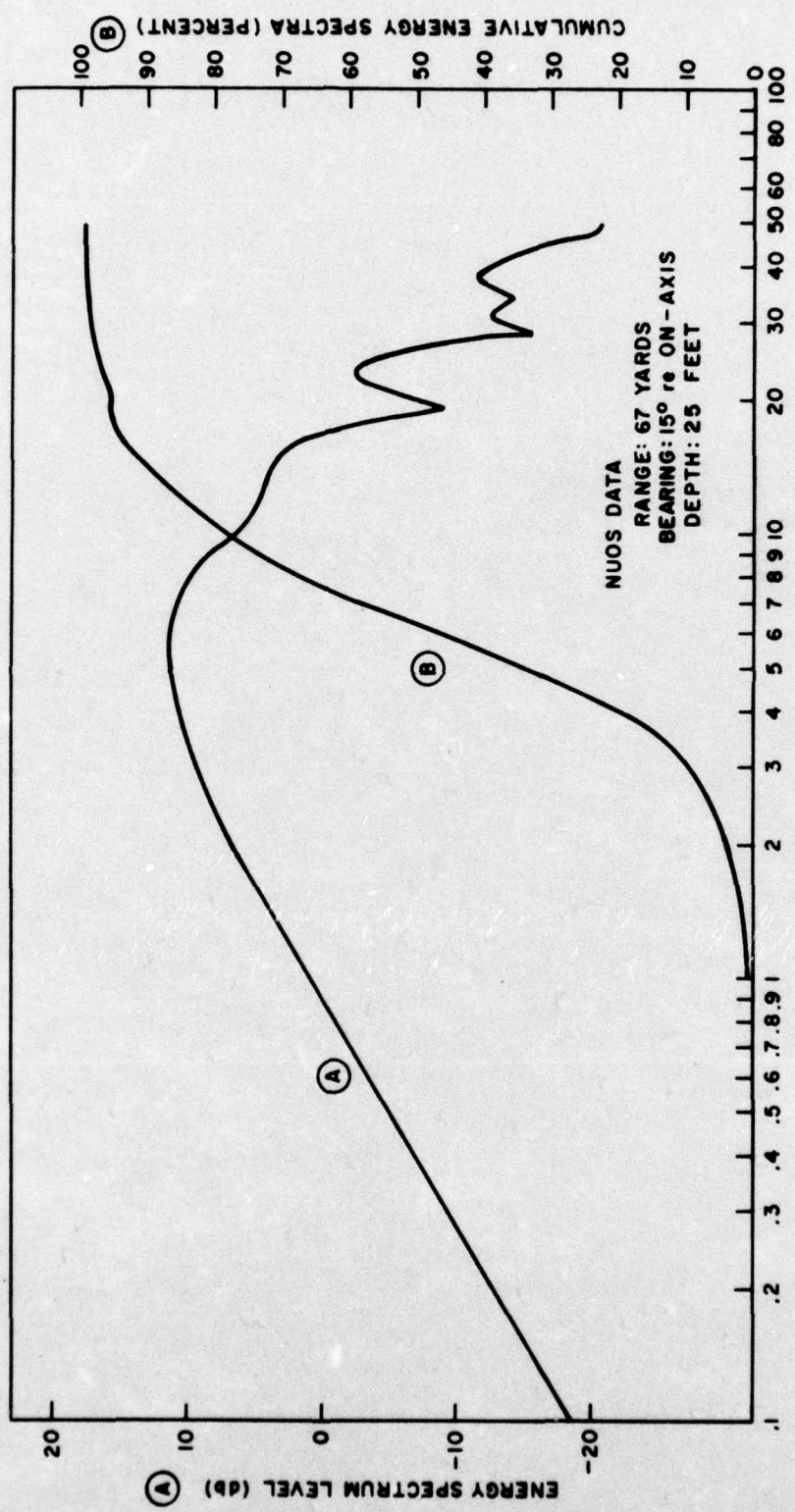

Figure 4C-15. Energy Spectrum and Cumulative Energy Spectra

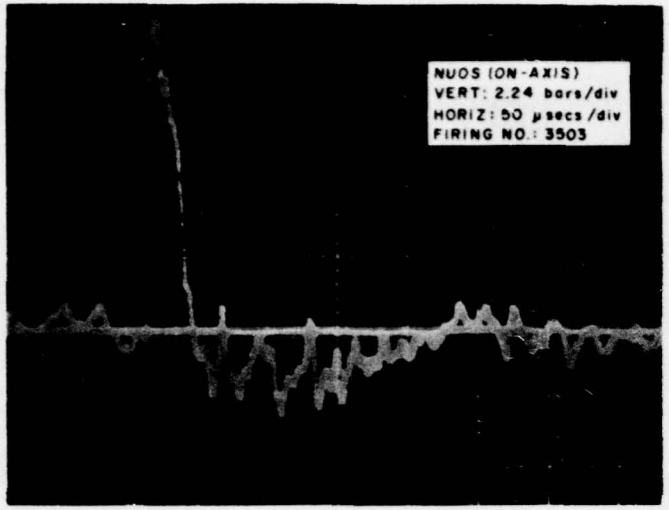

Figure 4C-16a. Pressure Waveform (1 Yard)

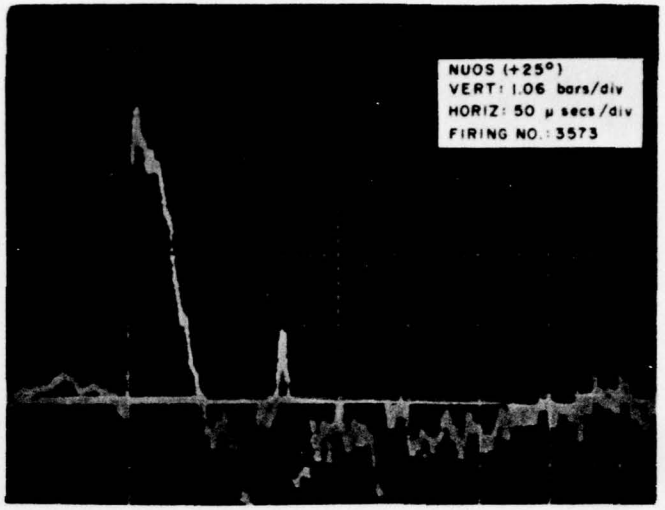

Figure 4C-16b. Pressure Waveform (1 Yard)

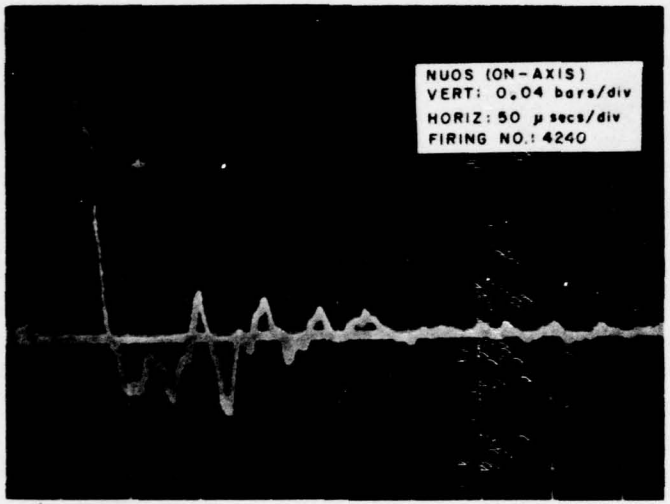

Figure 4C-17a. Pressure Waveform (67 Yards)

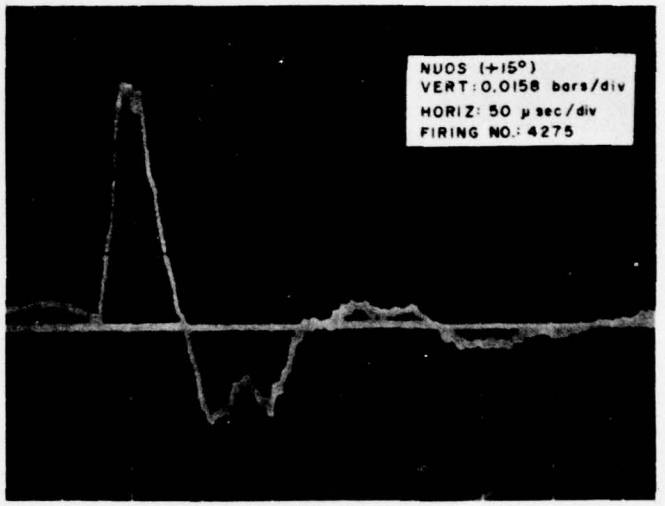

Figure 4C-17b. Pressure Waveform (67 Yards)

A measure of the concentration of the IMP signal in the time and frequency domain was obtained by computing the rms time (D_t) and frequency (D_f) durations. The rms bandwidth-time product ($D_t D_f$) is an estimate of the amount of information contained in the signal and of the complexity of the instrumentation necessary for processing. The results of these computations were:

EDO DATA

RANGE (feet)	D_t (μ secs)	D_f (kc)	$D_t D_f$
1	25.0	26.3	0.66
2	28.9	34.1	0.99
3	29.3	34.5	1.01
9	20.9	37.2	0.78
12	24.2	34.6	0.83
AVERAGE:	25.7	33.3	0.85

NUOS DATA

RANGE (yards)	D_t (μ sec)	D_f (kc)	$D_t D_f$
1	45.0	32.1	1.44
3	35.8	36.6	1.31
5	38.1	36.5	1.39
30	50.9	32.9	1.67
67	41.6	38.4	1.60
107	33.4	35.3	1.18
AVERAGE:	40.8	35.3	1.43

The frequency durations at both test sites showed very good agreement but differed markedly in the time durations. The long time durations computed for the NUOS data may be attributed to the high ripple in the frequency response of the LC-10 probe. Figure 4C-18 shows the rms bandwidth-time product as a function of range (on-axis). The product averaged 0.85 and 1.43 at Edo and NUOS, respectively. This implies that there are essentially two samples available for coherent processing for every signal pulse received.

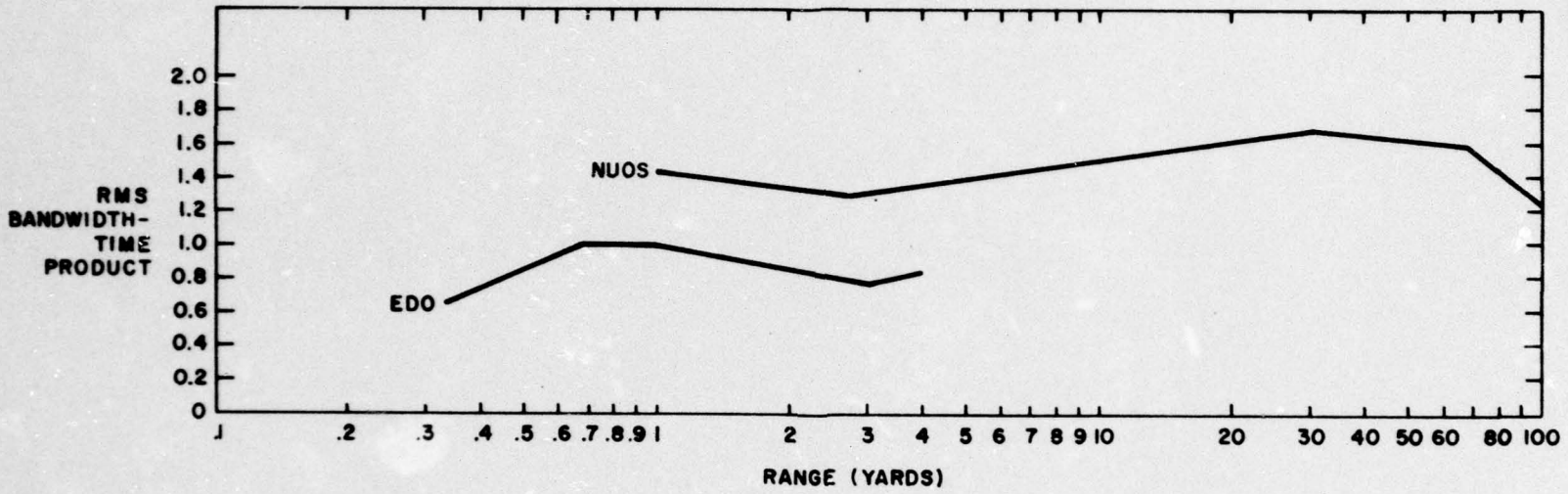

Figure 4C-18. RMS Bandwidth - Time Product vs Range (On-Axis)

Part 4D

Directivity

The transient signal generated by the IMP was highly directional. The directive properties of the signal are dependent on the pulse duration and the physical dimensions of the piston. Directivity patterns were constructed from pressure waveforms recorded in 7-1/2 (Edo) and 5 (NUOS) degree increments ± 45 degrees with respect to the acoustic axis in the azimuthal plane.

At ranges of 1 foot to 5 yards, the receiving probe was rotated about an axis lying in the plane of the acoustic window. For ranges greater than 5 yards the probe was fixed at the desired range by the tower-tripod and the IMP rotated via a turntable. Although the axis of rotation was now at the center of the IMP, the error incurred was negligible for the ranges under consideration. The time required to measure a directivity pattern was approximately 2-1/2 hours.

The directive properties of the IMP waveform were characterized by peak and iso-time patterns. The iso-time pattern was computed at the time that the pressure waveform reached its maximum value on-axis. Both patterns were rather symmetrical at all ranges. At the time of the peak maxima on-axis, the pressures at other bearings had not reached their peak values due to the increase in rise time which resulted in the iso-time pattern being steeper than the peak pattern. The increase in rise time was caused by the high frequency content off-axis being significantly reduced as compared to the on-axis spectra.

The peak and iso-time patterns at ranges of 1 foot, 2 feet, and 1 yard at Edo are shown in figures 4D-1 through 4D-3, and are normalized with respect to the peak pressure at 1 foot (on-axis). The beamwidth of the peak patterns at the -3 db level was approximately 30°. The influence of range upon the shape of the peak patterns is shown in figure 4D-4.

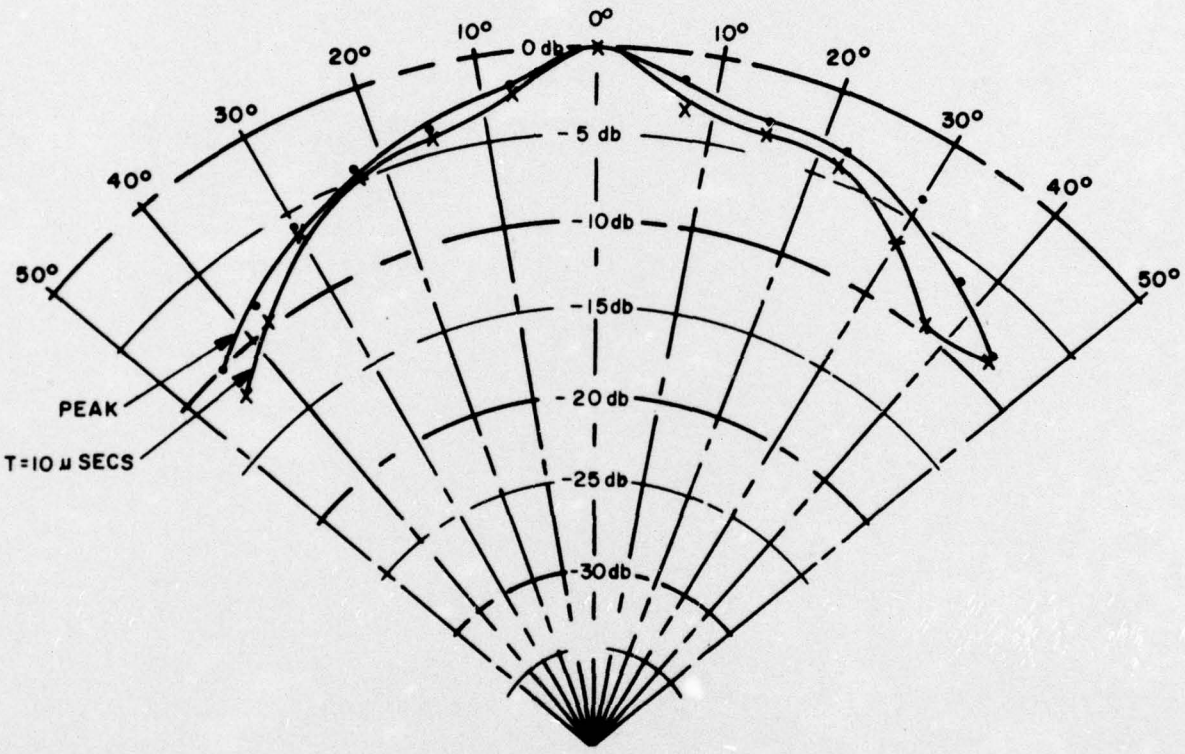

Figure 4D-1. Peak and Iso-Time Patterns at 1 Foot (Edo)

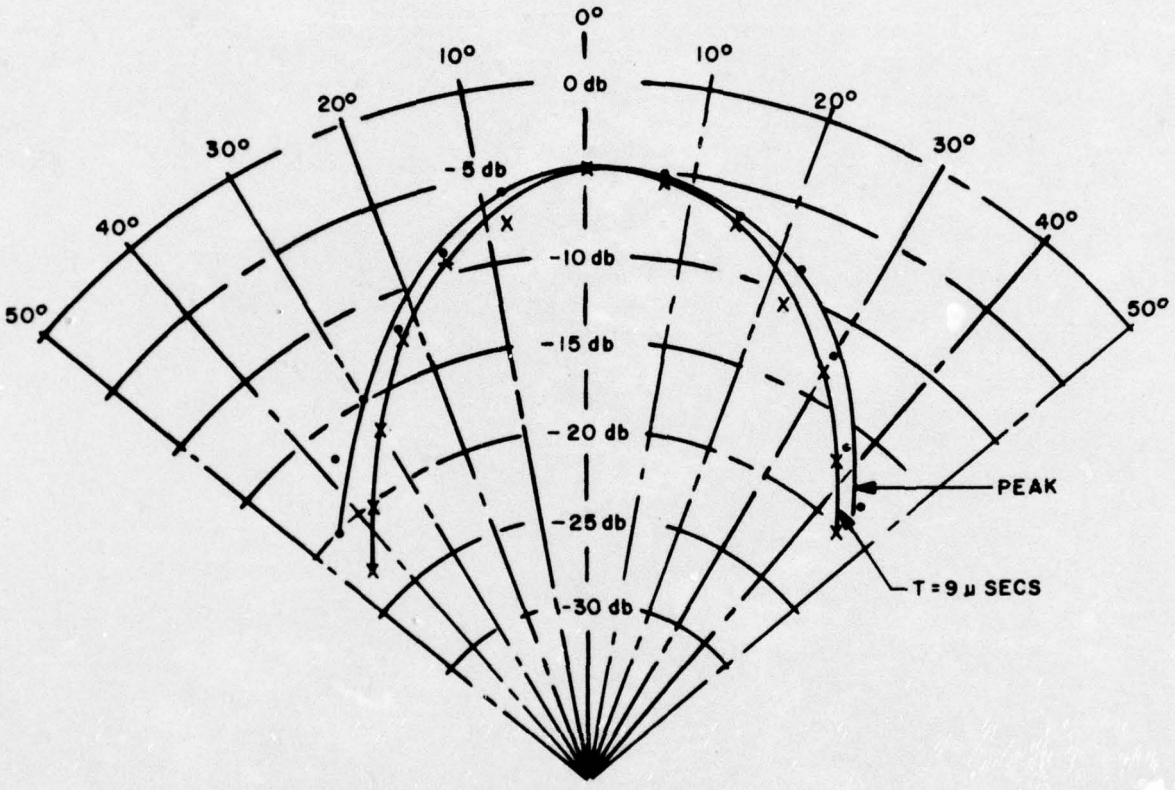

Figure 4D-2. Peak and Iso-Time Patterns at 2 Feet (Edo)

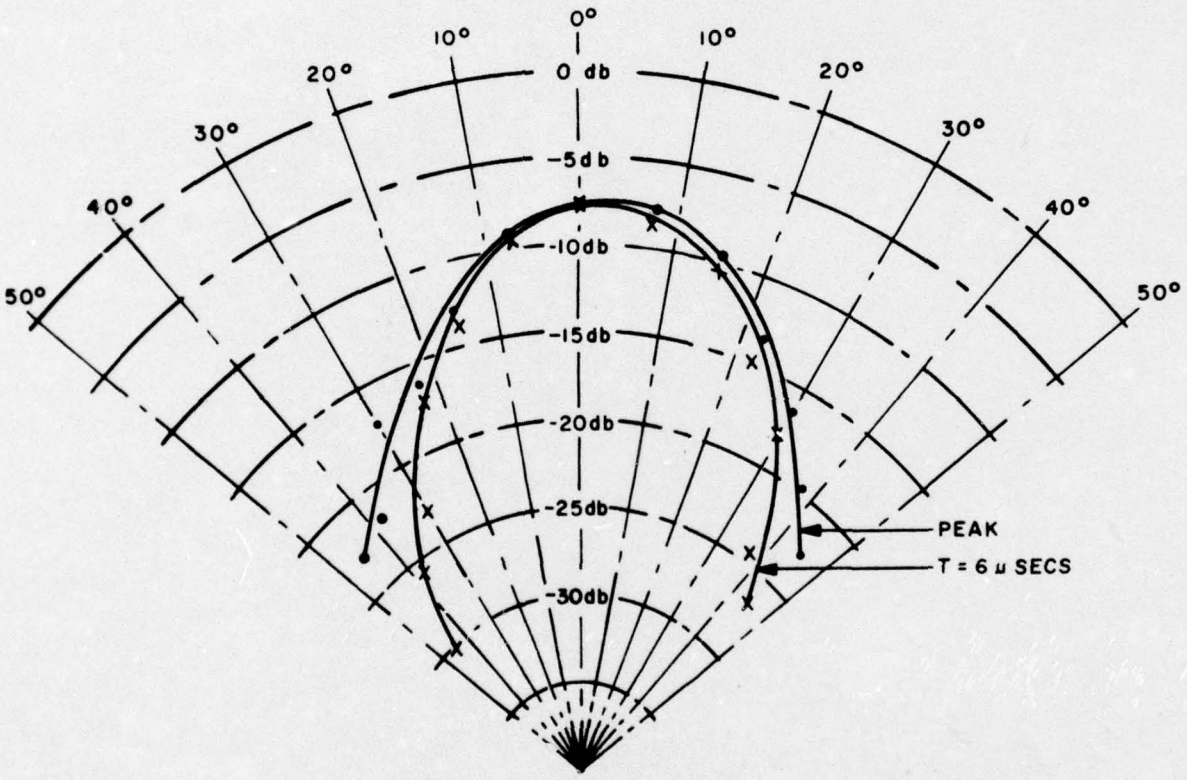

Figure 4D-3. Peak and Iso-Time Patterns at 1 Yard (Edo)

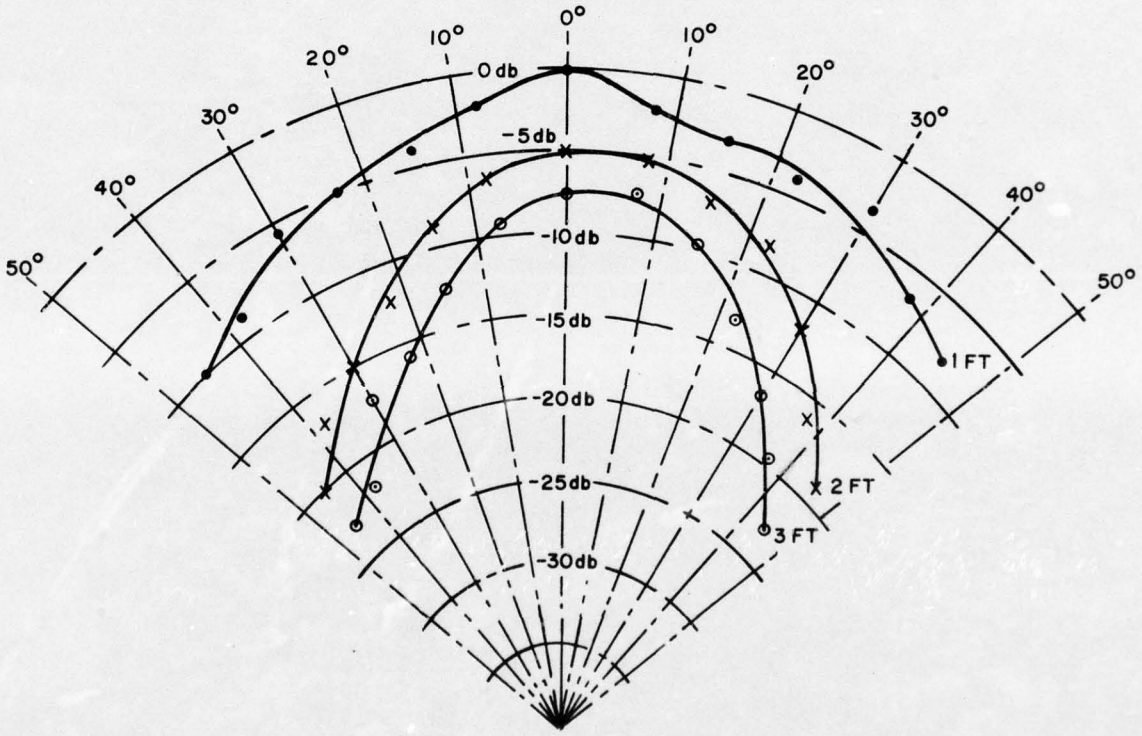

Figure 4D-4. Influence of Range on Peak Patterns (Edo)

The directivity patterns taken at NUOS are shown in figures 4D-5 though 4D-12. For distances of 1 yard and less, the patterns were quite broad, similar to those measured at Edo. At 1 yard, the -3 db beamwidth measured approximately 26°. For ranges greater than 3 yards, the patterns were much narrower where the beamwidth varied from 14° to 20° (17 ±3°).

It is highly significant that none of the patterns indicated any sidelobe structure within the ±45° sector. A rigid C-W circular piston with a -3 db beamwidth of 17° would have its first sidelobe maxima at a bearing 30° with respect to its maximum response axis. This suggests that the wideband nature of the transient acts to smooth or suppress the sidelobes inherent in the "single-frequency" pattern.

The effective C-W pressure patterns having the amplitude-phase spectra of the IMP signals generated on-axis are shown in figures 4D-13 and 4D-14, which are enclosed in an envelope bound to the back cover of this report. The transparencies are to be superimposed on the patterns at the indicated ranges for proper comparison. The effective C-W pressure patterns were generally much broader and more consistent with range than the peak or iso-time patterns and had a -3 db beamwidth of 22°. These pattern differences may have been caused by an anomaly resulting in a departure from the law of linear superposition or by selecting an incorrect "single-frequency" directivity pattern for spectral weighting (the IMP was considered a rigid circular piston). The -3 db beamwidth as a function of range is shown in figure 4D-15 for the peak, iso-time, and effective C-W pressure patterns at NUOS.

Measurements have shown that the acoustic pulse increases in width as the bearing increases with respect to the acoustic axis. This is due to the natural suppression of the high frequency content off-axis. There was relatively little dependence of pulsewidth with range for those ranges where frequency absorption was negligible. The pulsewidth as a function of bearing is shown for several ranges in figures 4D-16 and 4D-17.

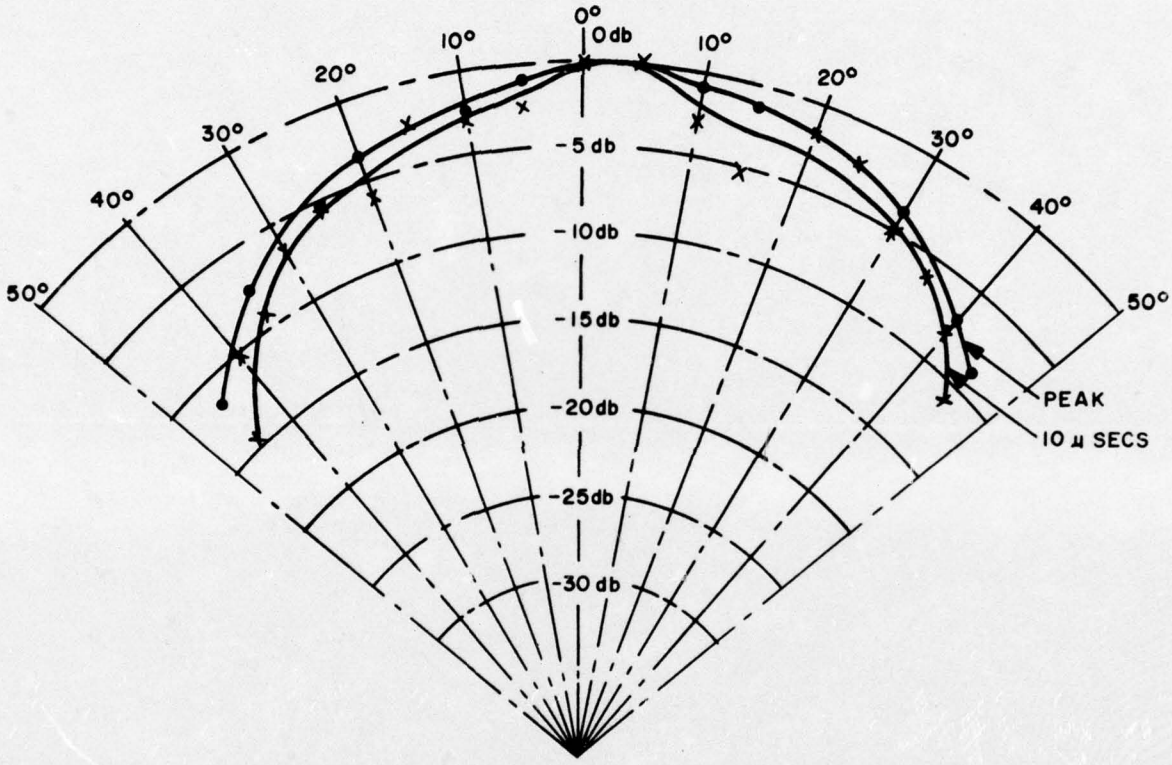

Figure 4D-5. Peak and Iso-Time Patterns at 1 Foot (NUOS)

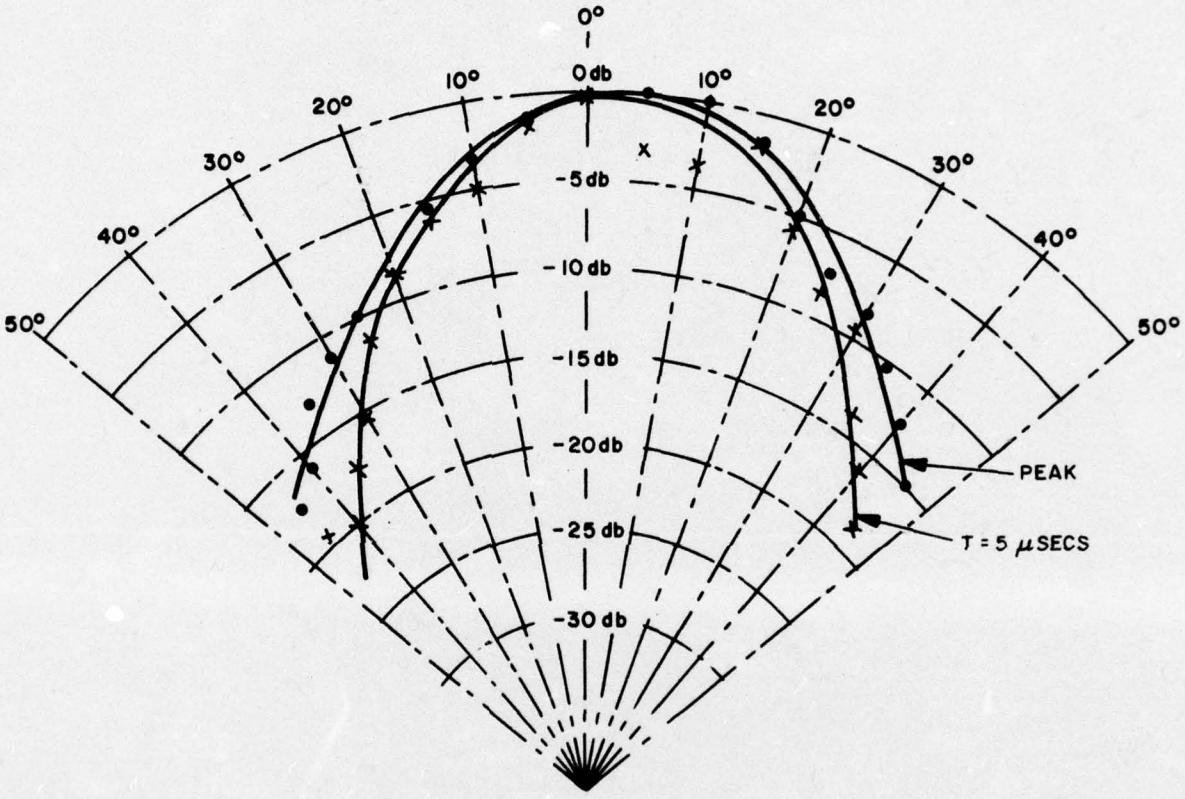

Figure 4D-6. Peak and Iso-Time Patterns at 2 Feet (NUOS)

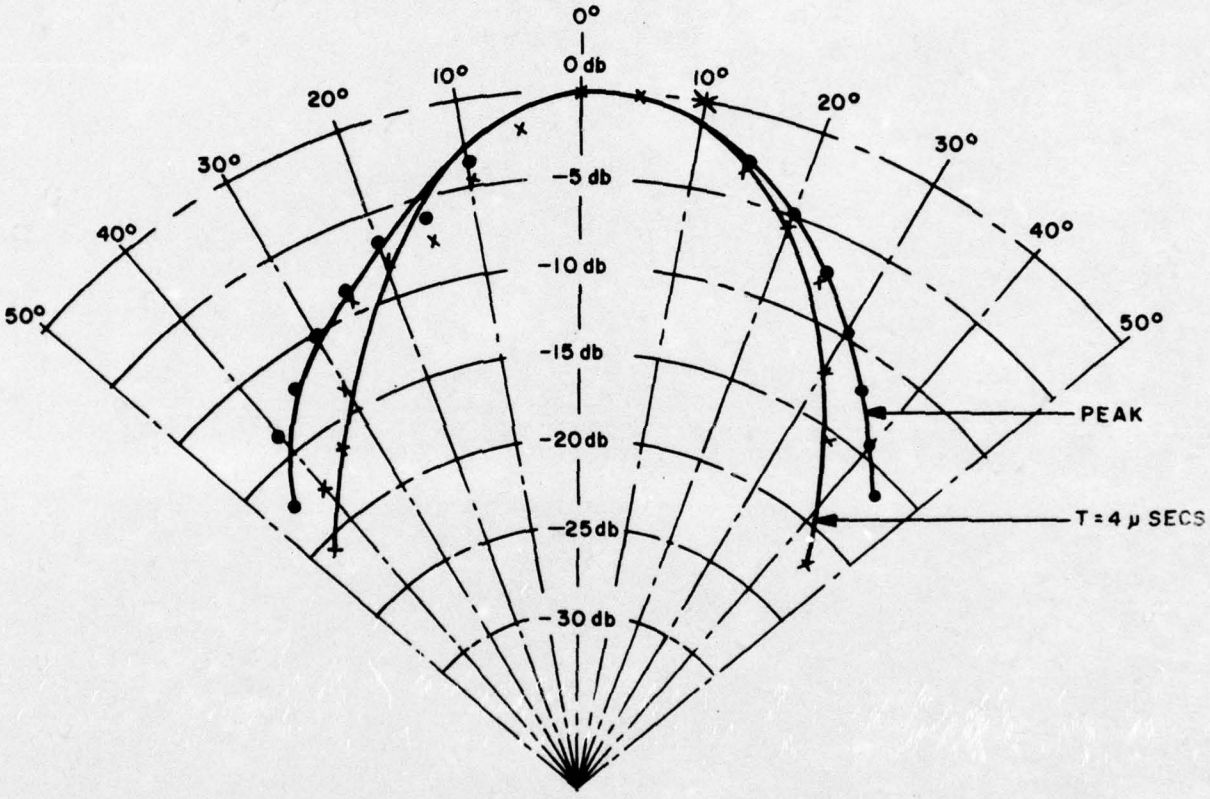

Figure 4D-7. Peak and Iso-Time Patterns at 1 Yard (NUOS)

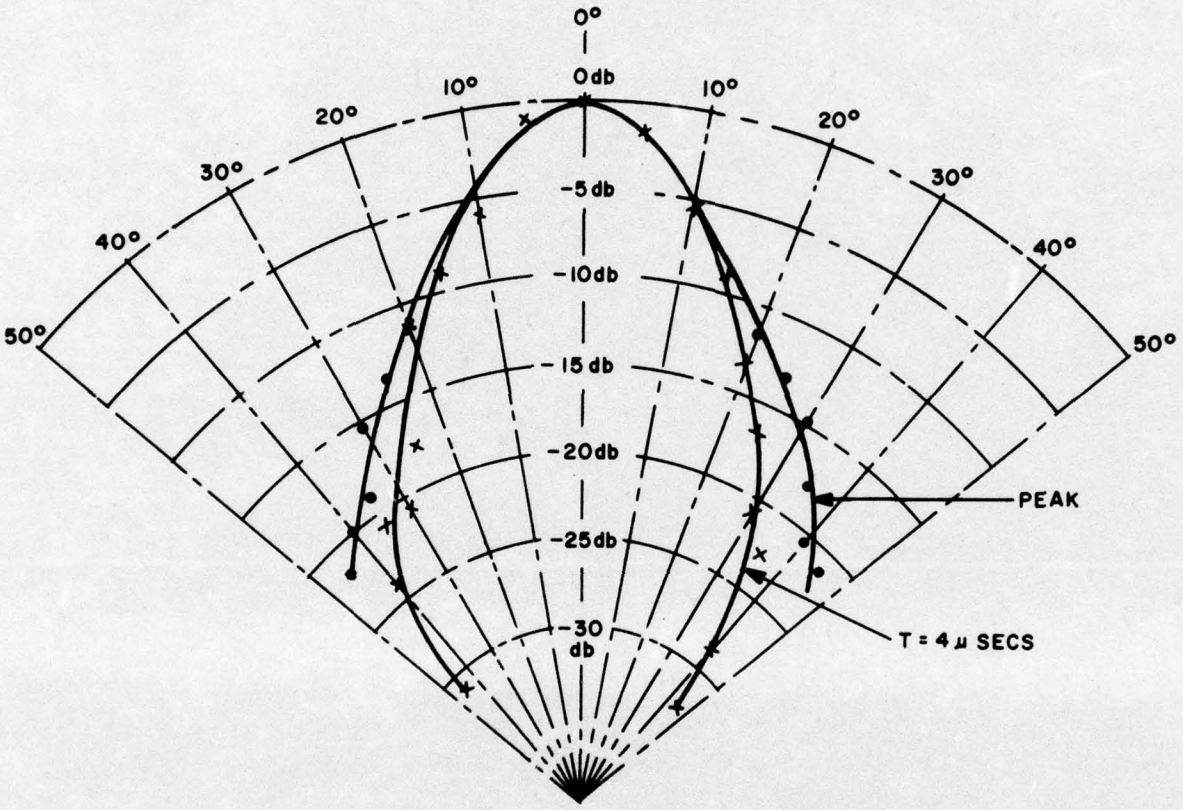

Figure 4D-8. Peak and Iso-Time Patterns at 3 Yards (NUOS)

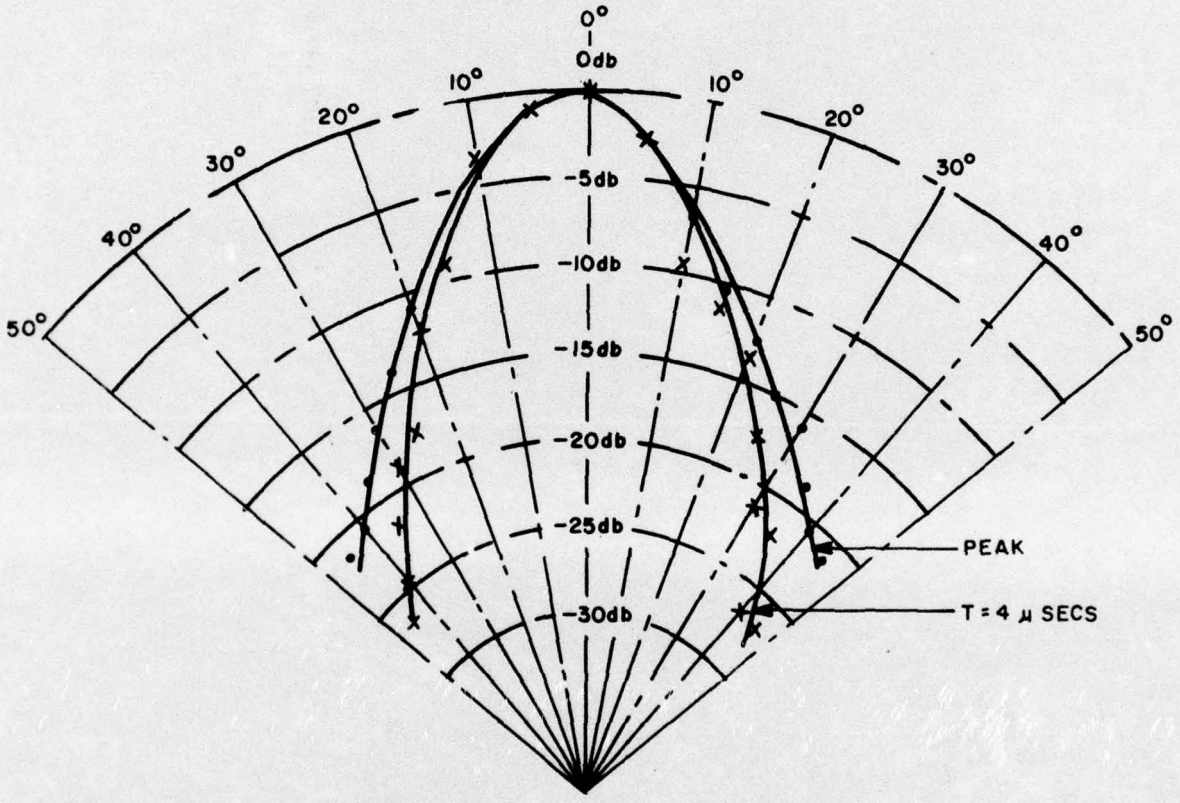

Figure 4D-9. Peak and Iso-Time Patterns at 5 Yards (NUOS)

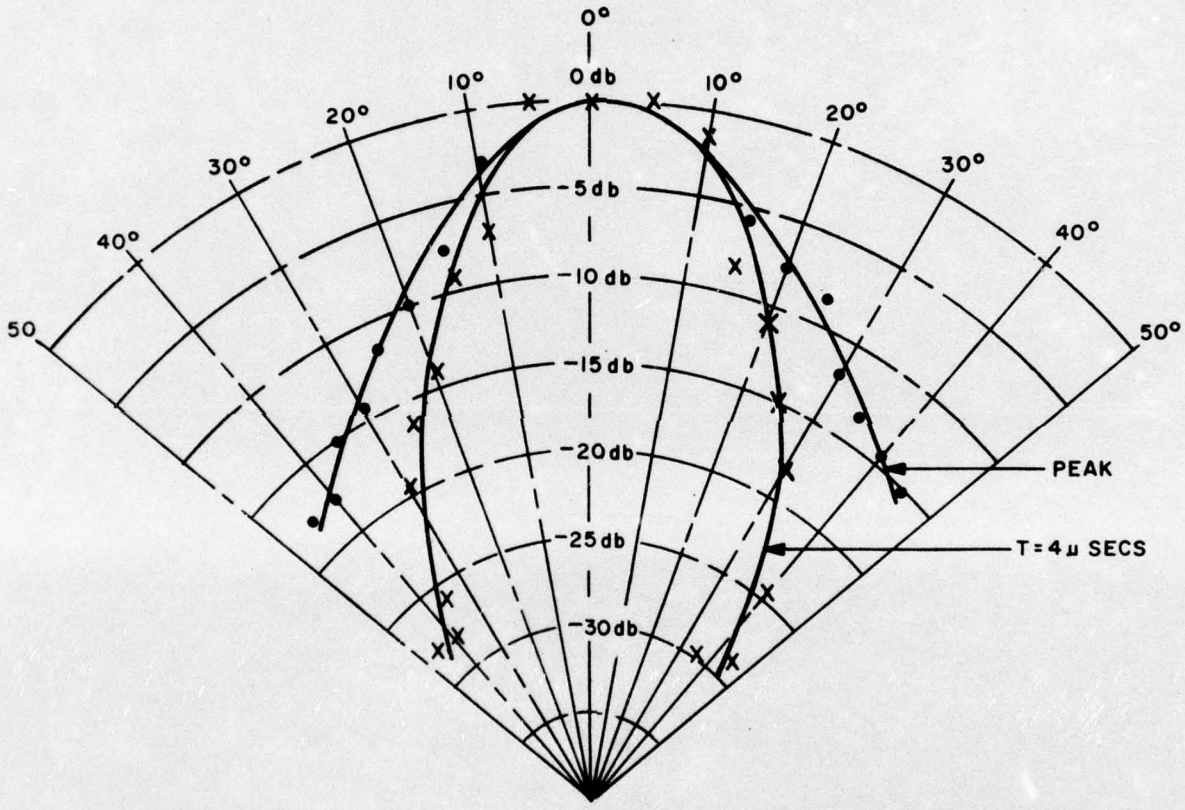

Figure 4D-10. Peak and Iso-Time Patterns at 30 Yards (NUOS)

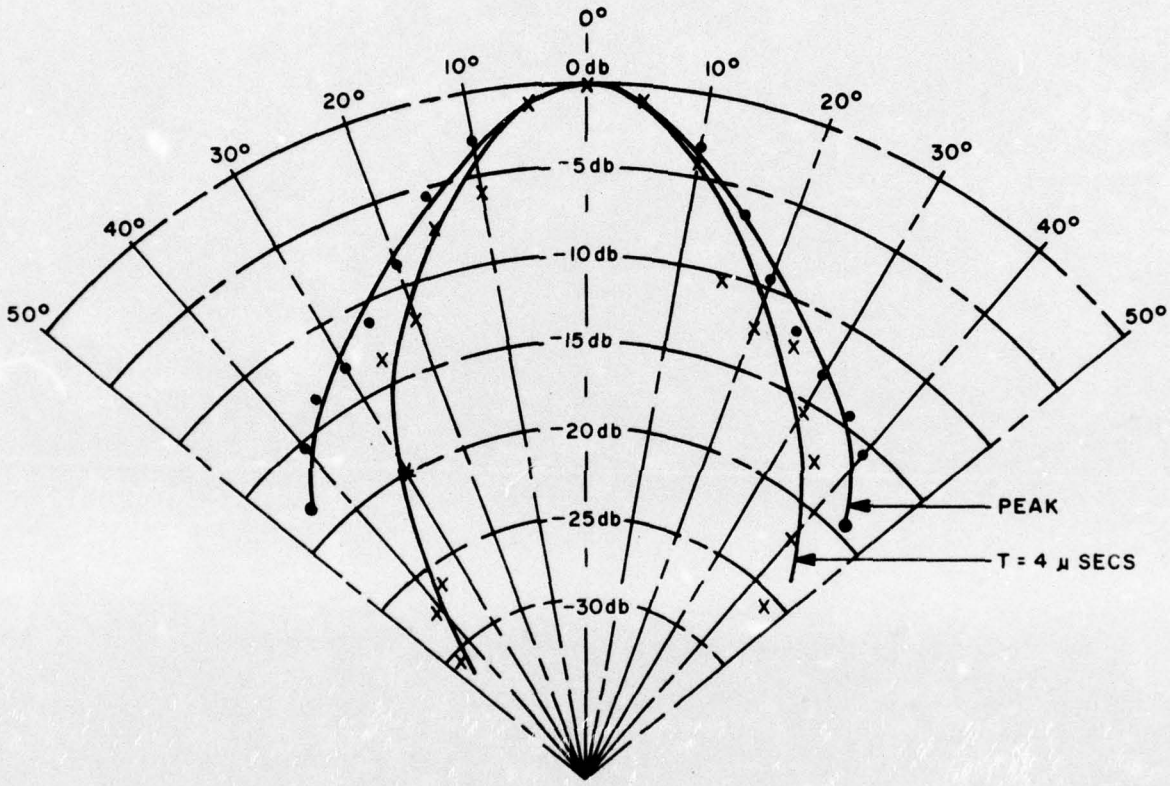

Figure 4D-11. Peak and Iso-Time Patterns at 67 Yards (NUOS)

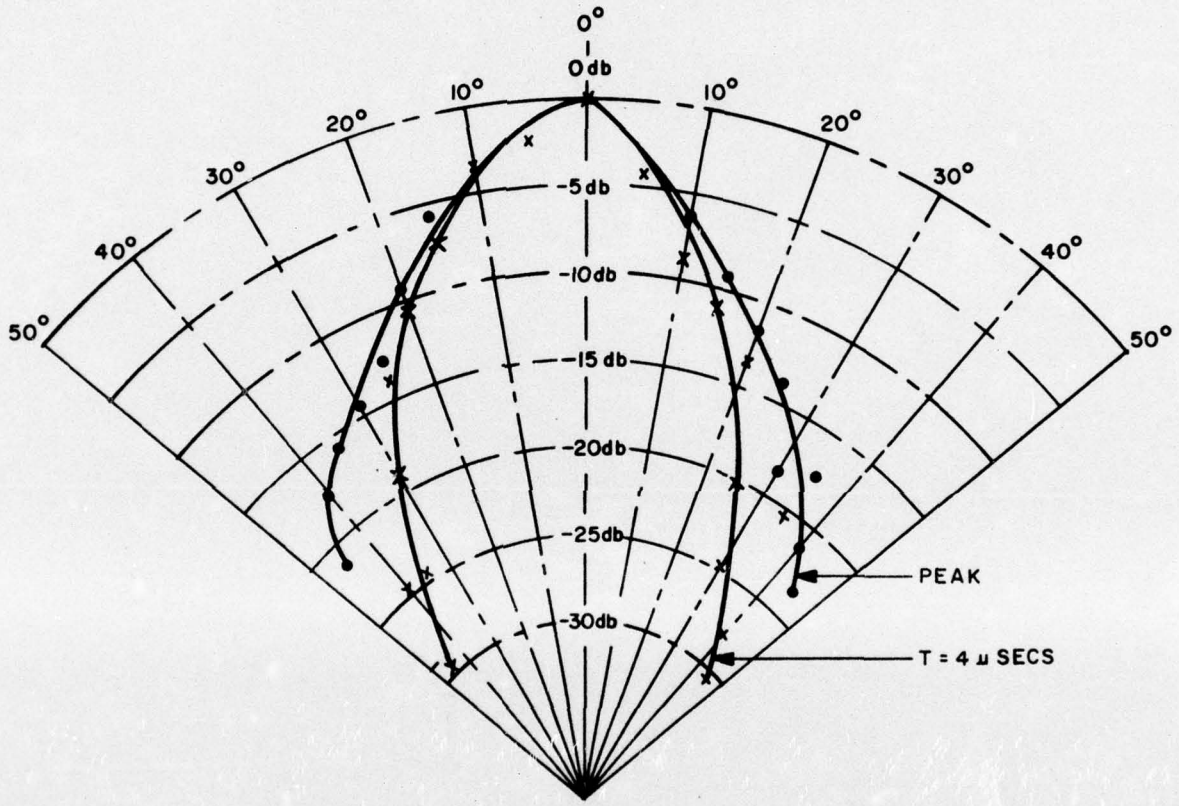

Figure 4D-12. Peak and Iso-Time Patterns at 107 Yards (NUOS)

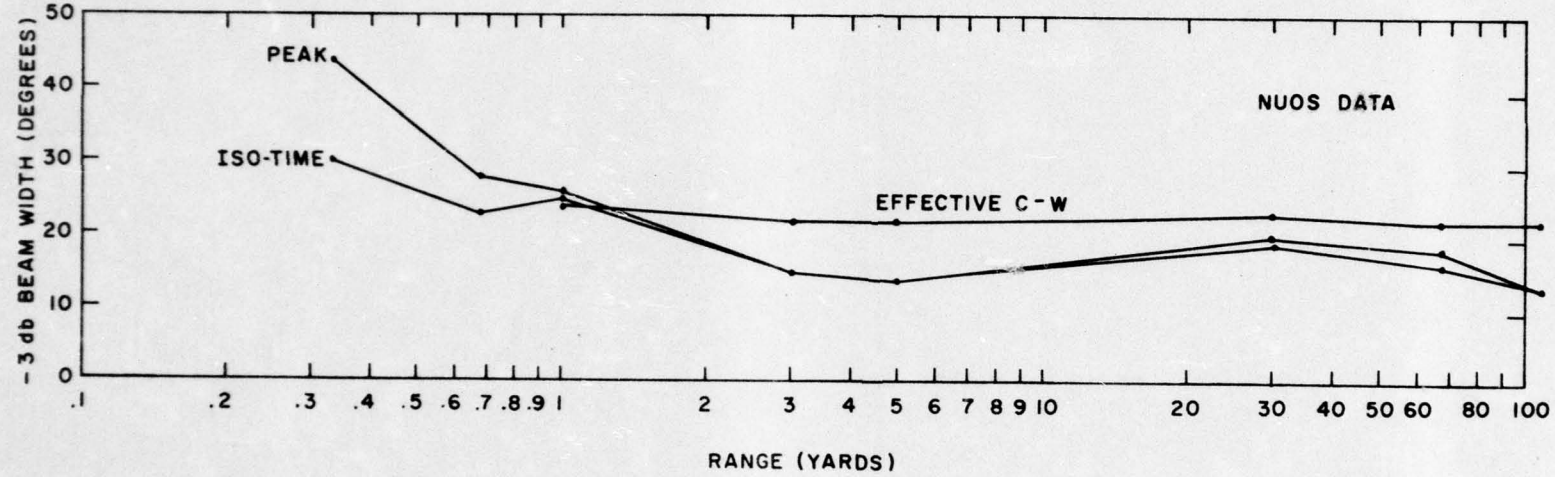

Figure 4D-15. The -3 db Beamwidth vs Range

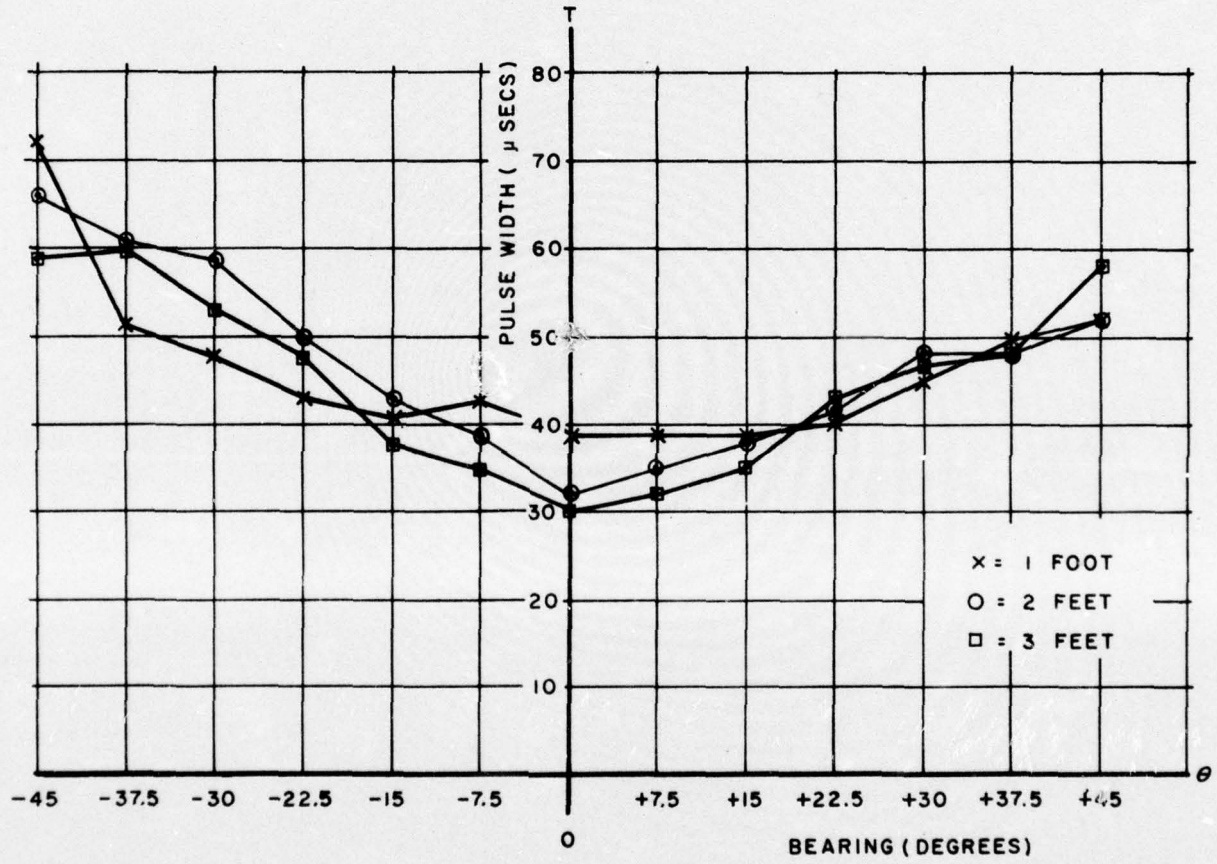

Figure 4D-16. Pulsewidth vs Bearing (Edo)

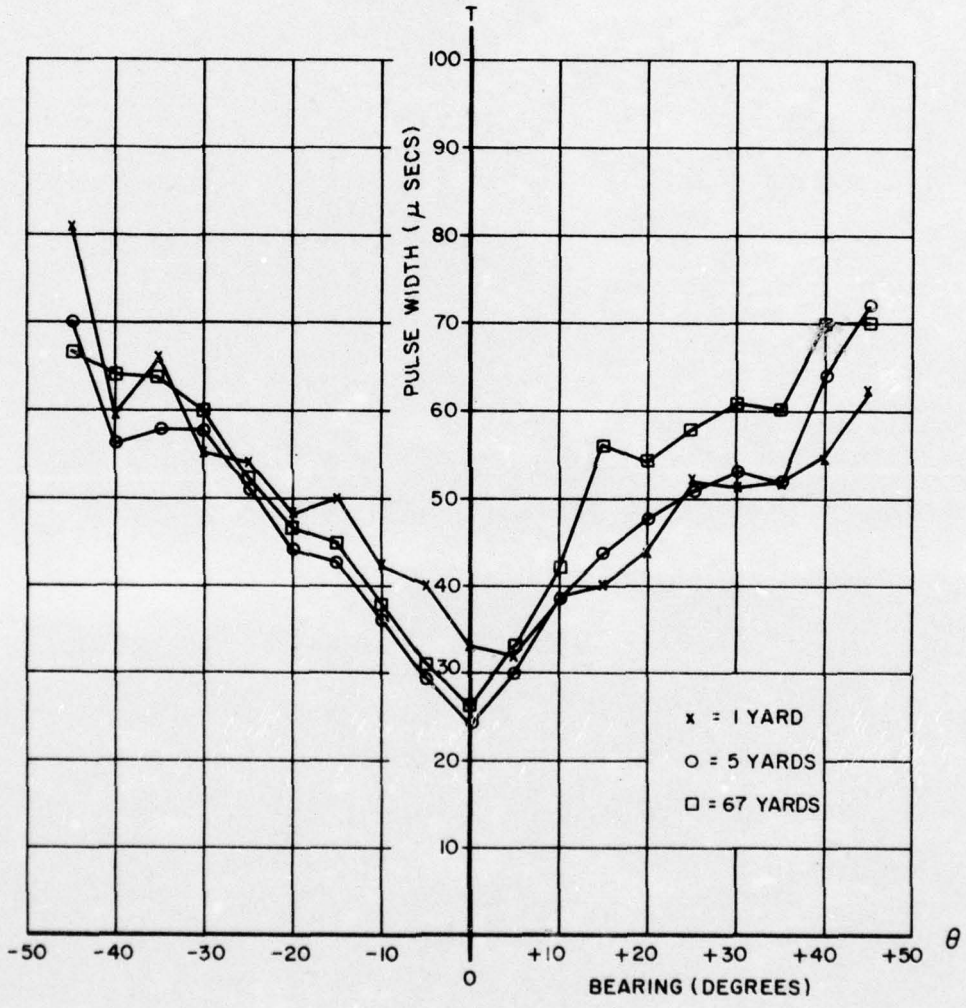

Figure 4D-17. Pulsewidth vs Bearing (NUOS)

In general, the resultant waveform at any point in the acoustic field is the superposition of waves which radiate from different points on the radiating aperture. Consider a single frequency and two arbitrary points on the aperture. If these points were spaced such that the difference in their distances to a given field point was equal to a half-wavelength, then the energy emanating from the aperture points would cancel each other completely. If the path difference was equal to a wavelength, there would be complete addition. For a wide-band signal, the physical picture is much more complicated since this process of signal formation would occur for every component in the spectrum. As the bearing deviation is increased, the interference between the energy from various aperture points will decrease the amplitude response relative to that at broadside and will cause the response to be spread over a longer period of time. A further increase in bearing would eventually minimize the interference resulting in a time response comprised of more than one pulse. In the test program, the waveform at large bearing deviations was approaching two separate pulses. This is shown in the recorded waveform in figure 4D-18 where the probe (LC-10M-1) was placed in the end-fire position. The total duration of the waveform was 180 microseconds which corresponds approximately to the diameter of the IMP divided by the velocity of sound.

The temporal growth and decay of the transient pattern at 67 yards is shown in figures 4D-19 and 4D-20a through 4D-20f which are essentially iso-time patterns. The temporal decay from t = 4 to approximately t = 20 microseconds was characterized by a progressive flattening and broadening of the pattern with loss of peak amplitude. The time instant for determining the pattern was then approaching the pulsewidth on-axis. At this time, the responses at bearings greater than 5° off the acoustic axis were starting to reach their peak values. This resulted in a "difference-type" pattern as shown in figure 4D-20f.

AD-A031 794 EDO CORP COLLEGE POINT N Y F/G 17/1
ACOUSTIC TRANSIENT SIGNAL STUDY.(U)
JUN 66 A A WINDER, A N COHEN NONR-3346(00)
UNCLASSIFIED EDO-7087 NL

2 OF 2
AD A031794

END

DATE FILMED
12-76

Figure 4D-18. Pressure Waveform at End-fire
(26-3/4 inches from the acoustic center)

Vertical Scale: 0.1 bars/div
Horizontal Scale: 50 usecs/div

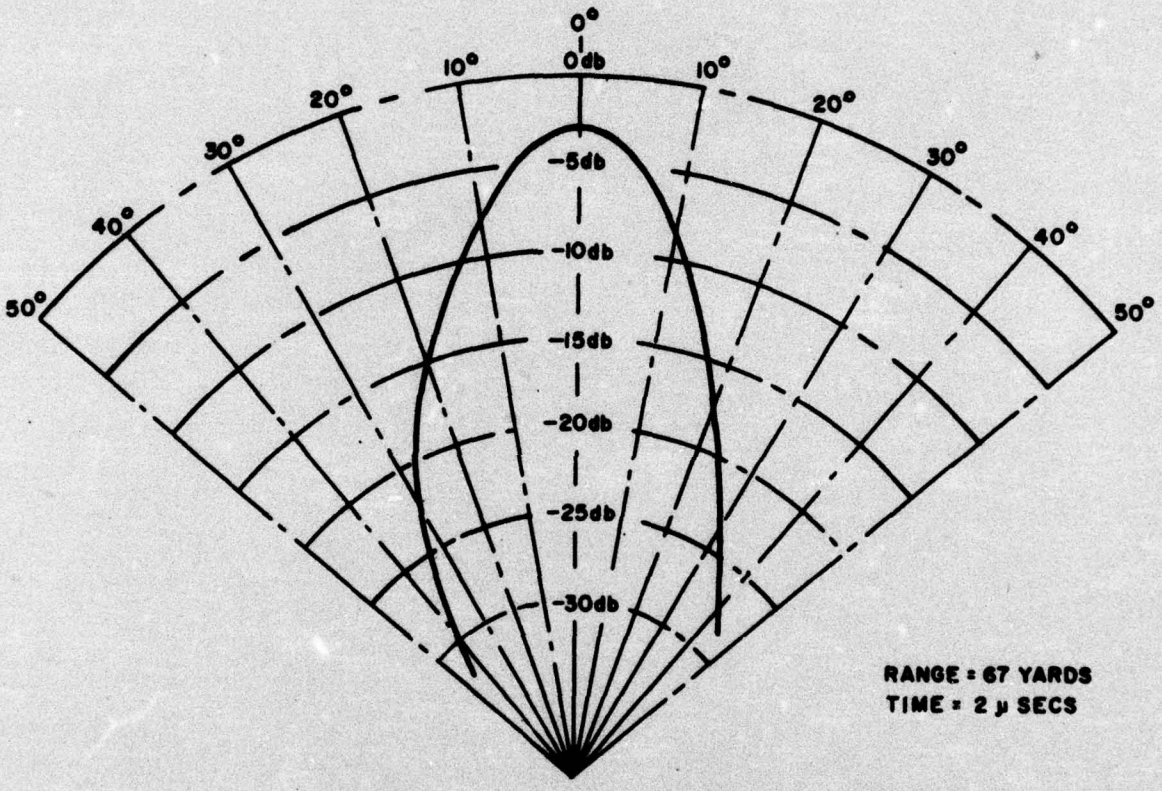

Figure 4D-19. Transient Pattern Growth

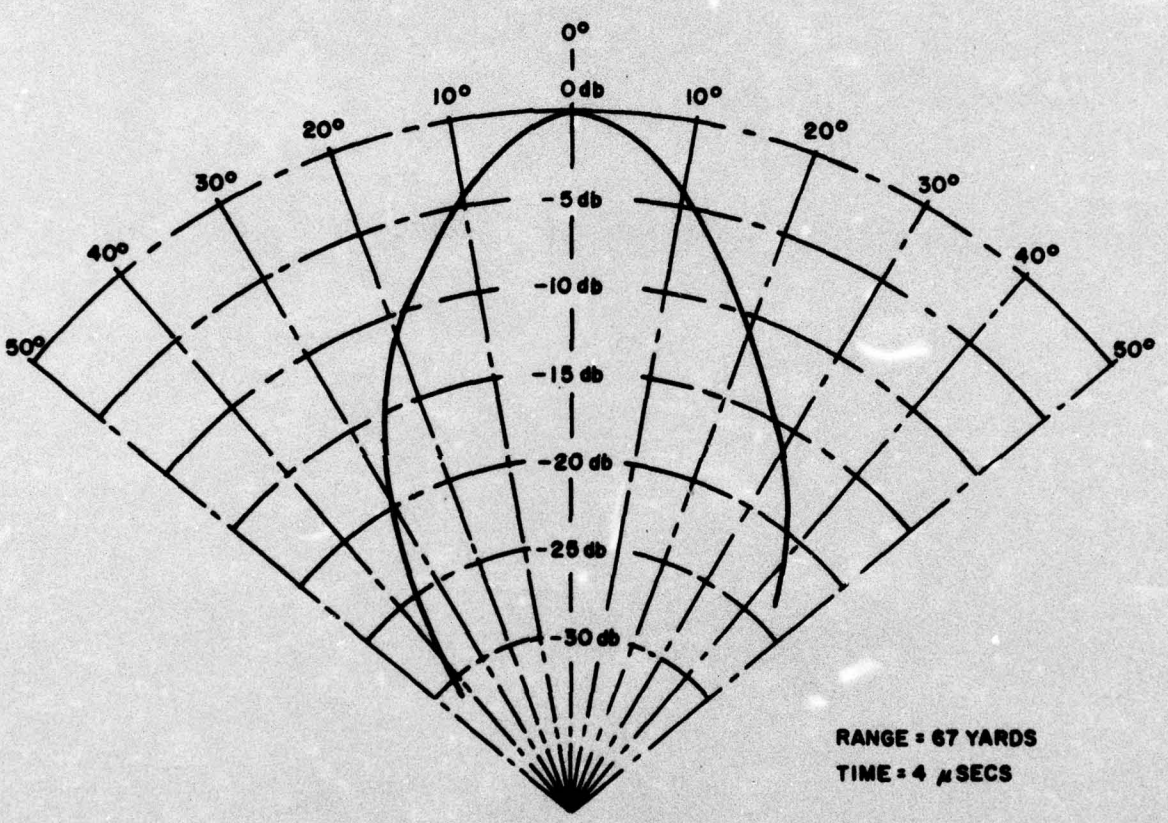

Figure 4D-20a. Transient Pattern Decay (Sheet 1 of 6)

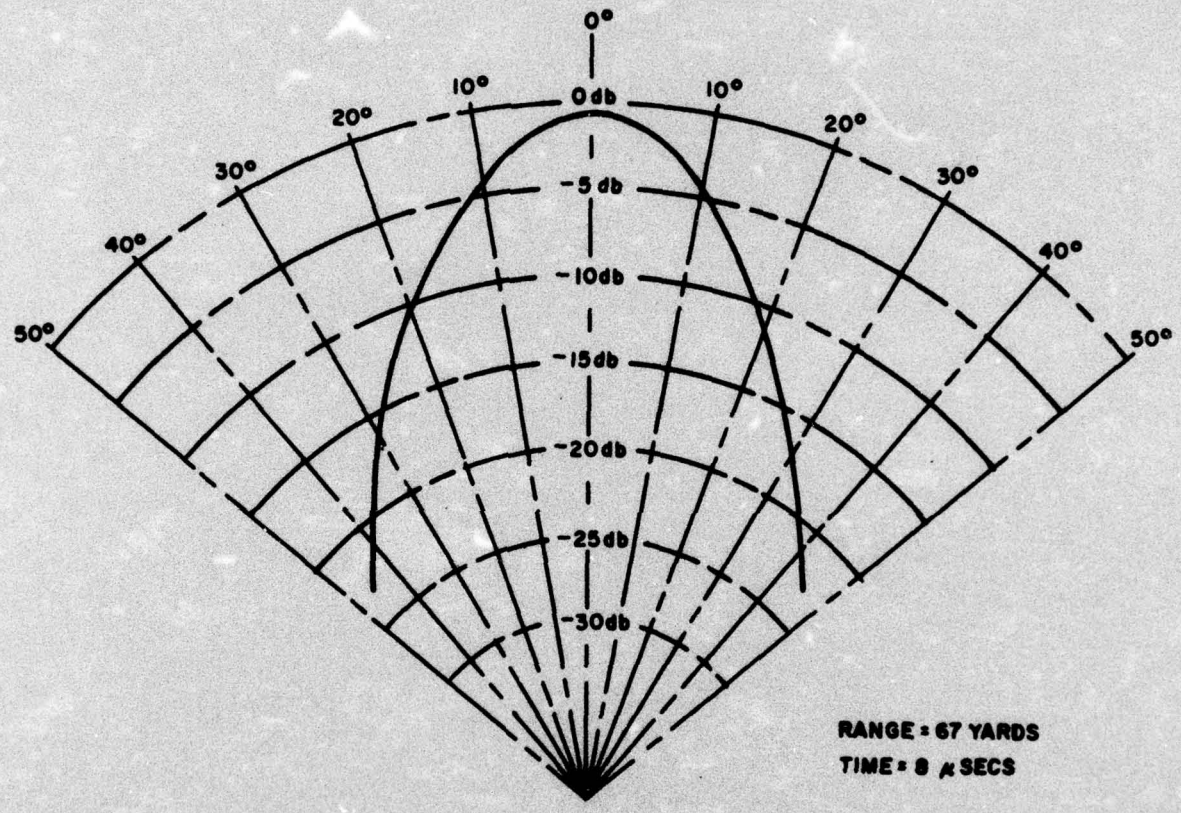

Figure 4D-20b. Transient Pattern Decay (Sheet 2 of 6)

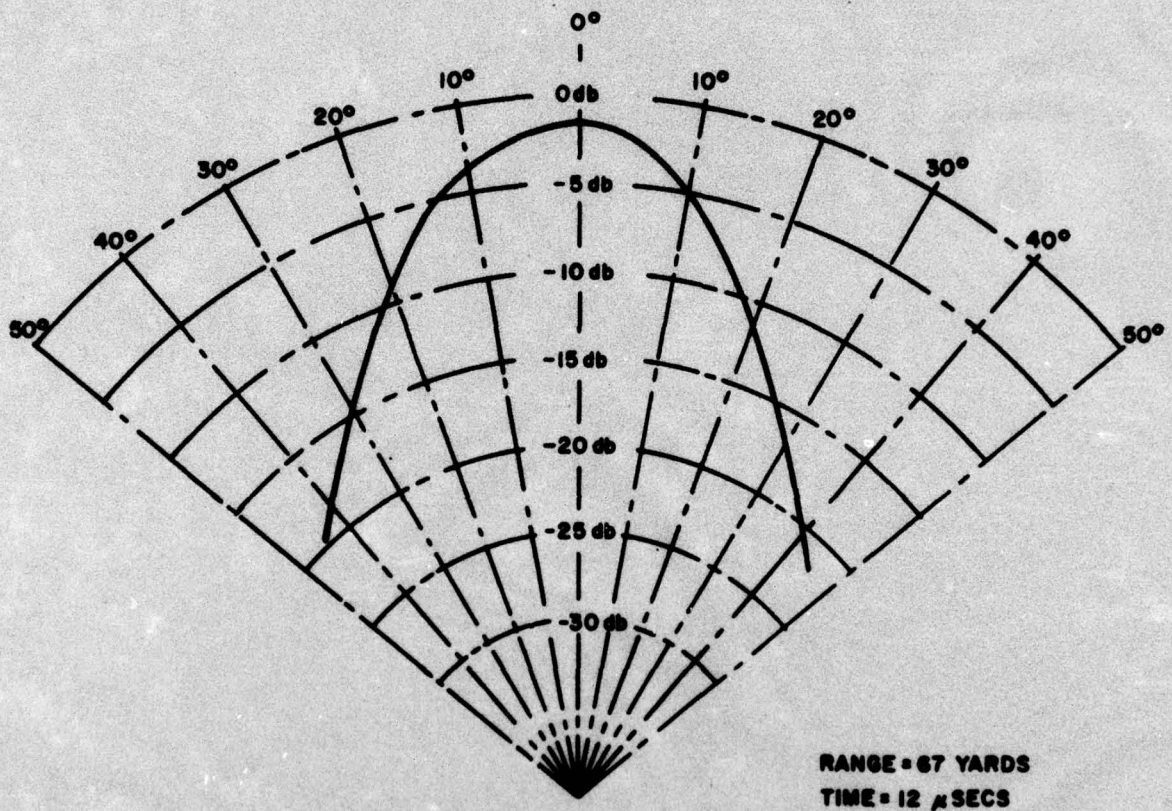

Figure 4D-20c. Transient Pattern Decay (Sheet 3 of 6)

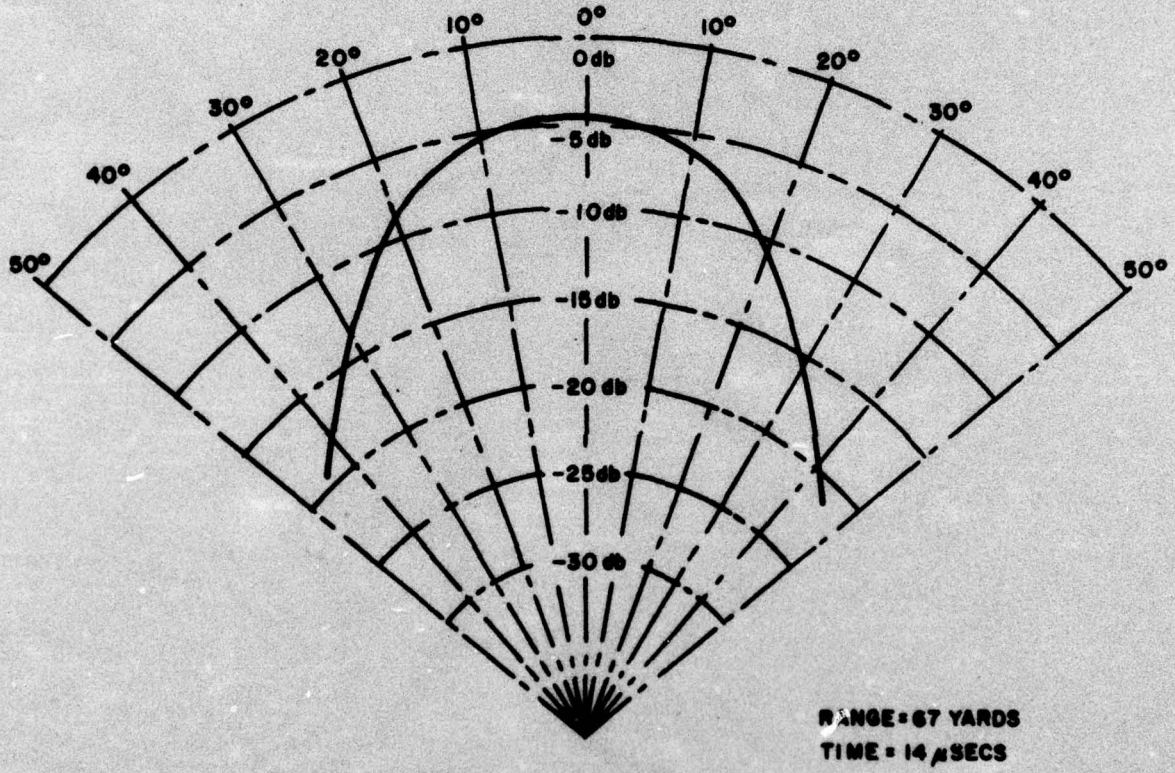

Figure 4D-20d. Transient Pattern Decay (Sheet 4 of 6)

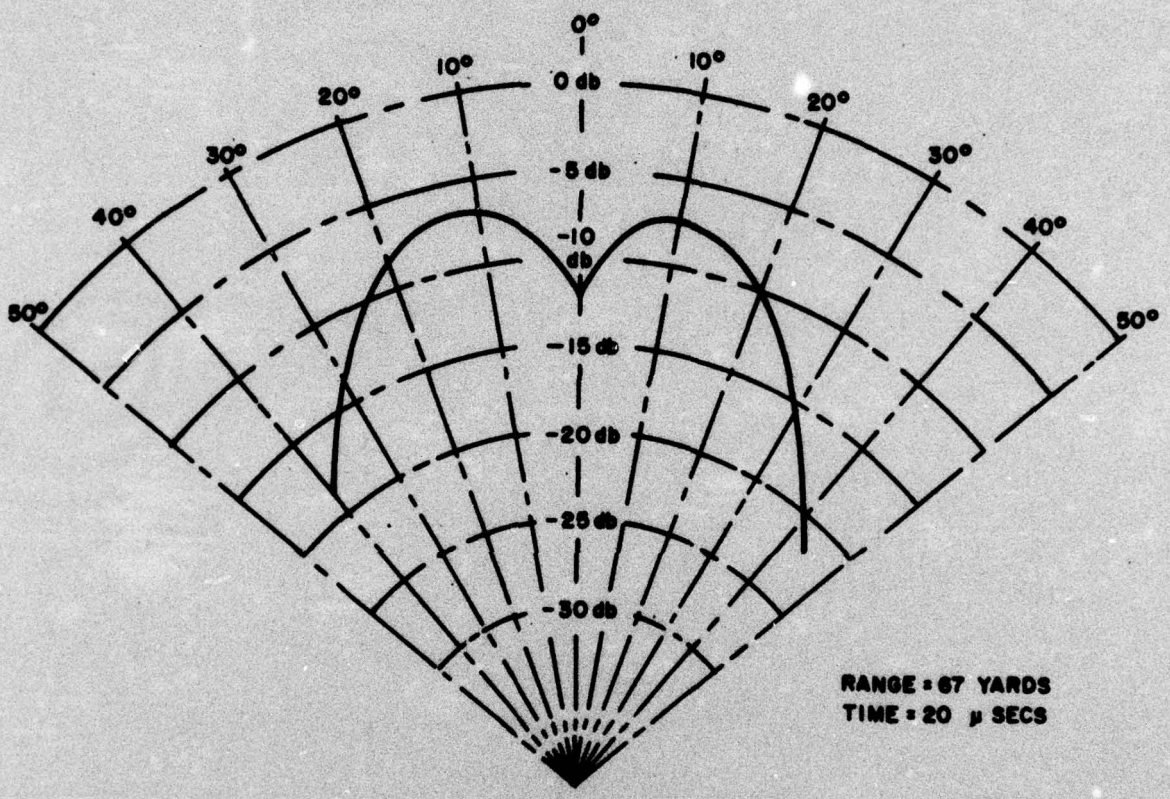

Figure 4D-20e. Transient Pattern Decay (Sheet 5 of 6)

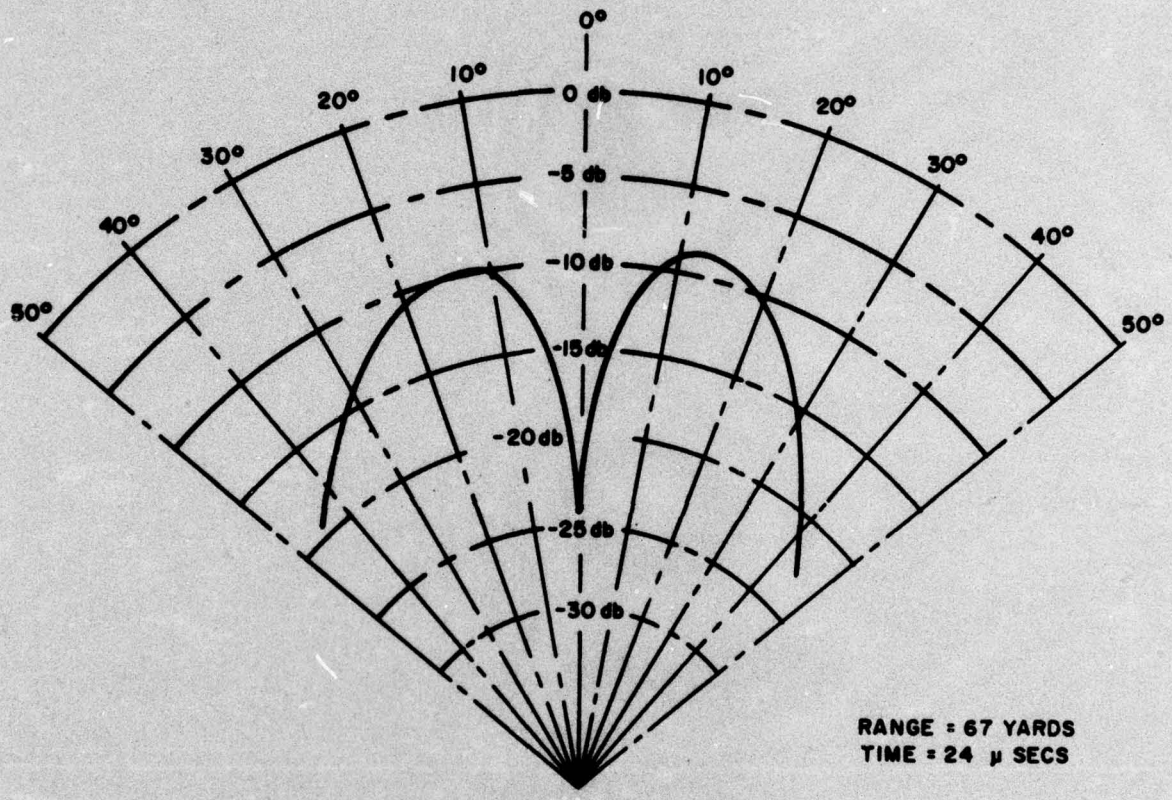

Figure 4D-20f. Transient Pattern Decay (Sheet 6 of 6)

Part 4E

Orthogonal Exponential Decomposition

Photographic slides of the IMP waveforms recorded at Edo at ranges of 1, 2, 3, 4, and 12 feet were projected on 11" × 17" graph paper and sampled manually at 4 microsecond intervals. Each signal produced on array of 50 points for computer analysis or an effective record length of 200 microseconds. The epoch, t_o, was selected to be the time of the sharp high-amplitude rise for each signal. Both the pre- and post-epoch parts of the signals were subjected to analysis, but only the post-epoch results are described. Experimentally, it was shown that with N = 10 the representation errors were in the range of

$0.007 < \frac{\langle e^2 \rangle}{\langle f^2 \rangle} < 0.027$. With N = 8, the errors were equal to or greater than 0.04.

Computer-generated plots of the five signals analyzed, together with their approximate representations, are shown in figures 4E-1 through 4E-5. The abcissae are sample numbers from 1 to 50 and the ordinates are to an arbitrary scale. The errors for post-epoch parts of the signals are:

Range (Feet)	Error (Percent)
1	2.66
2	1.01
3	0.79
4	1.04
12	1.50

The plots indicate excellent waveform fidelity for large signals and show deterioration for the low-amplitude signal tails. This is characteristic of the mean-squared-error criterion. If the lower-amplitude parts of the signal are considered to be important, then a weighting of the squared error inversely to the signal amplitude would improve the representation (at the expense of the fit at large amplitudes). Alternatively, values of N > 10

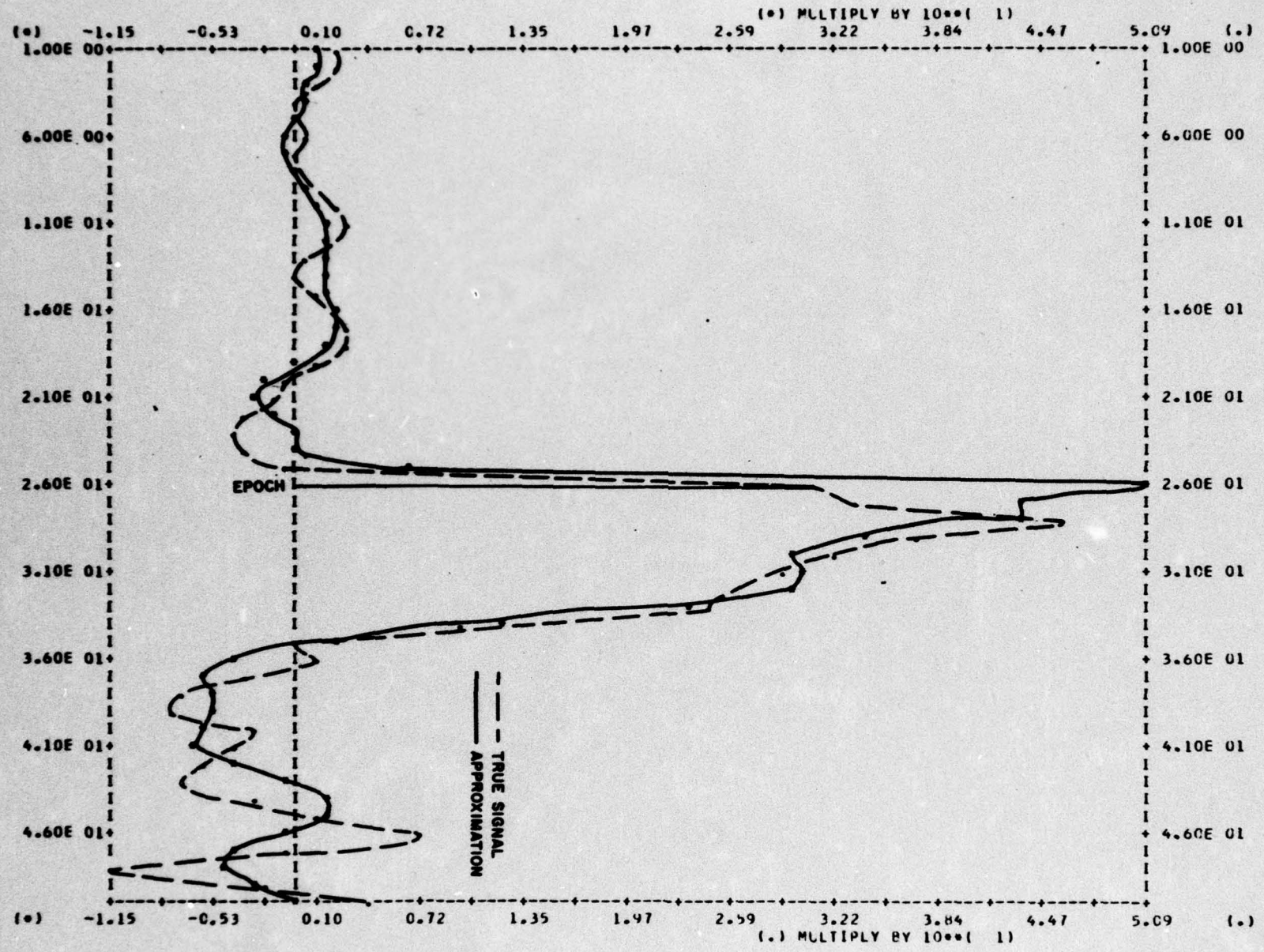

Figure 4E-1. Pressure Waveform and its Exponential Representation at 1 Foot

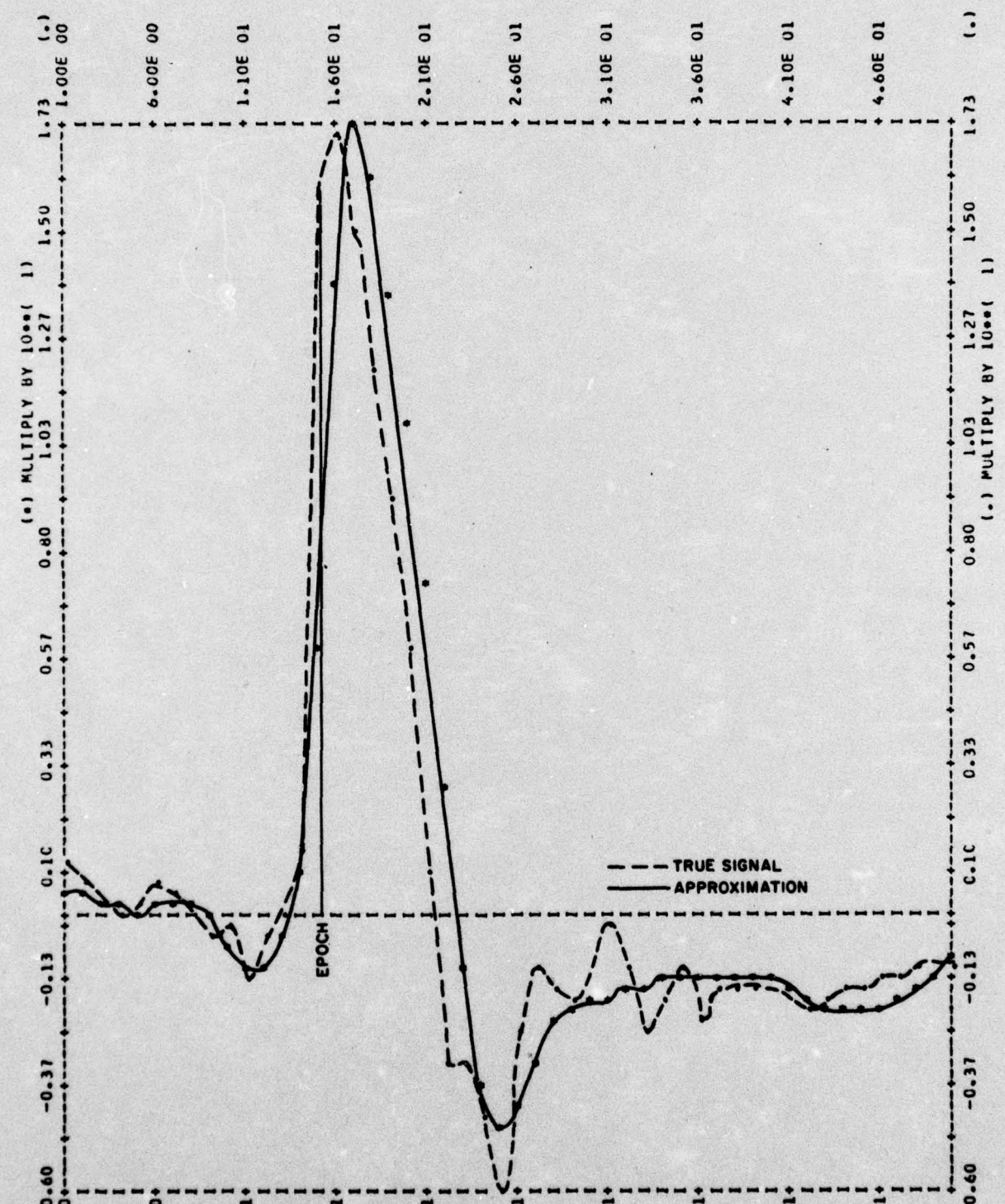

Figure 4E-2. Pressure Waveform and its Exponential Representation at 2 Feet

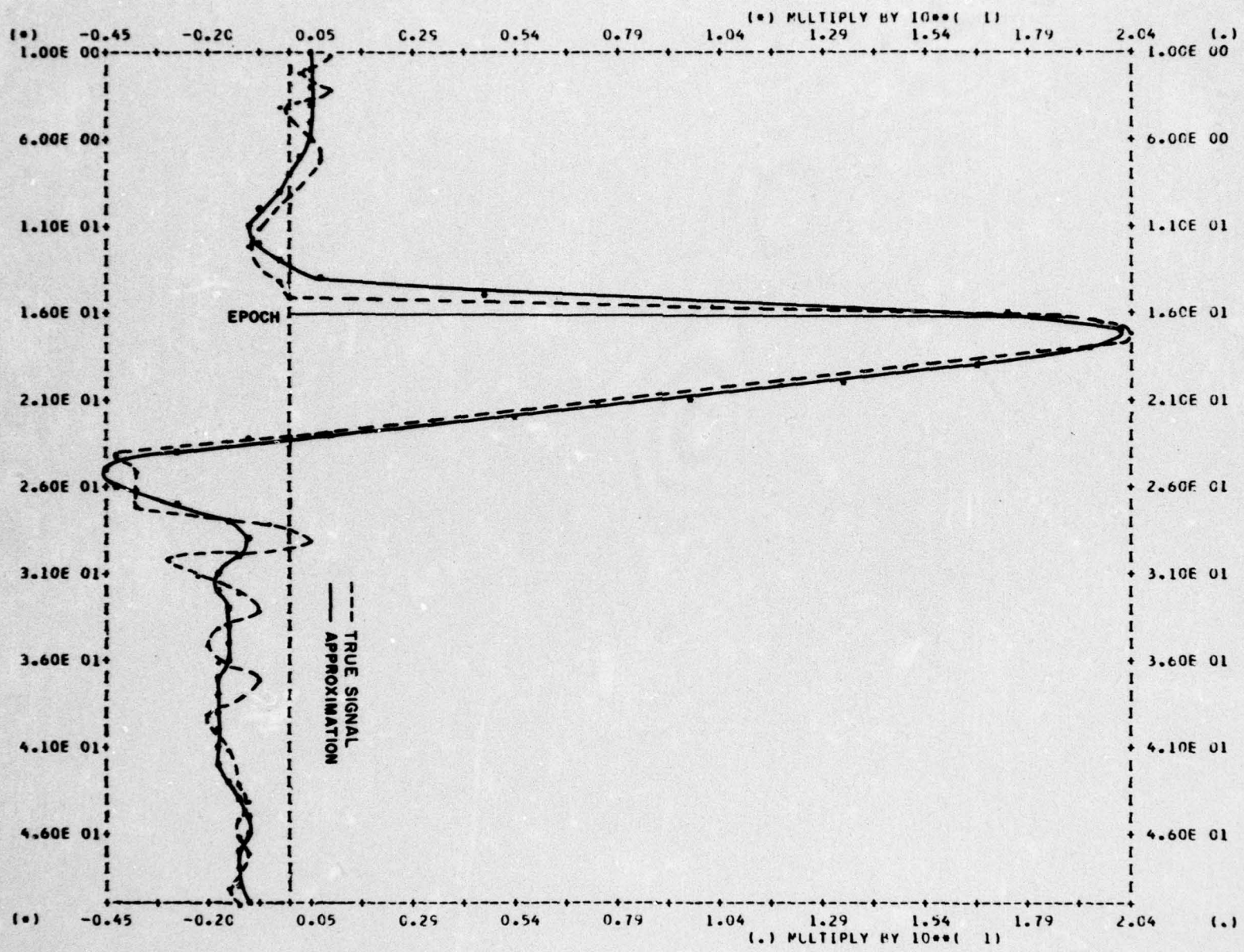

Figure 4E-3. Pressure Waveform and its Exponential Representation at 3 Feet

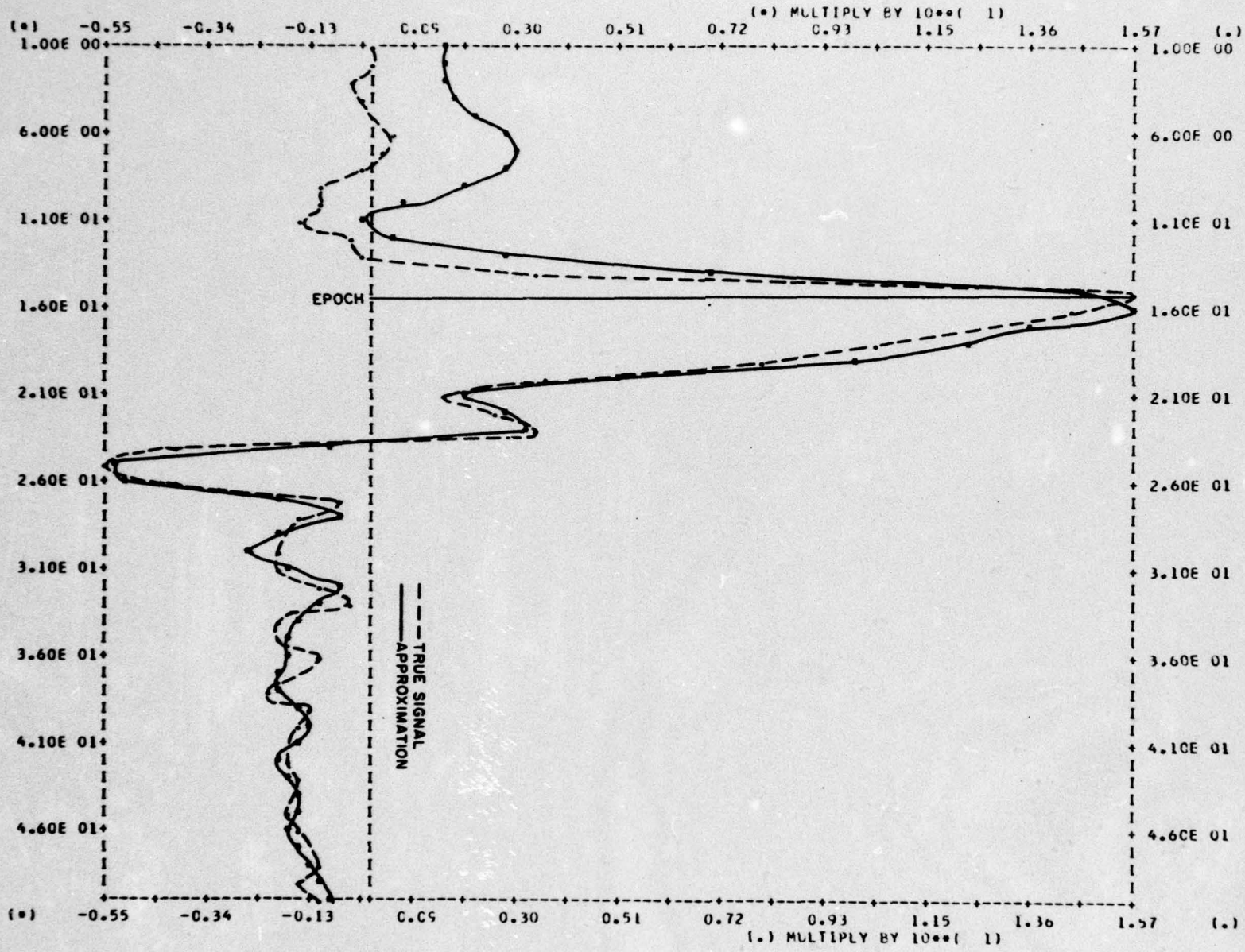

Figure 4E-4. Pressure Waveform and its Exponential Representation at 4 Feet

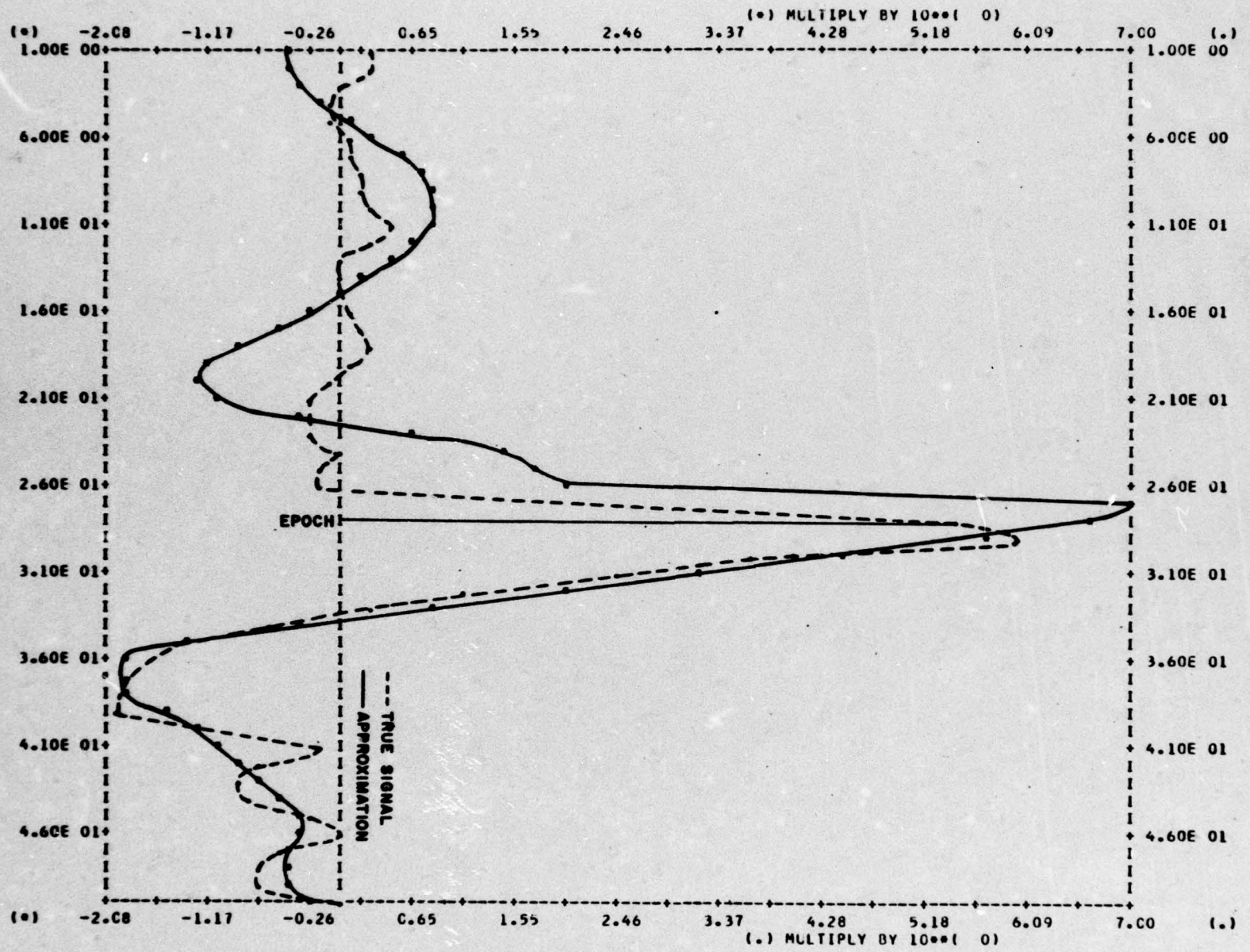

Figure 4E-5. Pressure Waveform and its Exponential Representation at 12 Feet

could be used. However, the data was not sufficient to warrant much larger values unless the sampling rate can be increased above 250 kc. Experiments are now being considered using the weighted mean-squared-error criterion and a Chebyshev (maximum absolute error) criterion.

Figure 4E-6 shows the energy spectra of the approximate post-epoch signals, i.e., of the $\left\{f_a\right\}_1^5$, from 100 cps to 10 kc. The ordinate values are an arbitrary scale. These spectra differ from the spectra of the actual signals $\left\{f\right\}_1^5$ because the pre-epoch signals were not included and the $\left\{f_a\right\}_1^5$ signals are inherently less complicated than the $\left\{f\right\}_1^5$ signals. However, general features of the spectra of the $\left\{f\right\}_1^5$ are present, including the approximate locations of maximum energy density and the apparent shift of energy to higher frequencies in the 12 foot signal. The energy spectra obtained from the exponential representations agreed well with those estimated from the correlation functions, shown in Part 4C.

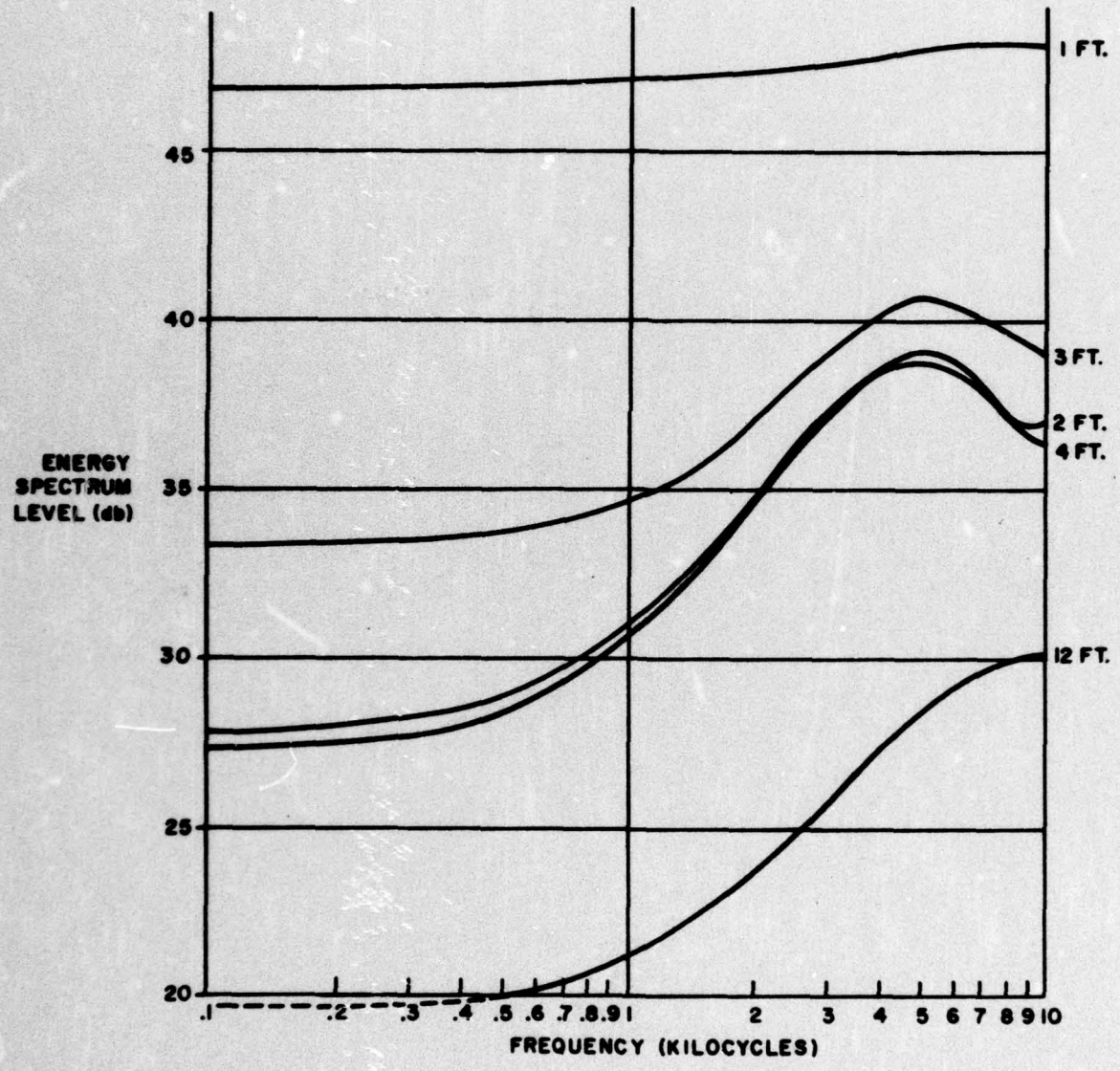

Figure 4E-6. IMP Mod X-1 Energy Spectra obtained from Exponential Representations

SECTION 5

FUTURE TRANSIENT PROGRAM

The experimental-study program described in this report has carried out its objectives. The waveshape, reproducibility, energy spectra, and directivity of the mechanical impact generator, IMP MOD X-1, was completely determined. In addition, the influence of the propagating medium upon the spatial and temporal properties of the IMP signal was also investigated.

There are many vital areas in the field of acoustic transients that need to be extensively studied before transient signals can be utilized effectively in future sonar systems. In order to help carry out this objective, a program is proposed to study the following:

★ Transient Response of Multidimensional Arrays

A linear and plane array of wideband probes will be designed to receive the IMP signal. The arrays will be adaptable to uniform and non-uniform interelement spacings and variable bandwidths. Data analysis will include determining the cross-correlation and cross-power spectra between elements and establishing the transform relationship between the pressure field and total array response. The effect of hydrophone length upon the hydrophone's transient response will also be determined.

★ Amplitude - Time Pattern of Ambient Noise

The effect of hydrophone directivity upon the impulsive nature and coherence of ambient noise will be examined. It is anticipated that as the directivity increases, the noise sources in the vicinity of the main lobe of the hydrophone will become more prominent, thereby increasing the peakedness of the received noise background. This may prove to be a major consideration in processing weak transient signals effectively.

★ **Digital Data Processing System**

A digital data processing system will be assessed to automatically process (electronically sample and digitize) the raw transient data into computer format in real time. The data processor will not only eliminate the errors due to manual digitization but will also permit, by employing time multiplexing, many points in the acoustic field to be monitored almost simultaneously. Ease of monitoring the acoustic field will facilitate characterizing the environment which would be required for realizing any technique for processing transient signals.

LIST OF REFERENCES

1. A. Winder, "A Survey of Acoustic Transient Processes and Experimental Evaluation of IMP MOD X-1," Edo Report 6299, January 1964.

2. H. W. Marsh, R. H. Mellen, and W. L. Konrad, "Anomalous Absorption of Pressure Waves from Explosions in Sea Water," AVCO Marine Electronics Office, New London, Connecticut, March 1965.

3. H. E. Sawyer, "Impact Sound Source Research," JUA(USN), 7, 221-224 (1957)

4. H. E. Sawyer, "Measurements of IMP Performance," JUA(USN), 10, 777-784 (1959)

5. H. E. Sawyer, W. S. Shultz, and C. S. Purington, "Status Report: Impact Sound Source," Contract Nonr 2129(00), (1957)

6. R. B. Blackman and J. W. Tukey, "The Measurement of Power Spectra," Dover Publications, Inc., New York, 1958

7. A. Papoulis, "The Fourier Integral and its Applications," sections 4-4 and 4-5, McGraw-Hill Book Company, Inc., 1962

8. M. I. Skolnik, "Introduction to Radar Systems," section 7-10, McGraw-Hill Book Company, Inc., 1962

9. J. W. Horton, "Fundamentals of Sonar," Chapter 4, United States Naval Institute, 1959

LIST OF REFERENCES (cont)

10. For history, development and application of exponential signal representations, refer to the series of reports "Representation and Analysis of Signals," Parts I - XVIII, originated by the Electrical Engineering Department, The Johns Hopkins University, under Contracts AF 19(604) - 1941, Nonr - 248(53) and Nonr - 4010(13). The reports are available from DDC.

11. "Representation and Analysis of Signals, Part XV. Matched Exponents for the Representation of Signals," R. N. McDonough, 1963.

12. Rosenblatt (editor) "Time Series Analysis".

GENERAL

DISTRIBUTION LIST

Office of Naval Research (Code 468) Department of the Navy Washington, D. C. 20360	2
Director, U. S. Naval Research Laboratory Technical Information Division Washington, D. C. 20390	6
Director, U. S. Naval Research Laboratory Sound Division Washington, D. C. 20390	1
Commanding Officer Office of Naval Research Branch Office 1030 East Green Street Pasadena, California 91101	1
Commanding Officer Office of Naval Research Branch Office 495 Summer Street Boston, Massachusetts 02210	1
Commanding Officer Office of Naval Research Branch Office 219 South Dearborn Street Chicago, Illinois 60604	1
Commanding Officer Office of Naval Research Branch Office 207 West 24th Street New York, New York 10011	1
Commanding Officer Office of Naval Research Branch Office Box 39 FPO New York 09510	9

Commander, U. S. Naval Ordnance Laboratory Acoustics Division White Oak, Silver Spring, Maryland 20910	1
Commanding Officer and Director U. S. Navy Electronics Laboratory San Diego, California 92152	1
Director, U. S. Navy Underwater Sound Reference Laboratory Office of Naval Research P. O. Box 8337 Orlando, Florida 32806	1
Commanding Officer and Director U. S. Navy Underwater Sound Laboratory Fort Trumbull New London, Connecticut 06321	1
Commander, U. S. Naval Air Development Center Johnsville, Pennsylvania	1
Commanding Officer and Director David Taylor Model Basin Washington, D. C. 2007	1
Superintendent, U. S. Naval Postgraduate Monterey, California Attn: Prof. L. E. Kinsler Prof. Herman Medwin	2
Commanding Officer U. S. Navy Mine Defense Laboratory Panama City, Florida 32402	1
U. S. Naval Academy Annapolis, Maryland 21402	1
Chief, Weapons Systems Command Department of the Navy Washington, D. C. 20360	1 Code RU-222 1 Code RUTO-3

Chief, Ships Systems Command Department of the Navy Washington, D. C. 20360	1 Code 343 1 Code 370 1 Code 1610
Commander, U. S. Naval Ordnance Test Station Pasadena Annex 3203 E. Foothill Blvd. Pasadena, California 91108	1
Hudson Laboratories Columbia University 145 Palisade Street Dobbs Ferry, New York 10522	1
Brown University Research Analysis Group Providence, Rhode Island 02906	1
Woods Hole Oceanographic Institution Woods Hole, Massachusetts 02543	1
Institute for Defense Analyses Communications Research Division von Neumann Hall Princeton, New Jersey 08540	1
Ordnance Research Laboratory Pennsylvania State University University Park, Pennsylvania 16801	1
U. S. Navy SOFAR Station APO, New York 09856 Attn: Dr. G. R. Hamilton	1
AVCO Marine Electronics Office 33 Union Street New London, Connecticut 06321 Attn: Dr. H. W. Marsh	1
Defense Research Laboratory University of Texas Austin, Texas 78712	1

Edo

University of Miami 1
Marine Laboratory
#1 Rickenbacker Causeway
Miami, Florida 33149

Director, Applied Physics Laboratory 1
University of Washington
Seattle, Washington 98105

Director, 1
Marine Physical Laboratory of the
Scripps Institution of Oceanography
University of California
San Diego, California 92152

Dr. J. V. Bouyoucos 1
General Dynamics/Electronics
1400 N. Goodman Street
P. O. 226
Rochester, New York 14609

Dr. W. H. Huggins 1
Department of Electrical Engineering
Johns Hopkins University
Baltimore, Maryland 21218

Mr. T. G. Birdsall 1
Cooley Electronics Laboratory
University of Michigan Research Institute
Ann Arbor, Michigan 48105

Dr. C. A. Stutt 1
Research Laboratory
General Electric Company
P. O. Box 1088
Schenectady, New York 12301

Dr. Steven S. Wolff 1
Department of Electrical Engineering
Johns Hopkins University
Baltimore, Maryland 21218

Unclassified
Security Classification

3ND PPSO 13152

DOCUMENT CONTROL DATA - R&D

(Security classification of title, body of abstract and indexing annotation must be entered when the overall report is classified)

1 ORIGINATING ACTIVITY (Corporate author)
Edo Corporation
College Point, N.Y. New York, U.S.A.

2a. REPORT SECURITY CLASSIFICATION
Unclassified

2b. GROUP
None

(6) 3. REPORT TITLE
Acoustic Transient Signal Study.
Interim Yearly Engineering Report

(10) Alan A. Winder
Allan N. Cohen

(9) 4. DESCRIPTIVE NOTES (Type of report and inclusive dates)
Interim Yearly Engineering Report 1 Sept 1964 — 1 Sept 1965

5. AUTHOR(S) (Last name, first name, initial)
Winder, Alan A. Research Project Engineer
Cohen, Allan N. Research Senior Engineer

(11) 6. REPORT DATE
30 June 1966

(12) 121p.

7a. TOTAL NO. OF PAGES
115

7b. NO. OF REFS
12

(15) 8a. CONTRACT OR GRANT NO.
NOnr-3346 (00)
None

b. None

c. None NOnr-4678(00)

d. None

(14) 9a. ORIGINATOR'S REPORT NUMBER(S)
EDO-7087

9b. OTHER REPORT NO(S) (Any other numbers that may be assigned this report)
None

10. AVAILABILITY/LIMITATION NOTICES
Distribution of this Document is Unlimited

11. SUPPLEMENTARY NOTES
None

12. SPONSORING MILITARY ACTIVITY
Office of Naval Research
Washington, D. C.

13. ABSTRACT

The acoustic properties of a mechanical impact generator, the IMP MOD X-1, were measured in the near and far field. The pressure waveform had excellent reproducibility in peak pressure, pulsewidth, rise time, and decay. The peak pressure at 1 yard, on-axis, was 141 db re 1 ~~uber~~ and the pulsewidth was 33 ~~ubees~~. In general, about 50% of the energy was below 14kc and 85% below 35kc. For ranges greater than 3 yards, the -3db beamwidth was 17 degrees ± 3 degrees. The waveform was represented by five (5) complex conjugate pairs of decaying exponentials with an accuracy (in the mean-squared sense) at 2.66% or better. Although the cavitation limit for C-W intensity was greatly exceeded during tests, there was no evidence of cavitation.

microbar
microsec.
+ or -

DD FORM 1 JAN 64 1473 IIA 0101 807 6800

122150

Unclassified
Security Classification

4B

Security Classification

14 KEY WORDS	LINK A		LINK B		LINK C	
	ROLE	WT	ROLE	WT	ROLE	WT
Mechanical Impact Generator, IMP MOD X-1 Transient Response Acoustic Reproducibility Energy Spectrum Cumulative Energy Spectra RMS Bandwidth-time product Peak and Iso-time patterns Effective C-W Pressure Pattern Truncation, Aliasing Manual Digitization Orthogonal Exponential Decomposition						

INSTRUCTIONS

1. **ORIGINATING ACTIVITY:** Enter the name and address of the contractor, subcontractor, grantee, Department of Defense activity or other organization *(corporate author)* issuing the report.

2a. **REPORT SECURITY CLASSIFICATION:** Enter the overall security classification of the report. Indicate whether "Restricted Data" is included. Marking is to be in accordance with appropriate security regulations.

2b. **GROUP:** Automatic downgrading is specified in DoD Directive 5200.10 and Armed Forces Industrial Manual. Enter the group number. Also, when applicable, show that optional markings have been used for Group 3 and Group 4 as authorized.

3. **REPORT TITLE:** Enter the complete report title in all capital letters. Titles in all cases should be unclassified. If a meaningful title cannot be selected without classification, show title classification in all capitals in parenthesis immediately following the title.

4. **DESCRIPTIVE NOTES:** If appropriate, enter the type of report, e.g., interim, progress, summary, annual, or final. Give the inclusive dates when a specific reporting period is covered.

5. **AUTHOR(S):** Enter the name(s) of author(s) as shown on or in the report. Enter last name, first name, middle initial. If military, show rank and branch of service. The name of the principal author is an absolute minimum requirement.

6. **REPORT DATE:** Enter the date of the report as day, month, year; or month, year. If more than one date appears on the report, use date of publication.

7a. **TOTAL NUMBER OF PAGES:** The total page count should follow normal pagination procedures, i.e., enter the number of pages containing information.

7b. **NUMBER OF REFERENCES:** Enter the total number of references cited in the report.

8a. **CONTRACT OR GRANT NUMBER:** If appropriate, enter the applicable number of the contract or grant under which the report was written.

8b, 8c, & 8d. **PROJECT NUMBER:** Enter the appropriate military department identification, such as project number, subproject number, system numbers, task number, etc.

9a. **ORIGINATOR'S REPORT NUMBER(S):** Enter the official report number by which the document will be identified and controlled by the originating activity. This number must be unique to this report.

9b. **OTHER REPORT NUMBER(S):** If the report has been assigned any other report numbers *(either by the originator or by the sponsor)*, also enter this number(s).

10. **AVAILABILITY/LIMITATION NOTICES:** Enter any limitations on further dissemination of the report, other than those imposed by security classification, using standard statements such as:

(1) "Qualified requesters may obtain copies of this report from DDC."

(2) "Foreign announcement and dissemination of this report by DDC is not authorized."

(3) "U. S. Government agencies may obtain copies of this report directly from DDC. Other qualified DDC users shall request through _____."

(4) "U. S. military agencies may obtain copies of this report directly from DDC. Other qualified users shall request through _____."

(5) "All distribution of this report is controlled. Qualified DDC users shall request through _____."

If the report has been furnished to the Office of Technical Services, Department of Commerce, for sale to the public, indicate this fact and enter the price, if known.

11. **SUPPLEMENTARY NOTES:** Use for additional explanatory notes.

12. **SPONSORING MILITARY ACTIVITY:** Enter the name of the departmental project office or laboratory sponsoring *(paying for)* the research and development. Include address.

13. **ABSTRACT:** Enter an abstract giving a brief and factual summary of the document indicative of the report, even though it may also appear elsewhere in the body of the technical report. If additional space is required, a continuation sheet shall be attached.

It is highly desirable that the abstract of classified reports be unclassified. Each paragraph of the abstract shall end with an indication of the military security classification of the information in the paragraph, represented as *(TS), (S), (C), or (U)*.

There is no limitation on the length of the abstract. However, the suggested length is from 150 to 225 words.

14. **KEY WORDS:** Key words are technically meaningful terms or short phrases that characterize a report and may be used as index entries for cataloging the report. Key words must be selected so that no security classification is required. Identifiers, such as equipment model designation, trade name, military project code name, geographic location, may be used as key words but will be followed by an indication of technical context. The assignment of links, roles, and weights is optional.

Security Classification

Edo Corporation. Report 7087.

ACOUSTIC TRANSIENT SIGNAL STUDY INTERIM YEARLY ENGINEERING REPORT

1 SEPT. 1964 - 1 SEPT. 1965

by A. A. Winder, A. N. Cohen 115 p. p., transient photos, graphs, tables.

UNCLASSIFIED

The acoustic properties of a mechanical impact generator, the IMP MOD X-1, were measured in the near and far field. The pressure waveform had excellent reproducibility in peak pressure, pulsewidth, rise time, and decay. The peak pressure at 1 yard, on-axis, was 141 db re 1 μ bar and the pulsewidth was 33 μ secs. In general, about 50% of the energy was below 14 kc and 85% below 35 kc. For ranges greater than 3 yards, the -3 db beamwidth was 17° ± 3°. The waveform was represented by five (5) complex conjugate pairs of decaying exponentials with an accuracy (in the mean-squared sense) of 2.66% or better. Although the cavitation limit for C-W intensity was greatly exceeded during tests, there was no evidence of cavitation.

i. Acoustic Transient Signal Study

1. Winder, A. A.
2. Cohen, A. N.

Edo Corporation. Report 7087.

ACOUSTIC TRANSIENT SIGNAL STUDY INTERIM YEARLY ENGINEERING REPORT

1 SEPT. 1964 - 1 SEPT. 1965

by A. A. Winder, A. N. Cohen 115 p. p., transient photos, graphs, tables.

UNCLASSIFIED

The acoustic properties of a mechanical impact generator, the IMP MOD X-1, were measured in the near and far field. The pressure waveform had excellent reproducibility in peak pressure, pulsewidth, rise time, and decay. The peak pressure at 1 yard, on-axis, was 141 db re 1 μ bar and the pulsewidth was 33 μ secs. In general, about 50% of the energy was below 14 kc and 85% below 35 kc. For ranges greater than 3 yards, the -3 db beamwidth was 17° ± 3°. The waveform was represented by five (5) complex conjugate pairs of decaying exponentials with an accuracy (in the mean-squared sense) of 2.66% or better. Although the cavitation limit for C-W intensity was greatly exceeded during tests, there was no evidence of cavitation.

i. Acoustic Transient Signal Study

1. Winder, A. A.
2. Cohen, A. N.

Edo Corporation. Report 7087.

ACOUSTIC TRANSIENT SIGNAL STUDY INTERIM YEARLY ENGINEERING REPORT

1 SEPT. 1964 - 1 SEPT. 1965

by A. A. Winder, A. N. Cohen 115 p. p., transient photos, graphs, tables.

UNCLASSIFIED

The acoustic properties of a mechanical impact generator, the IMP MOD X-1, were measured in the near and far field. The pressure waveform had excellent reproducibility in peak pressure, pulsewidth, rise time, and decay. The peak pressure at 1 yard, on-axis, was 141 db re 1 μ bar and the pulsewidth was 33 μ secs. In general, about 50% of the energy was below 14 kc and 85% below 35 kc. For ranges greater than 3 yards, the -3 db beamwidth was 17° ± 3°. The waveform was represented by five (5) complex conjugate pairs of decaying exponentials with an accuracy (in the mean-squared sense) of 2.66% or better. Although the cavitation limit for C-W intensity was greatly exceeded during tests, there was no evidence of cavitation.

i. Acoustic Transient Signal Study

1. Winder, A. A.
2. Cohen, A. N.

Edo Corporation. Report 7087.

ACOUSTIC TRANSIENT SIGNAL STUDY INTERIM YEARLY ENGINEERING REPORT

1 SEPT. 1964 - 1 SEPT. 1965

by A. A. Winder, A. N. Cohen 115 p. p., transient photos, graphs, tables.

UNCLASSIFIED

The acoustic properties of a mechanical impact generator, the IMP MOD X-1, were measured in the near and far field. The pressure waveform had excellent reproducibility in peak pressure, pulsewidth, rise time, and decay. The peak pressure at 1 yard, on-axis, was 141 db re 1 μ bar and the pulsewidth was 33 μ secs. In general, about 50% of the energy was below 14 kc and 85% below 35 kc. For ranges greater than 3 yards, the -3 db beamwidth was 17° ± 3°. The waveform was represented by five (5) complex conjugate pairs of decaying exponentials with an accuracy (in the mean-squared sense) of 2.66% or better. Although the cavitation limit for C-W intensity was greatly exceeded during tests, there was no evidence of cavitation.

i. Acoustic Transient Signal Study

1. Winder, A. A.
2. Cohen, A. N.

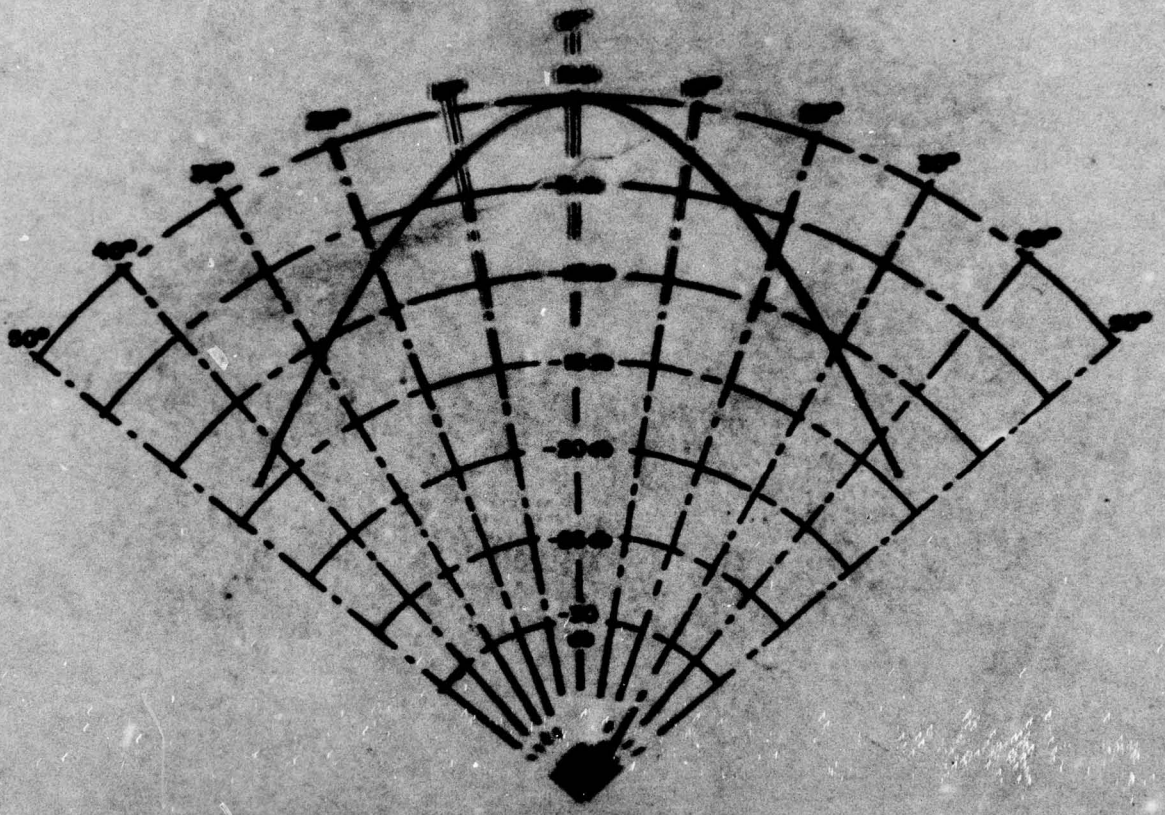

Figure 4D-12. Effective C-W Pressure Pattern at 8, 6, 67, and 107 Yards (NUCE)

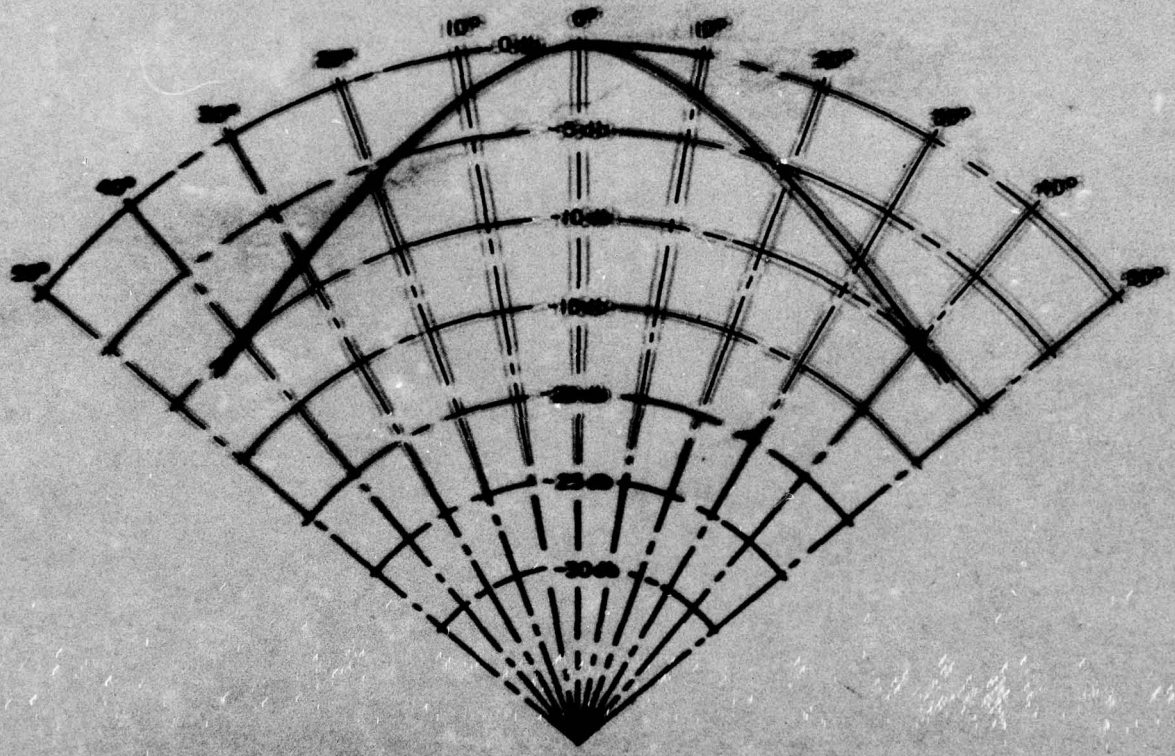

Figure 4D-14. [illegible] Pressure Pattern at 20 Yards (NUOS)